# 3. The Nuclear Shell Model

## 3.1 One-particle Excitations

### 3.1.1 Introduction

The basic assumption in the nuclear shell model is that, to first order, each nucleon (proton or neutron) is moving in an independent way in an average field. This is not so, a priori, since the nucleus constitutes an $A$-body problem interacting via the nucleon-nucleon force in the nuclear medium. It is clear from the very beginning that this nucleon-nucleon force will be different from the free nucleon-nucleon interaction (Bohr, Mottelson 1969). As was already expressed in the introduction to this book, the non-relativistic form of the nucleon-nucleon interaction behaves as shown in Fig. 3.1. At large separations $|\boldsymbol{r}_i - \boldsymbol{r}_j| \cong 1.5 - 2\,\mathrm{fm}$, the force behaves according to a one-pion exchange potential (OPEP) which has an analytic dependence on $r = |\boldsymbol{r}_i - \boldsymbol{r}_j|$ of (Bohr, Mottelson 1969)

$$V(r) = -\frac{\mathrm{e}^{-\mu r}}{\mu r}\left(1 + \frac{3}{\mu r} + \frac{3}{(\mu r)^2}\right). \tag{3.1}$$

For small distances the attractive part turns over and becomes repulsive at distances $r < 0.5\,\mathrm{fm}$; this is the hard-core potential. At such short distances the energy for interactions between nucleons becomes so high that non-relativistic treatments are no longer justified. In this region, exchange of more pions or heavy mesons is needed. It is probably even more correct to go to QCD where nucleons are

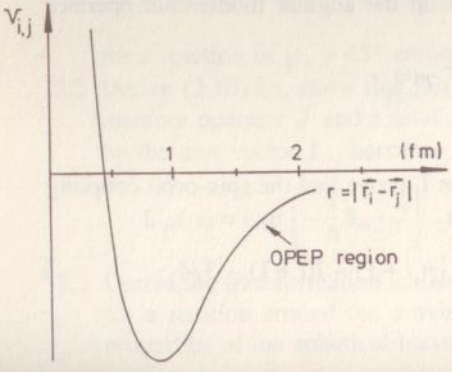


**Fig. 3.1.** Schematic illustration of the nucleon two-body interaction $V_{i,j}$ as a function of the nucleon separation $r = |\boldsymbol{r}_i - \boldsymbol{r}_j|$. For large separation ($r \cong 1.5 - 2fm$), the OPEP tail results. For short distances, a short range repulsive core shows up

considered as being obtained from their quark constituents and so, a nucleon-nucleon interaction process can be better depicted, as in Fig. 3.2.

One of the most unexpected features is still the very large nuclear mean free path in the nuclear medium (Fig. 3.3).

In the study of the nuclear structure observed at low excitation energy ($E_x <$ 8 MeV), two important aspects show up:

- how to handle (even in a non-relativistic way) the $A$-nucleon problem,
- how to describe the nuclear average field starting from the nucleon-nucleon force $V(|\boldsymbol{r}_i - \boldsymbol{r}_j|)$ between free nucleons.

In the atomic case, a shell structure was shown to exist by N. Bohr. Starting from an average Coulomb field $V(r) = -Z\,e^2/r$, the corresponding one-electron Schrödinger equation can be solved and the atomic orbits studied in detail. According to the Pauli principle, only one fermion particle can be in a specific quantum state defined by the radialquantum number ($n$), and the orbital ($l$), total ($j$) and

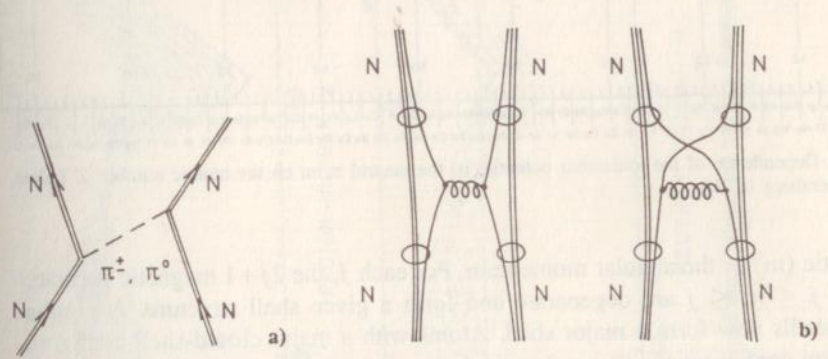


**Fig. 3.2.** The nucleon-nucleon interaction (**a**) on the level of QHD (quantum hadro-dynamics) where the force is mediated by the exchange of pions ($\pi^{\pm}, \pi^0$) between the interacting nucleons, or (**b**) on the level of QCD (quantum chromo-dynamics) where a gluon is exchanged between one of the three quarks constituting the nucleon. The left-hand side diagram is zero due to the colour selection rules, the right-hand diagram contributes since colour selection rules are obeyed

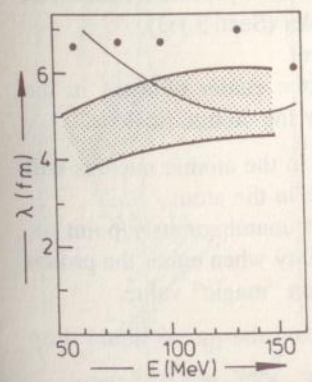


**Fig. 3.3.** The empirical mean free path ($\lambda(fm)$). The shaded band denotes the range of values determined from reaction cross sections for Ca, Zr and Pb in (Nadasen 1981), the solid line indicates the representative values selected in (Bohr 1969) and the data points are determined from optical potential fits for $^{208}$Pb in (Nadasen 1981) [taken from (Negele 1983)]

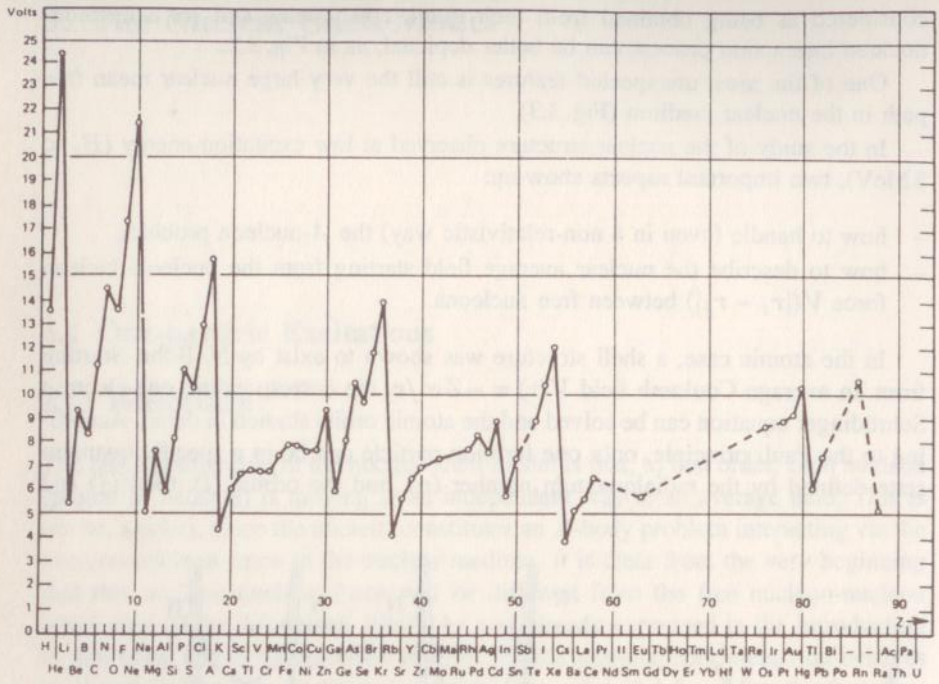


**Fig. 3.4.** Dependence of the ionization potential of the neutral atom on the atomic number $Z$ [taken from (Herzberg 1944)]

magnetic ($m$) of the angular momentum. For each $j$, the $2j+1$ magnetic substates with $-j \leq m \leq j$ are degenerate and form a given shell structure. A number of subshells now form a major shell. Atoms with a major closed-shell configuration form configurations that are particularly stable against losing the last electron (Figure 3.4 shows the ionization potentials of the elements).

In the nucleus a similar description seems to be possible. However, a number of distinct differences to the atomic case arise:

i) The nuclear mean field is very different from the Coulomb potential. Moreover, strong spin-orbit coupling is shown to exist in nuclei (Sect. 3.1.3).
ii) In the nucleus both protons and neutrons are present.
iii) There is no preferential central point other than the center of mass in the nucleus in contrast to the atomic field generated by the atomic nucleus.

Because of the above conditions the shell structure in the atomic nucleus will be very different from the corresponding shell structure in the atom.

We now quote a number of nuclear properties that unambiguously point towards nuclear shell structure and increased nuclear stability when either the proton number ($Z$) and/or the neutron number ($N$) has a certain "magic" value.

i) Deviations of the nuclear mass (binding energy) from the mean, liquid drop value exist (Fig. 3.5).

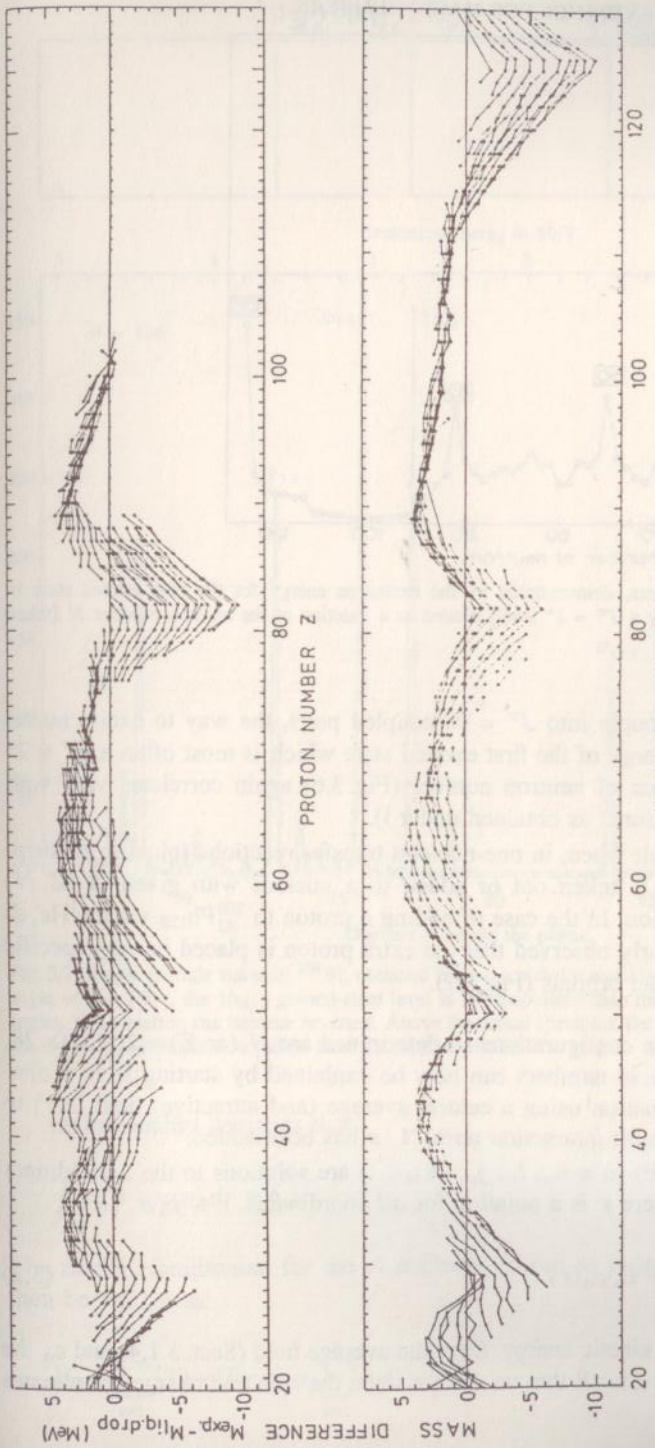


Fig. 3.5. Deviations of nuclear masses from their mean (liquid drop) values, and this as a function of neutron and proton number [taken from (Myers 1966)]

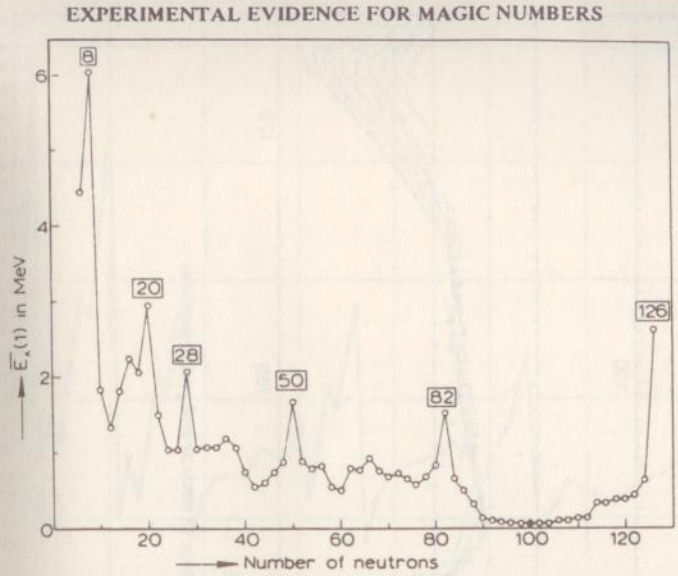


**Fig. 3.6.** The magic numbers, demonstrated by the excitation energy for the first excited state in doubly-even nuclei (mainly a $J^\pi = 2^+$ level) plotted as a function of the neutron number $N$ [taken from (Brussaard 1977)]

ii) Since nucleons couple into $J^\pi = 0^+$ coupled pairs, the way to excite nuclei (the excitation energy of the first excited state which is most often a $J^\pi = 2^+$ state) as a function of neutron number (Fig. 3.6) again correlates very well with the shell closures as obtained under i).

iii) Specific tests result when, in one-nucleon transfer reactions (pick-up or stripping), a nucleon is taken out or added to a nucleus with given $A$ $(Z, N)$ nucleon constitution. In the case of adding a proton to $^{208}_{82}\mathrm{Pb}_{126}$ via a $(^3\mathrm{He}, d)$ reaction, it is clearly observed that the extra proton is placed in very specific nuclear shell model orbitals (Fig. 3.7).

The stable nucleon configurations so determined are $N$ (or $Z$) = 2, 8, 20, 28, 50, 82, 126, (...). These numbers can now be explained by starting from a one-body Schrödinger equation using a central average (and attractive) field $U(r)$ to which a strong spin-orbit interaction term $\zeta \boldsymbol{l} \cdot \boldsymbol{s}$ has been added.

Suppose that $\varphi_a(\boldsymbol{r})$ $(a = n_a, l_a, j_a, m_a, \ldots)$ are solutions to the Schrödinger one-body equation (here $\boldsymbol{r}$ is a notation for *all* coordinates, $\boldsymbol{r} \equiv \boldsymbol{r}, \sigma, \ldots$)

$$[T + U(r)]\varphi_a(\boldsymbol{r}) = \varepsilon_a \varphi_a(\boldsymbol{r}) \,. \tag{3.2}$$

Here $T$ describes the kinetic energy, $U(r)$ the average field (Sect. 3.1.4) and $\varepsilon_a$ the single-particle energy (recall that we do not write the spin and charge coordinates explicitly).

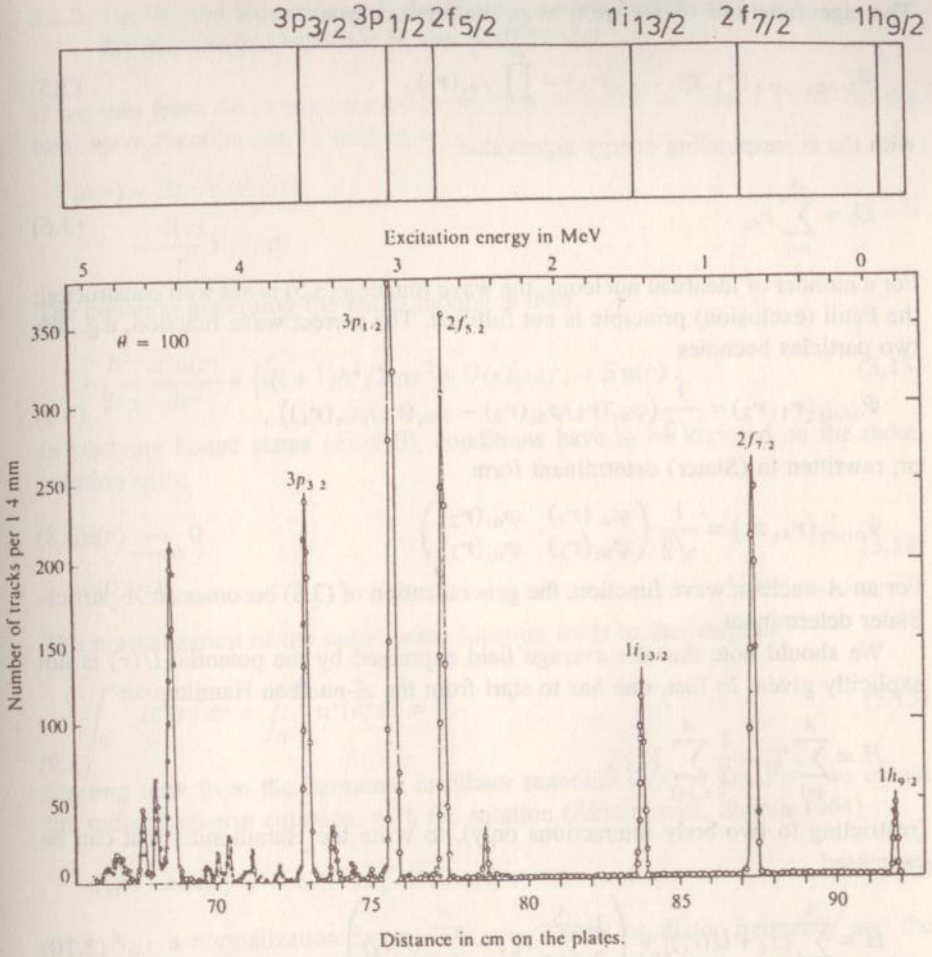


**Fig. 3.7.** Single-particle states in $^{209}$Bi, obtained from the pick-up reaction $^{208}$Pb ($^{3}$He,d)$^{209}$Bi. At the angle of $\theta = 100°$, the $1h_{9/2}$ ground-state level is less populated than the excited states but at other angles, this situation can become reversed. Above the actual spectrum, the proton single-particle states are drawn as an illustration [taken from (Mottelson 1967)]

Orthogonality demands that

$$\int \varphi_a^*(\boldsymbol{r})\varphi_b(\boldsymbol{r})\,d\boldsymbol{r} = \delta_{ab}\,. \tag{3.3}$$

The model Hamiltonian for the $A$ nucleons (taken as independent particles) can then be written as

$$H_0 = \sum_{i=1}^{A}\left(T_i + U(r_i)\right) = \sum_{i=1}^{A} h_0(i)\,. \tag{3.4}$$

The eigenfunctions of $H_0$ are now of the product type

$$\Psi_{a_1,a_2,\ldots,a_A}(\boldsymbol{r}_1,\boldsymbol{r}_2,\ldots,\boldsymbol{r}_A)=\prod_{i=1}^{A}\varphi_{a_i}(\boldsymbol{r}_i)\,, \tag{3.5}$$

with the corresponding energy eigenvalue

$$E_0=\sum_{i=1}^{A}\varepsilon_{a_i}\,. \tag{3.6}$$

For a number of identical nucleons, the wave function (3.5) is not well constructed: the Pauli (exclusion) principle is not fulfilled. The correct wave function, e.g., for two particles becomes

$$\Psi_{a_1,a_2}(\boldsymbol{r}_1,\boldsymbol{r}_2)=\frac{1}{\sqrt{2}}\left(\varphi_{a_1}(\boldsymbol{r}_1)\varphi_{a_2}(\boldsymbol{r}_2)-\varphi_{a_1}(\boldsymbol{r}_2)\varphi_{a_2}(\boldsymbol{r}_1)\right)\,, \tag{3.7}$$

or, rewritten in (Slater) determinant form

$$\Psi_{a_1,a_2}(\boldsymbol{r}_1,\boldsymbol{r}_2)=\frac{1}{\sqrt{2}}\begin{pmatrix}\varphi_{a_1}(\boldsymbol{r}_1) & \varphi_{a_1}(\boldsymbol{r}_2)\\ \varphi_{a_2}(\boldsymbol{r}_1) & \varphi_{a_2}(\boldsymbol{r}_2)\end{pmatrix}\,. \tag{3.8}$$

For an $A$-nucleon wave function, the generalization of (3.8) becomes an $A$-particle Slater determinant.

We should note that the average field expressed by the potential $U(r)$ is not explicitly given. In fact, one has to start from the $A$-nucleon Hamiltonian

$$H=\sum_{i=1}^{A}T_i+\frac{1}{2}\sum_{i,j=1}^{A}V_{i,j}\,, \tag{3.9}$$

(restricting to two-body interactions only), to write the Hamiltonian that can be expressed

$$H=\sum_{i=1}^{A}\left[T_i+U(r_i)\right]+\left(\frac{1}{2}\sum_{i,j=1}^{A}V_{i,j}-\sum_{i=1}^{A}U(r_i)\right) \tag{3.10}$$

$$\begin{aligned}&=H_0+H_{\mathrm{res}}\\ &=\sum_{i=1}^{A}h_0(i)+H_{\mathrm{res}}\,,\end{aligned} \tag{3.11}$$

where $H_0$ describes the motion of $A$ nucleons, independent of each other in the same average field. The smaller the effect of $H_{\mathrm{res}}$, the better the assumption of an average, independent field becomes. The method of determining $U(r)$, starting from a known $V_{i,j}$ and a Slater determinant $A$-nucleon wave function that is a good approximation to the total ground state wave function for the full Hamiltonian $H$, is carried out by using the Hartree-Fock method (Sect. 3.1.4). Before that, however, we study the independent nucleon motion with a harmonic oscillator potential $U(r)=\frac{1}{2}m\omega^2r^2$.

### 3.1.2 The Radial Equation and the Single-particle Spectrum: the Harmonic Oscillator in the Shell Model

If we start from the central, one-body problem discussed in Chap. 1 (1.14–18) the total wave function can be written as

$$\begin{aligned}\varphi(\boldsymbol{r}) &= R(r)Y(\theta,\varphi)\,,\\ &= \frac{u(r)}{r}Y(\theta,\varphi)\,.\end{aligned} \tag{3.12}$$

The equation governing the radial motion is then

$$-\frac{\hbar^2}{2m}\frac{d^2u(r)}{dr^2} + \left[l(l+1)\hbar^2/2mr^2 + U(r)\right]u(r) = Eu(r)\,. \tag{3.13}$$

In studying bound states ($E < 0$), conditions have to be imposed on the radial solution $u(r)$:

$$\begin{aligned}&u(r) \underset{r\to\infty}{\to} 0\,,\\ &u(0) = 0\,.\end{aligned} \tag{3.14}$$

The normalization of the radial wave function leads to the integrals

$$\int_0^\infty R^2(r)\,dr = \int_0^\infty u^2(r)\,dr = 1\,. \tag{3.15}$$

Starting now from the harmonic oscillator potential $U(r) = \frac{1}{2}m\omega^2r^2$, we obtain the radial Laguerre equation, with the solution (Abramowitz, Stegun 1964)

$$u_{kl}(r) = N_{k,l}\cdot r^{l+1}\,\mathrm{e}^{-\nu r^2}\,L_k^{l+1/2}\left(2\nu r^2\right)\,, \tag{3.16}$$

with $N_{k,l}$ a normalization factor, $\nu = m\omega/2\hbar$ the oscillator frequency and the Laguerre polynomial, given by (Abramowitz, Stegun 1964)

$$L_k^{l+1/2}(x) = \sum_{k'=0}^{k} a_{k'}^{l}(-1)^{k'}x^{k'}\,. \tag{3.17}$$

A number of radial solutions are illustrated for $Z = 82$, $N = 126$ for the neutron motion. Although the wave functions in Fig. 3.8 are calculated for a more realistic potential, a Woods-Saxon potential (Blomqvist, Wahlborn 1960), the overall behavior is the same as for the harmonic oscillator potential.

The energy eigenvalues corresponding with the eigenfunctions (3.16) are given by

$$E = \hbar\omega\left(2k + l + \tfrac{3}{2}\right) = \hbar\omega\left(N + \tfrac{3}{2}\right)\,, \tag{3.18}$$

with

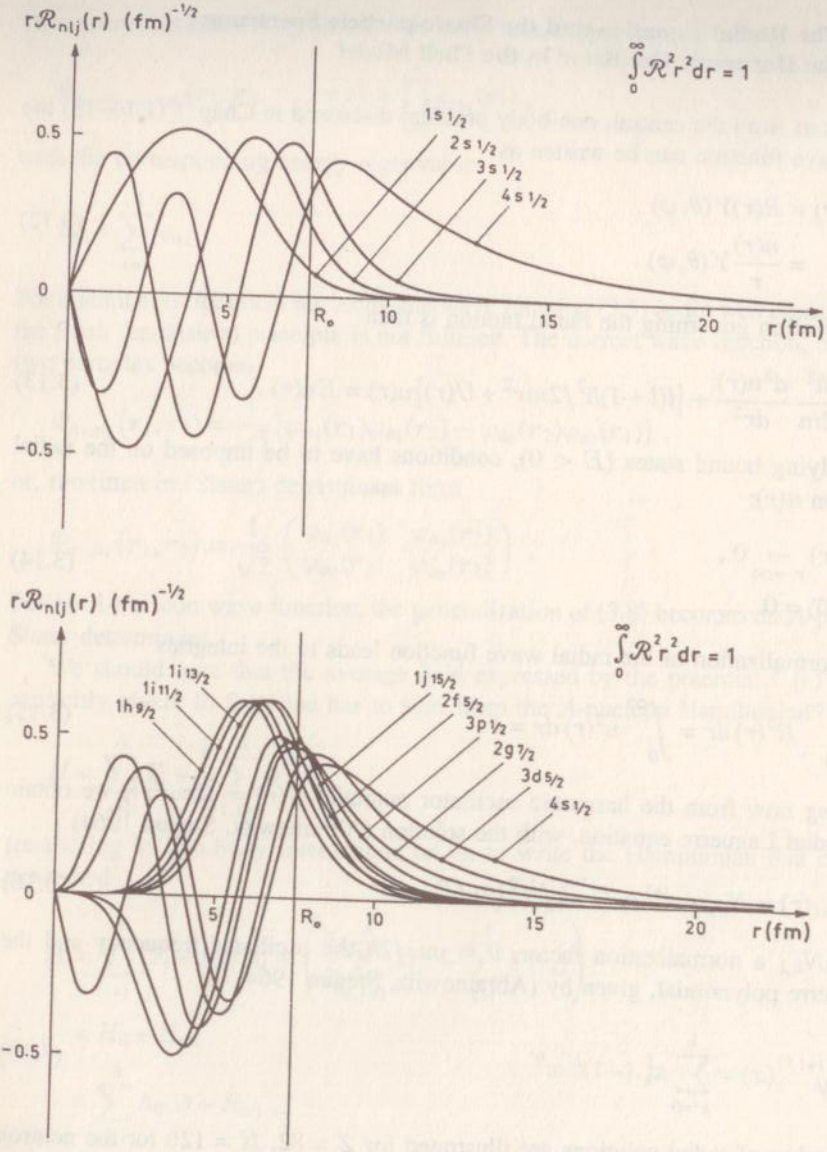


**Fig. 3.8.** Neutron radial wave functions for $A = 208$ and $Z = 82$ $u_{nlj}(r)$ $(n = 1, 2, \ldots)$ [based on the calculations with a Woods-Saxon potential by (Blomqvist 1960)] [taken from (Bohr, Mottelson 1969)]

$$\begin{aligned} &N = 0,\ 1,\ 2\,, && \text{(major oscillator quantum number)}\,,\\ &l = N,\ N-2,\ \ldots,\ 1 \text{ or } 0 && \text{(orbital quantum number)}\,,\\ &k = (N-l)/2 && \text{(radial quantum number)}\,. \end{aligned} \tag{3.19}$$

Thus, the spectrum of eigenvalues presents a large number of degenerate $(l, k)$ quantum numbers corresponding to a fixed $N$ major oscillator quantum number (Fig. 3.9).

The radial quantum number more often used (de-Shalit, Talmi 1963) is related to $k$ via

$$n = k + 1 = (N - l + 2)/2\,, \tag{3.20}$$

and expresses the number of nodes of the radial wave function in the interval $(0, \infty)$ including the node at the origin (excluding the one at infinity).

We now give a number of interesting properties of the Laguerre polynomials that allow for an elegant calculation of the normalization factor $N_{k,l}$ (Abramowitz, Stegun 1964)

$$\int_0^\infty z^a\, \mathrm{e}^{-z}\, L_k^a(z) L_{k'}^a(z)\, dz = \delta_{kk'} \cdot \Gamma(k + a + 1)^3/k!\,. \tag{3.21}$$

We use (3.21) in calculating the norm $N_{k,l}$ by putting $z = 2\nu r^2$, $r = (z/2\nu)^{1/2}$ and $dr = dz/[2(2\nu z)^{1/2}]$ and evaluate the integral

$$\begin{aligned} &N_{k,l}^2 \int_0^\infty r^{2l+2}\, \mathrm{e}^{-2\nu r^2} \left[L_k^{l+1/2}(2\nu r^2)\right]^2 dr\\ &\quad = N_{k,l}^2 \int_0^\infty z^{l+1/2}/\left(2(2\nu)^{l+3/2}\right) \mathrm{e}^{-z} \left[L_k^{l+1/2}(z)\right]^2 dz \end{aligned}$$

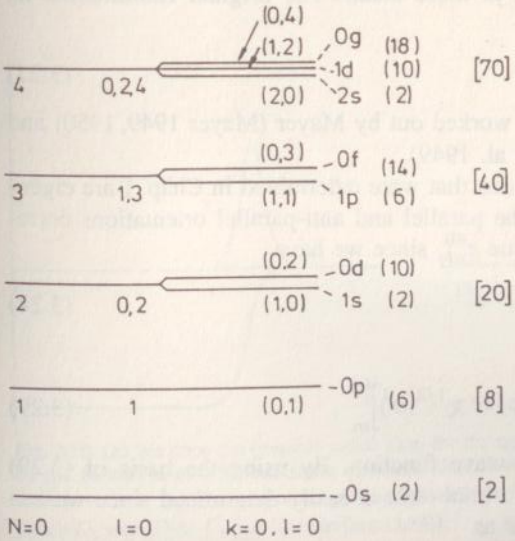


**Fig. 3.9.** Illustration of the degenerate harmonic oscillator energy spectrum up to $N = 4$. Besides the major shell quantum number $(N)$, the $(k, l)$ degeneracies are drawn explicitly. Partial and cumulative occupation numbers are given in round and squared brackets, respectively

$$= N_{k,l}^2/\left(2(2\nu)^{l+3/2}\right)\cdot\Gamma\left(l+\tfrac{3}{2}+k\right)^3/k! = 1 \quad \text{or}$$

$$N_{k,l} = \left(2(2\nu)^{l+3/2}k!/\Gamma(l+k+3/2)^3\right)^{1/2} . \tag{3.22}$$

Summarizing some properties:

$$\Gamma(z+1) = z\Gamma(z), \quad \Gamma\left(\tfrac{1}{2}\right) = \sqrt{\pi}\,,$$
$$L_0^a(z) = \Gamma(a+1), \quad L_0^{1/2}(z) = \sqrt{\pi}/2\,. \tag{3.23}$$

The radial wave functions can be determined as follows, since

$$L_k^a(z) = \Gamma(a+k+1)/k!\,\mathrm{e}^z\, z^{-a}\frac{d^k}{dz^k}\left(z^{a+k}\,\mathrm{e}^{-z}\right), \tag{3.24}$$

($k$ = entire). As an example, we illustrate the above equation for $L_1^{1/2}(z)$:

$$L_1^{1/2}(z) = \tfrac{3}{2}\cdot\frac{\sqrt{\pi}}{2}\left(\tfrac{3}{2}-z\right). \tag{3.25}$$

A number of often used expressions relating to the calculation of radial integrals are

$$\int_0^\infty x^{2n}\,\mathrm{e}^{-px^2}\,dx = (2n-1)!!/\left(2(2p)^n\right)\sqrt{\pi/p} \quad (p>0)\,,$$
$$\int_0^\infty x^{2n+1}\,\mathrm{e}^{-px^2}\,dx = n!/2p^{n+1} \qquad (p>0)\,. \tag{3.26}$$

Having determined the solutions to the radial equation for a single-particle harmonic oscillator potential, we observe a large degeneracy in the orbitals. Moreover, the nucleon numbers that form the stable configurations are $N$, $Z$ = 2, 8, 20, 40, 70 and do not agree with the experimental numbers. There is a strong spin-orbit term $\zeta(r)\,\boldsymbol{l}\cdot\boldsymbol{s}$ that is modifying the single-particle spectrum in the right direction. We shall work this out in more detail. The original Hamiltonian $h_0$ becomes

$$h = h_0 + \zeta(r)\boldsymbol{l}\cdot\boldsymbol{s}\,. \tag{3.27}$$

The consequences were originally worked out by Mayer (Mayer 1949, 1950) and Haxel, Jensen and Suess (Haxel et al. 1949).

The single-particle wave functions that were determined in Chap. 1 are eigenfunctions of $h_0$. Moreover, both the parallel and anti-parallel orientations correspond to the same energy eigenvalue $\varepsilon_{nlj}^{(0)}$ since we have

$$\langle nlj, m|h_0|nlj, m\rangle = \varepsilon_{nlj}^{(0)}\,, \tag{3.28}$$

with

$$\langle \boldsymbol{r}, \boldsymbol{\sigma}|nlj, m\rangle = \frac{u_{nl}(r)}{r}\left[\boldsymbol{Y}_l(\theta,\varphi)\otimes\boldsymbol{\chi}^{1/2}(\boldsymbol{\sigma})\right]_m^{(j)}, \tag{3.29}$$

the $(l, \frac{1}{2})j$ coupled single-particle wave function. By using the basis of (3.29) the energy correction for the spin-orbital term is easily determined since we can express the spin-orbit term $\zeta(r)\boldsymbol{l}\cdot\boldsymbol{s}$ as

$$\zeta(r)\tfrac{1}{2}\left(j^2 - l^2 - s^2\right) . \tag{3.30}$$

Thus we obtain

$$\varepsilon_{nlj} = \varepsilon^{(0)}_{nlj} + \Delta\varepsilon_{nlj} , \tag{3.31}$$

with

$$\Delta\varepsilon_{nlj} = \langle nlj, m|\zeta(r)\boldsymbol{l}\cdot\boldsymbol{s}|nlj, m\rangle , \tag{3.32}$$

or

$$\Delta\varepsilon_{nlj} = \frac{D}{2}\left[j(j+1) - l(l+1) - \tfrac{3}{4}\right] . \tag{3.33}$$

We define

$$D = \int u^2_{nl}(r)\zeta(r)\,dr . \tag{3.34}$$

This gives rise to a spin-orbit splitting of

$$\begin{aligned} \Delta\varepsilon_{nl\,j=l+1/2} &= \frac{D}{2}\cdot l \\ \Delta\varepsilon_{nl\,j=l-1/2} &= -\frac{D}{2}(l+1) , \end{aligned} \tag{3.35}$$

as illustrated in Fig. 3.10b.

A much used form of $\zeta(r)$ is the derivative of the average $U(r)$ potential and is shown for a Woods-Saxon potential in Fig. 3.10a. One can thus express $\zeta(r)$ as

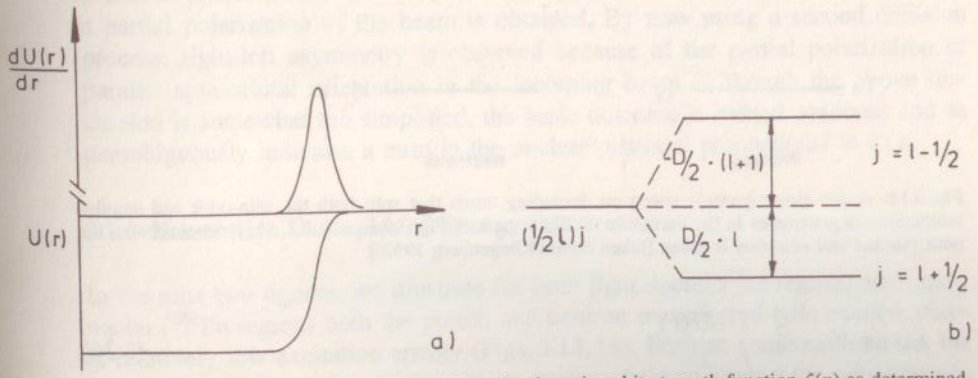


**Fig. 3.10.** (**a**) We draw the possible radial form for the spin-orbit strength function $\zeta(r)$ as determined by the derivative of a Woods-Saxon potential, described by (3.36). This function $\zeta(r)$ peaks at the nuclear surface. (**b**) The spin-orbit splitting between $j = l \pm \frac{1}{2}$ partners, according to (3.35), using the factor $D$, with $D \equiv \int u^2_{nl}(r)\zeta(r)dr$ [see (3.34)]

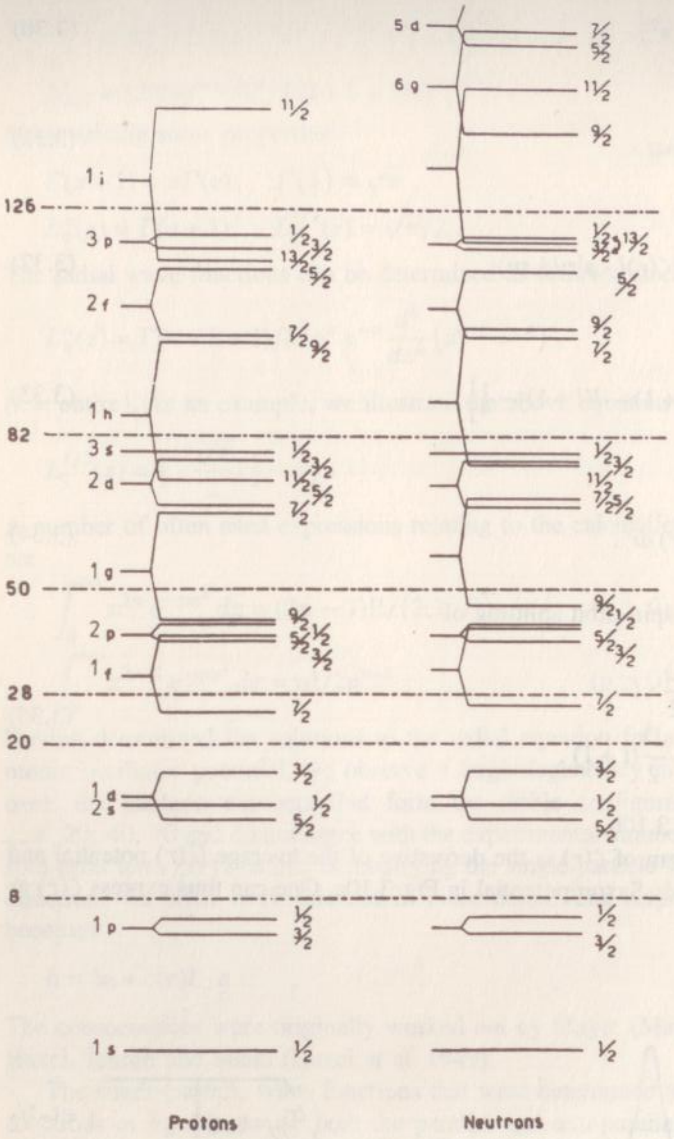


**Fig. 3.11.** A full single-particle spectrum, including terms that split both the spin-orbit and angular momentum degeneracies in the harmonic oscillator case of Fig. 3.9 ($n = 1, 2, \ldots$). A level scheme for both protons and neutrons is given [taken from (Klingenberg 1952)]

$$\zeta(r) = V_{ls} \cdot r_0^2 \cdot \frac{1}{r} \frac{\partial U(r)}{\partial r} \,. \tag{3.36}$$

A full single-particle spectrum, including a term proportional to $l^2$ for splitting the remaining degeneracies on $(k, l)$ for given $N$ in addition to the spin-orbit interaction, is illustrated in Fig. 3.11. This figure gives a general idea of

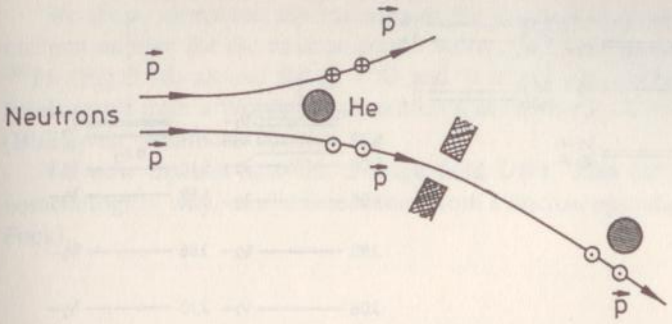


**Fig. 3.12.** Classical illustration of the existence of a spin-orbit interaction. A beam of unpolarized neutrons is directed to $^4$He scattering nuclei. If the coefficient multiplying the spin-orbit interaction is such as to favour parallel orientation, then neutrons passing on the lower side have their spin pointing *out* of the plane ($\odot$), the neutrons on the upper side have their spin pointing *into* the plane ($\otimes$). By collimating the beam, a polarized beam is selected. For a 100% polarized beam and scattering on a second $^4$He nucleus, *all* neutrons should pass on the lower side. This asymmetry is indeed observed in realistic cases. This experiment is an example of the polarizer-analyzer set-up

the nucleon shell structure with, this time, the correct "magic" numbers $N$, $Z = 2, 8, 20, 28, 50, 82, 126, \ldots$ .

Besides the correct reproduction of the stable nucleon configurations, there exists experimental evidence for a spin-orbit term in the nucleon-nucleon interaction as observed from nucleon-nucleus scattering (Bohr, Mottelson 1969). In a first collision of neutrons or protons with He nuclei of energy between 5 and 15 MeV, the beam is partially polarized. Classically, we can present the scattering in the following way (Fig. 3.12). The potential that an incoming nucleon feels in the nucleus is $U(r) + \zeta(r)\boldsymbol{l} \cdot \boldsymbol{s}$ with a negative value of $V_{ls}$ in (3.36). Thus the parallel orientation is favored by the scattering process. The nucleons scattered to the right now have their spin preferentially in the forward direction; the ones scattered to the left have their spin in the opposite direction. Using a diaphragm, a partial polarization of the beam is obtained. By now using a second collision process, right-left asymmetry is observed because of the partial polarization of parallel spin-orbital orientation in the incoming beam. Although the above discussion is somewhat too simplified, the basic outcome is indeed observed and so unambiguously indicates a term in the nuclear potential proportional to $\boldsymbol{l} \cdot \boldsymbol{s}$.

### 3.1.3 Illustrative Examples of Energy Spectra

In the next two figures, we illustrate for both light nuclei ($^{16}$O region) and heavy nuclei ($^{208}$Pb region) both the proton and neutron particle and hole excited states at relatively low excitation energy (Figs. 3.13, 14). Besides some extra states, the concept of single-particle motion in an average field following the structure obtained in Sect. 3.1.2 is indeed very well realized. Also, it is clear that in the heavier $^{208}$Pb nucleus the average field is better determined compared to $^{16}$O where only 16 particles are present.

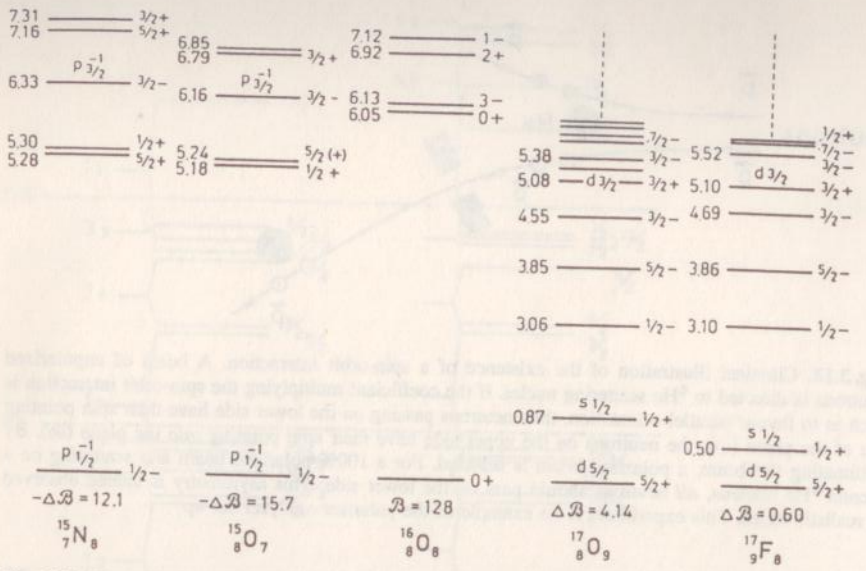


**Fig. 3.13.** Illustration of both proton and neutron single-particle and single-hole states around $^{16}$O. On each nucleus, the binding energy difference $\Delta B$, relative to $^{16}$O is given. The levels where the major single-particle (single-hole) character is concentrated are given with the quantum numbers $(lj)$ although these quantities are not good quantum numbers in general (only $J^\pi$ is). The level scheme is taken from (Bohr, Mottelson 1969)

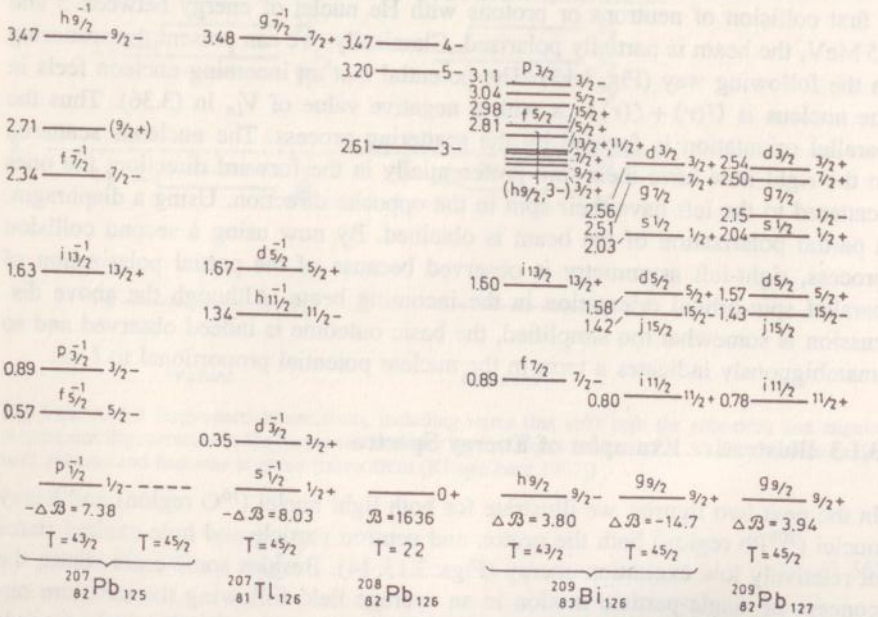


**Fig. 3.14.** See caption to Fig. 3.13, but now for the proton and neutron single-particle and single-hole states around the nucleus $^{208}$Pb. Details on the origin of the experimental data can be found in the Nuclear Data Sheets for the appropriate nuclei [Figure taken from (Bohr, Mottelson 1969)]

We show, moreover, the variation of the single-particle states as a function of nucleon number for the neutron bound states (Fig. 3.15), as well as an excerpt for $^{208}$Pb (Fig. 3.16) around the $Z = 82$ and $N = 126$ closed shells. [The calculated levels result from a Woods-Saxon potential as studied by Blomqvist and Wahlborn (Blomqvist, Wahlborn 1960).]

We now discuss how the average field $U(r)$, used before in a rather phenomenological way, can be determined from a microscopic starting point (Hartree-Fock).

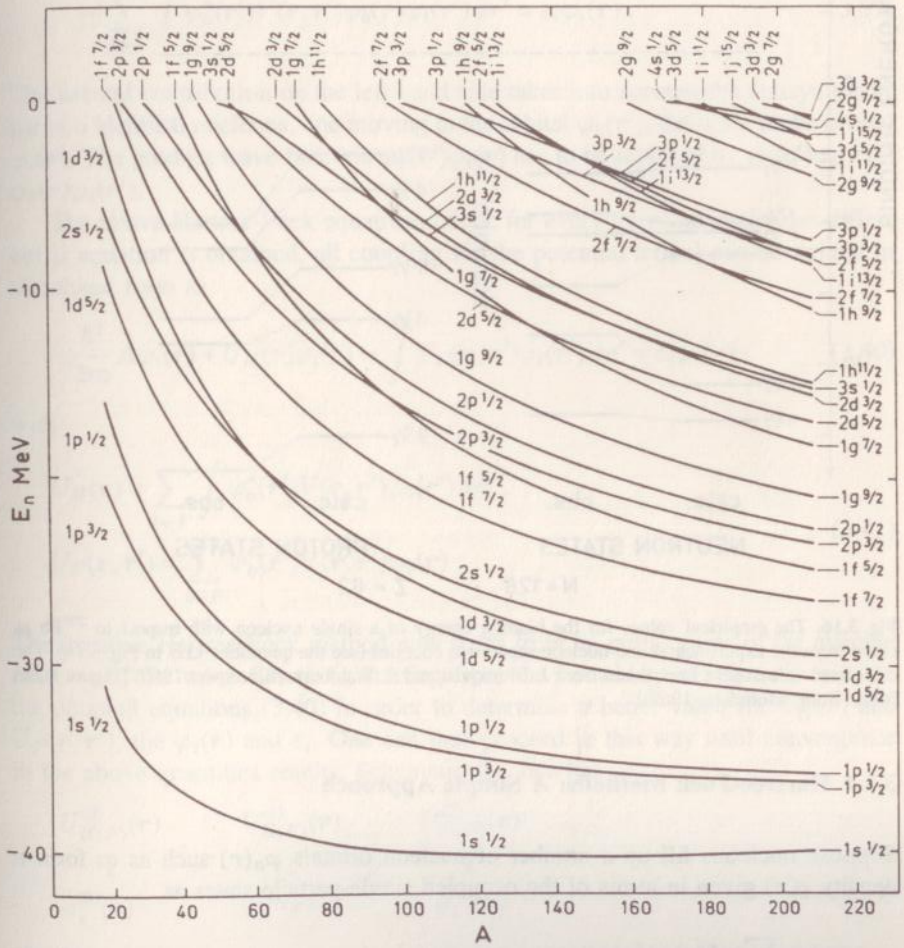


**Fig. 3.15.** Energies of neutron orbitals, calculated by C.J. Veje as quoted in (Bohr 1969). Use has been made of a Woods-Saxon potential $U = Vf(r) + V_{ls}(\vec{l} \cdot \vec{s})r_0^2(1/r)(d/dr)f(r)$, with $f(r)$ having a Woods-Saxon shape $[1 + \exp(r - R_0/a)]^{-1}$, and $R_0 = r_0 A^{1/3}$ ($r_0 = 1.27\ fm$) and $a = 0.67\ fm$. The potentials $V$ and $V_{ls}$ are given as $V = (-51 + 33((N - Z)/A))$ MeV, $V_{ls} = -0.44$ V, [taken from (Bohr, Mottelson 1969)]

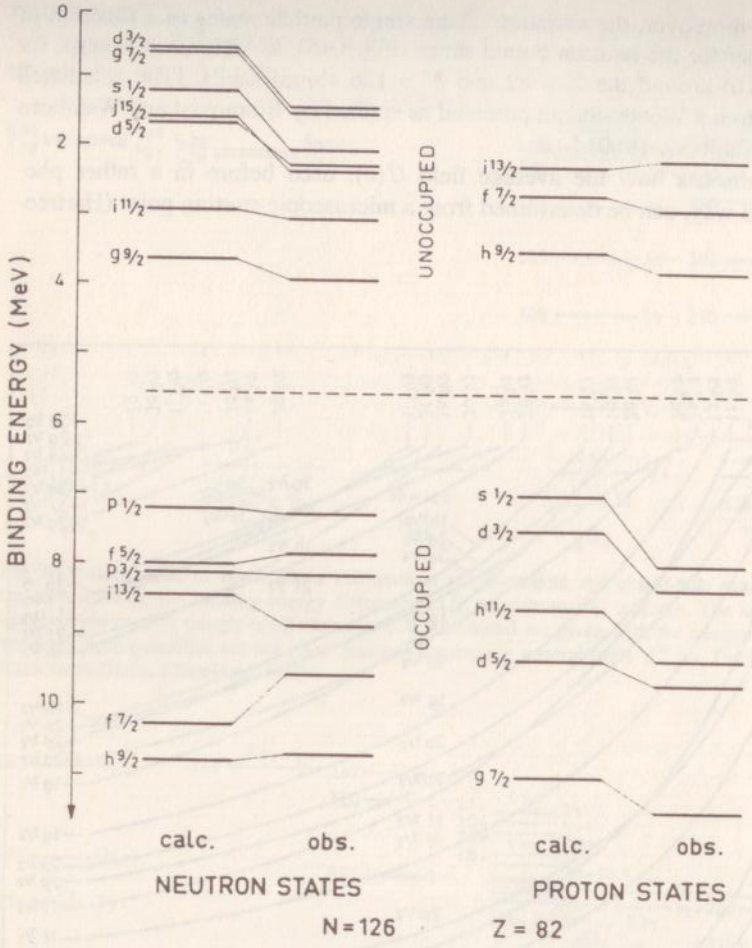


**Fig. 3.16.** The empirical values for the binding energy of a single nucleon with respect to $^{208}$Pb as taken from the experimental one-nucleon separation energies (see the quantities $\Delta B$ in Fig. 3.14). The calculated values have been taken from J. Blomqvist and S. Wahlborn (Blomqvist 1960) [Figure taken from (Bohr, Mottelson 1969)]

### 3.1.4 Hartree-Fock Methods: A Simple Approach

Suppose nucleons fill up a number of nucleon orbitals $\varphi_a(\boldsymbol{r})$ such as to form a density $\varrho(\boldsymbol{r})$ given in terms of the occupied single-particle states as

$$\varrho(\boldsymbol{r}) = \sum_{b \in F} \varphi_b^*(\boldsymbol{r}) \varphi_b(\boldsymbol{r}) \,. \tag{3.37}$$

Then the potential at a point $\boldsymbol{r}'$, generated because of the nucleon-nucleon two-body interaction $V(\boldsymbol{r}, \boldsymbol{r}')$ reads

$$U_H(r') = \sum_{b\in F} \int \varphi_b^*(r) V(r,r') \varphi_b(r)\, dr \,. \tag{3.38}$$

We denote by $U_H(r')$, the Hartree term neglecting exchange effects, and this term is used in the case of atoms. Within the atomic nucleus, $U_H(r')$ is the direct term of the potential affecting the nucleon motion in the nucleus. The more correct, single-particle Schrödinger equation for the orbital $\varphi_i(r)$ now becomes

$$\begin{aligned} &-\frac{\hbar^2}{2m}\Delta\varphi_i(r) + \sum_{b\in F} \int \varphi_b^*(r') V(r,r') \varphi_b(r') dr' \cdot \varphi_i(r) \\ &- \sum_{b\in F} \int \varphi_b^*(r') V(r,r') \varphi_b(r) \varphi_i(r')\, dr' = \varepsilon_i \varphi_i(r) \,. \end{aligned} \tag{3.39}$$

The second contribution on the left hand side takes into account the antisymmetry for two identical nucleons, one moving in the orbital $\varphi_b(r')$, the other in the orbital $\varphi_i(r)$. The product wave function $\varphi_b(r')\varphi_i(r)$ has to be replaced by $\varphi_b(r')\varphi_i(r) - \varphi_b(r)\varphi_i(r')$.

The above Hartree-Fock equations [since for every $\varphi_i(r)$ an analogous differential equation is obtained, all coupling via the potential terms] can be written in shorthand form as

$$-\frac{\hbar^2}{2m}\Delta\varphi_i(r) + U_H(r)\varphi_i(r) - \int U_F(r,r')\varphi_i(r')\, dr' = \varepsilon_i \varphi_i(r) \,, \tag{3.40}$$

with

$$\begin{aligned} U_H(r) &= \sum_{b\in F} \int \varphi_b^*(r') V(r,r') \varphi_b(r')\, dr' \,, \\ U_F(r,r') &= \sum_{b\in F} \varphi_b^*(r') V(r,r') \varphi_b(r) \,. \end{aligned} \tag{3.41}$$

The iterative Hartree-Fock method now starts from an initial guess of the average field, or of the wave functions, starting from the knowledge of $V(r,r')$ to solve the coupled equations (3.40) in order to determine a better value for $U_H(r)$ and $U_F(r,r')$, the $\varphi_i(r)$ and $\varepsilon_i$. One can thus proceed in this way until convergence in the above quantities results. Schematically, one has

$$\begin{array}{ccccccc} U_{H(F)}^{(0)}(r) & & U_{H(F)}^{(1)}(r) & & U_{H(F)}^{(2)}(r) & \cdots \\ \downarrow & \nearrow & \downarrow & \nearrow & \downarrow & \nearrow \\ \varphi_i^{(0)}(r) & & \varphi_i^{(1)}(r) & & \varphi_i^{(2)}(r) & \\ \varepsilon_i^{(0)} & & \varepsilon_i^{(1)} & & \varepsilon_i^{(2)} & . \end{array} \tag{3.42}$$

At the end, a final field $U_H(r)$, wave function $\varphi_i(r)$, single-particle energy $\varepsilon_i$ is obtained. It is now possible to prove that with the wave functions so obtained, by calculating the energy expectation value

$$E_{HF} = \langle \Psi_{a_1,a_2,\ldots,a_A}(\boldsymbol{r}_1, \ldots, \boldsymbol{r}_A) | H | \Psi_{a_1,a_2,\ldots,a_A}(\boldsymbol{r}_1, \ldots, \boldsymbol{r}_A) \rangle \,, \tag{3.43}$$

with the $\Psi_{a_1,a_2,\ldots,a_A}(\boldsymbol{r}_1, \ldots, \boldsymbol{r}_A)$ defined in (3.5), the minimal value is obtained.

In the present discussion, one assumes that the original one and two-body Hamiltonian (3.9) does *not* contain strong short-range correlations nor density dependent two-body interactions. In those cases, the variational aspect of Hartree-Fock theory becomes lost (Ring, Schuck 1980, de-Shalit, Feshbach 1974). Detailed discussions on the determination of the Hartree-Fock energy and on variational approaches to the energy of an interacting many-body system can be found in (Ring, Schuck 1980, Irvine 1972). Since it is not our aim to devote an extensive treatment to those aspects of the nuclear $A$-body system, we refer the reader to the above references. The situation with two-body density dependent interactions will be discussed in some detail in Chap. 8.

There now exist many alternative methods in addition to the Hartree-Fock Schrödinger equations to derive this condition. We do not go into detail about these aspects. We only mention that an often used method to determine the "best" wave functions $\varphi_i(\boldsymbol{r})$ is to expand in a harmonic oscillator basis

$$\varphi_i(\boldsymbol{r}) = \sum_k a_k^i \varphi_k^{\text{h.o.}}(\boldsymbol{r}) \,, \tag{3.44}$$

after which the coefficients $a_k^i$ are determined so that the total energy $E_{HF}$ (3.43) is minimized.

The Hartree-Fock wave functions (and potential) indeed give a firm basis to the independent particle shell-model approach for the study of nuclear excited states. Besides the determination of the single-particle energies that can be compared with the data and show good overall agreement throughout the nuclear mass table (see Fig. 3.16 for a comparison in $^{208}$Pb), nuclear densities [charge densities $\varrho^c(\boldsymbol{r})$] have also been determined and compared in detail. We do this for $^{16}$O–$^{208}$Pb (Fig. 3.17a) and compare in Fig. 3.17b their nuclear matter densities $\varrho^m(r)$ with that for the corresponding densities of nuclear matter. Calculations have been carried out using Skyrme type of effective interactions (see also Chap. 8) but other interactions give very similar results. Very recently, using the difference of charge densities as obtained via $(e, e')$ scattering experiments at Saclay for $^{206}$Pb-$^{205}$Tl, (Cavedon et al. 1982, Frois et al. 1983, Doe 1983)

$$\begin{aligned} \varrho(^{206}\text{Pb}) - \varrho(^{205}\text{Tl}) &= \sum_{b \in F} |\varphi_b(\boldsymbol{r})|^2 (^{206}\text{Pb}) - \sum_{b \in F} |\varphi_b(\boldsymbol{r})|^2 (^{205}\text{Tl}) \\ &= |\varphi_{3s^2_{1/2}}(\boldsymbol{r})|^2 \,, \end{aligned} \tag{3.45}$$

the shape of the $3s_{1/2}$ orbit could unambiguously be determined (Fig. 3.18). This gives a sound basis for the independent motion of nucleons as a very good picture of the nuclear $A$-body problem. Thus this is a good point to study more detailed features related to the residual nucleon-nucleon interactions remaining outside the average field ($H_{\text{res}}$). We shall study the two-particle and three-particle systems

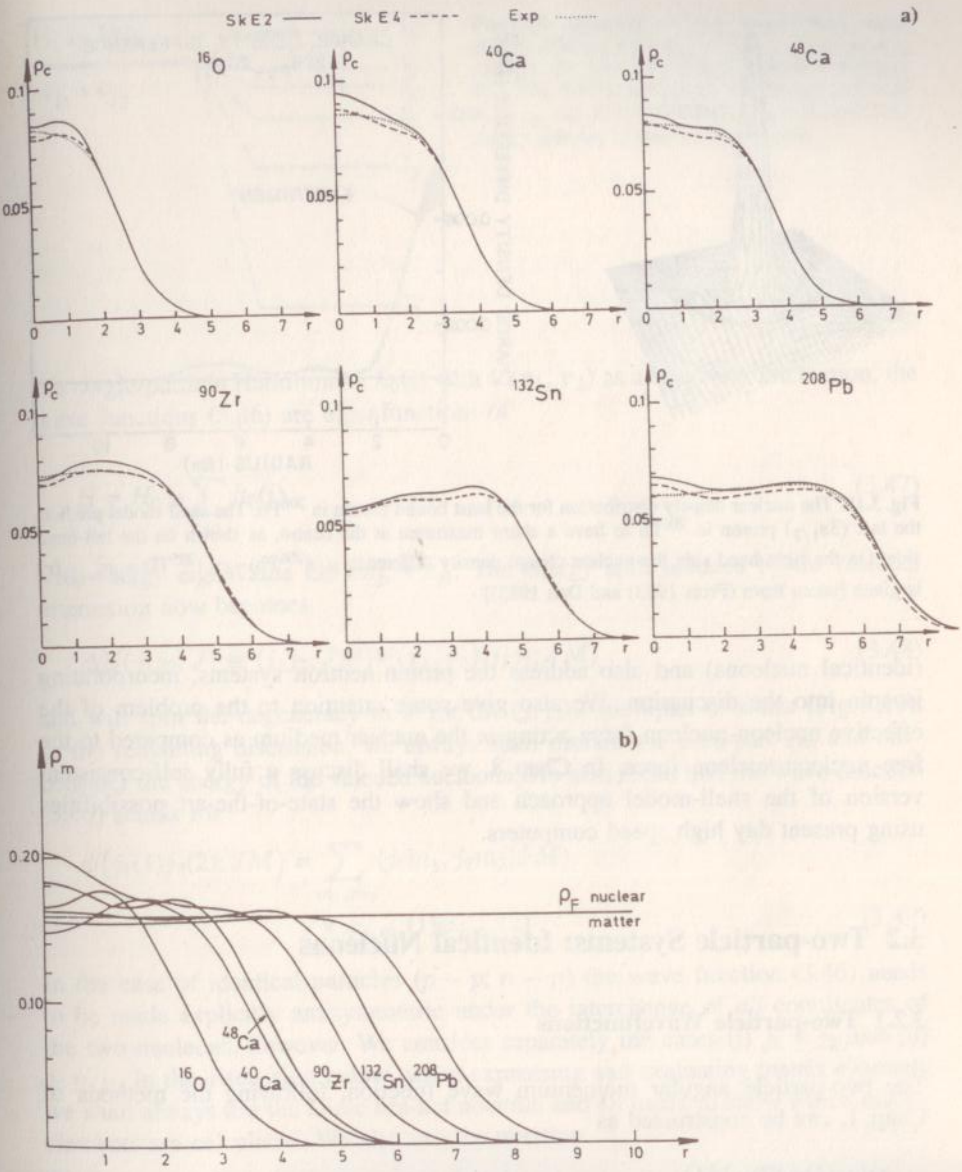


**Fig. 3.17.** (a) Charge densities for the magic nuclei $^{16}$O, $^{40}$Ca, $^{48}$Ca, $^{90}$Zr, $^{132}$Sn and $^{208}$Pb. The theoretical curves correspond to the effective interactions SkE2 and SkE4, respectively (see Chap. 8 for a detailed discussion of the extended Skyrme forces) and are compared with the data. The units for $\varrho_c$ are efm$^{-3}$, with the radius $r$ in fm. (b) Combined nuclear matter densities $\varrho_m$ (fm$^{-3}$) for the above set of doubly-closed shell nuclei. Nuclear matter density $\varrho_F$ (nuclear matter) is given as a "measure" for comparison

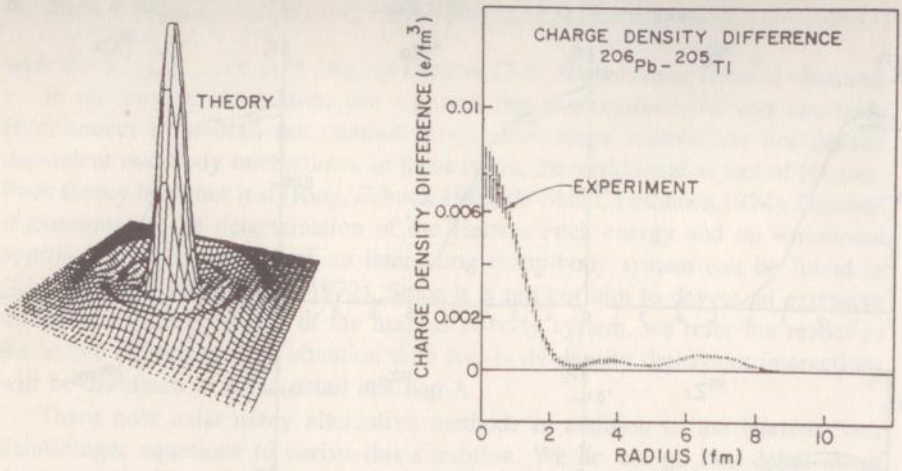


**Fig. 3.18.** The nuclear density distribution for the least bound proton in $^{206}$Pb. The shell-model predicts the last $(3s_{1/2})$ proton in $^{206}$Pb to have a sharp maximum at the centre, as shown on the left-hand side. On the right-hand side the nuclear charge density difference $\varrho_c\,(^{206}\mathrm{Pb}) - \varrho_c\,(^{205}\mathrm{Tl}) = \varphi^2_{3s_{1/2}}(r)$ is given [taken from (Frois 1983) and Doe 1983)]

(identical nucleons) and also address the proton-neutron systems, incorporating isospin into the discussion. We also give some attention to the problem of the effective nucleon-nucleon force acting *in* the nuclear medium as compared to the free nucleon-nucleon force. In Chap. 8, we shall discuss a fully self-consistent version of the shell-model approach and show the state-of-the-art possibilities using present day high speed computers.

## 3.2 Two-particle Systems: Identical Nucleons

### 3.2.1 Two-particle Wavefunctions

The two-particle angular momentum wave function, following the methods of Chap. 1, can be constructed as

$$\psi\big(j_1(1)j_2(2); JM\big)\,. \tag{3.46}$$

($\varphi$ will always be the notation for a single-particle wave function, $\psi$ and $\Psi$ for composite wave functions). In what follows we denote with $1 \equiv \boldsymbol{r}_1, \boldsymbol{\sigma}_1, \ldots$ all coordinates of particle 1, and $j_1$ is a notation for all quantum numbers necessary to specify the single-particle state in a unique way $j_1 \equiv n_1, l_1, j_1$.

In describing the full Hamiltonian for a nucleus formed by a closed shell system described by $H_0$ and two extra identical valence nucleons described by

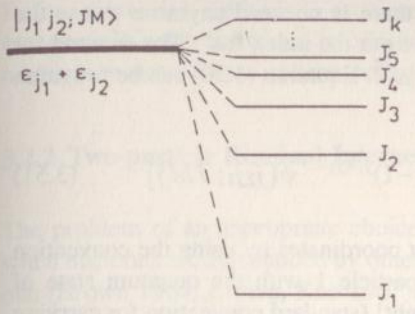


**Fig. 3.19.** Splitting of the two-particle states $\psi(j_1 j_2; JM)_{\text{nas}}$ with $|j_1 - j_2| \leq J \leq j_1 + j_2$ through the residual nucleon-nucleon interaction $V_{1,2}$. The unperturbed energy for the configurations, $\varepsilon_{j_1} + \varepsilon_{j_2}$ (all $J$) is given on the left-hand side. The energy splitting is drawn schematically

the single-particle Hamiltonian $h_0(i)$ with $V(\boldsymbol{r}_1, \boldsymbol{r}_2)$ as a two-body interaction, the wave functions (3.46) are eigenfunctions of

$$H = H_0 + \sum_{i=1}^{2} h_0(i) \,, \tag{3.47}$$

with energy eigenvalue $E_0 + \varepsilon_{j_1} + \varepsilon_{j_2}$. The energy shift induced by the residual interaction now becomes

$$\Delta E(j_1 j_2; J) \equiv \langle j_1 j_2; JM | V(\boldsymbol{r}_1, \boldsymbol{r}_2) | j_1 j_2; JM \rangle \,, \tag{3.48}$$

and will split the degeneracy in $J$ for the $(j_1 j_2)J$ multiplet of states (Fig. 3.19). In the remaining discussion, we always shall discard the core-part $H_0$ and only consider the energy of the valence nucleons. We also recall that the wave function (3.46) stands for

$$\psi(j_1(1) j_2(2); JM) = \sum_{m_1, m_2} \langle j_1 m_1, j_2 m_2 | JM \rangle \times \varphi_{j_1 m_1}(1) \varphi_{j_2 m_2}(2) \,. \tag{3.49}$$

In the case of identical particles ($p - p$; $n - n$) the wave function (3.46) needs to be made explicitly antisymmetric under the interchange of *all* coordinates of the two nucleons, however. We consider separately the cases (i) $j_1 \neq j_2$ and (ii) $j_1 = j_2$. In the discussion below, when expressing and evaluating matrix elements we shall always use the Dirac bra-ket notation and an index to show which matrix elements are calculated. We also use the notation

as : antisymmetrized wave function,
nas : normalized, antisymmetrized wave function,
no index : non-antisymmetrized wave function.

i) $j_1 \neq j_2$. We construct

$$\psi_{\text{as}}(j_1 j_2; JM) = N \sum_{m_1, m_2} \langle j_1 m_1, j_2 m_2 | JM \rangle \times \left[ \varphi_{j_1 m_1}(1) \varphi_{j_2 m_2}(2) - \varphi_{j_1 m_1}(2) \varphi_{j_2 m_2}(1) \right] \,. \tag{3.50}$$

Because of the explicit antisymmetrization, there is no need anymore to use the coordinates in the wave function on which we put the index "as". The demand for a normalized wave function results in $N = 1/\sqrt{2}$. Equation (3.50) can be rewritten as

$$\psi_{\text{nas}}(j_1 j_2; JM) = \frac{1}{\sqrt{2}} \left[\psi(j_1 j_2; JM) - (-1)^{j_1+j_2-J} \psi(j_2 j_1; JM)\right] . \tag{3.51}$$

On the right hand side, we can also leave out coordinates by using the convention of always coupling the quantum state for particle 1 with the quantum state of particle 2 in *that* order reading from left to right! (standard convention for carrying out Racah-Algebra within the nuclear shell-model) (de-Shalit, Talmi 1963).

ii) $j_1 = j_2$. We now construct, as above,

$$\begin{aligned}
\psi_{\text{nas}}(j^2; JM) &= N' \sum_{m_1,m_2} \langle jm_1, jm_2|JM\rangle \\
&\times \left[\varphi_{jm_1}(1)\varphi_{jm_2}(2) - \varphi_{jm_2}(1)\varphi_{jm_1}(2)\right] \\
&= N' \sum_{m_1,m_2} \left[\langle jm_1, jm_2|JM\rangle - \langle jm_2, jm_1|JM\rangle\right]\varphi_{jm_1}(1)\varphi_{jm_2}(2) \\
&= N'\left(1 - (-1)^{2j-J}\right) \sum_{m_1,m_2} \langle jm_1, jm_2|JM\rangle \varphi_{jm_1}(1)\varphi_{jm_2}(2) .
\end{aligned} \tag{3.52}$$

Thus, only even $J$ values are obtained ($J = 0, 2, \ldots, 2j-1$) and $N' = \frac{1}{2}$.

As an example, we give the possible states for

- the $1d_{5/2}\ 1d_{3/2}$ two-particle states

$$\psi_{\text{as}}(1d_{5/2}\, 1d_{3/2}; JM) \qquad J = 1, 2, 3, 4 ,$$

- the $1d_{5/2}\ 1d_{5/2}$ two-particle states

$$\psi_{\text{as}}((1d_{5/2})^2; JM) \qquad J = 0, 2, 4 .$$

The two-body matrix elements including the residual interaction can be written as ($j_1 \neq j_2$)

$$\begin{aligned}
\Delta E(j_1 j_2, J) &\equiv \langle j_1 j_2; JM|V_{12}|j_1 j_2; JM\rangle_{\text{nas}} \\
&= \langle j_1 j_2; JM|V_{12}|j_1 j_2; JM\rangle \\
&\quad - (-1)^{j_1+j_2-J} \langle j_1 j_2; JM|V_{12}|j_2 j_1; JM\rangle ,
\end{aligned} \tag{3.53}$$

by assuming $V_{12} = V_{21}$ [where $V_{12} \equiv V(\boldsymbol{r}_1, \boldsymbol{r}_2)$] and if $j_1 = j_2$, one gets

$$\Delta E(j^2, J) \equiv \langle j^2; JM|V_{12}|j^2; JM\rangle . \tag{3.54}$$

Before discussing methods to evaluate the matrix elements (3.53, 54) by using the two-particle wave functions as constructed above, we first discuss in some detail methods to get a better understanding of the effective interaction $V(\boldsymbol{r}_1, \boldsymbol{r}_2)$ itself.

### 3.2.2 Two-particle Residual Interaction

The problem of an appropriate choice for the two-nucleon interaction, especially when nucleons are surrounded by other nucleons (the nuclear medium) is a difficult one (Brown 1964, Brown, Kuo 1967). It does not have a unique answer since the "effective" force will be dependent on the particular model space that one considers in handling low-lying excited states. Still, a number of avenues have been followed in the past and we will discuss some of the more effective ones.

#### a) Effective Two-Body Matrix Elements

Within this approach, no attempt is made to pin down the (radial) shape of the interaction itself. Rather, the two-body matrix elements, together with the single-particle energies, are taken as "free" parameters for use in the Schrödinger equation to describe the nuclear excited states (Brussaard, Glaudemans 1977). Thus as parameters for a given model space one has

$$\varepsilon_{j_i} , \qquad \langle j_1 j_2; JM | V_{12} | j_3 j_4; JM \rangle .$$

If one takes as an example the full *sd* space (in order to discuss nuclei between $^{16}$O and $^{40}$Ca), the parameters are the two relative energies $\varepsilon_{2s_{1/2}} - \varepsilon_{1d_{5/2}}, \varepsilon_{2s_{1/2}} - \varepsilon_{1d_{3/2}}$ and the 63 two-body interaction matrix elements using as two-particle configurations all two particle states $|j_1 j_2; JM\rangle$ with $j_1, j_2 \in (2s_{1/2}, 1d_{3/2}, 1d_{5/2})$. Since in the Schrödinger equation for a given nucleus $A(Z, N)$ with $n$ valence nucleons (protons and neutrons) $0 \leq n \leq 24$, the eigenvalues $E_{J_i^\pi}$ are functions of the essential parameters given above,

$$H\Psi_{J_i^\pi}(n) = E_{J_i^\pi}\Psi_{J_i^\pi}(n) , \tag{3.55}$$

one can use iterative least-squares methods to get convergence to a final set of two-body matrix elements and relative single-particle energies (Fig. 3.20). This method has been in use for a long time, and with the advent of high-speed computers has been applied to a large variety of nuclei. In particular the Utrecht group (Brussaard, Glaudemans 1977) and Wildenthal-Brown (Wildenthal 1976, 1985) have studied *p* shell nuclei and, more recently, the full *sd* shell using a single set of two-body matrix elements. We illustrate this by some examples for $^{27}$Al, $^{28}$Si, $^{29}$Si in the middle of the *sd* shell for the excited states and for the full *sd* shell including binding energies (two-neutron separation energies (Figs. 3.21, 22).

Eventually, of course, one should try to compare and understand the fitted values with two-body matrix elements determined by other methods.

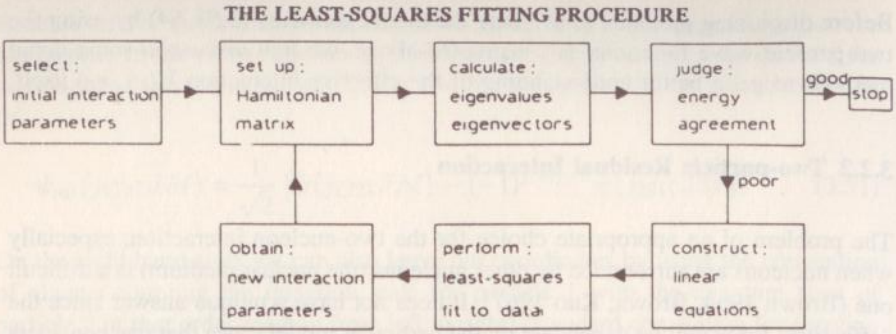


**Fig. 3.20.** Illustration of the various steps necessary in order to deduce an effective interaction (the two-body matrix elements $\langle j_1 j_2; J|V_{1,2}|j_3 j_4; J\rangle$ and single-particle energies $\varepsilon_{j_i}$) along the method discussed in Sect. 3.2.2a. Thereby a fit to experimental excitation energies and/or electromagnetic properties can be imposed [taken from (Brussaard 1977)]

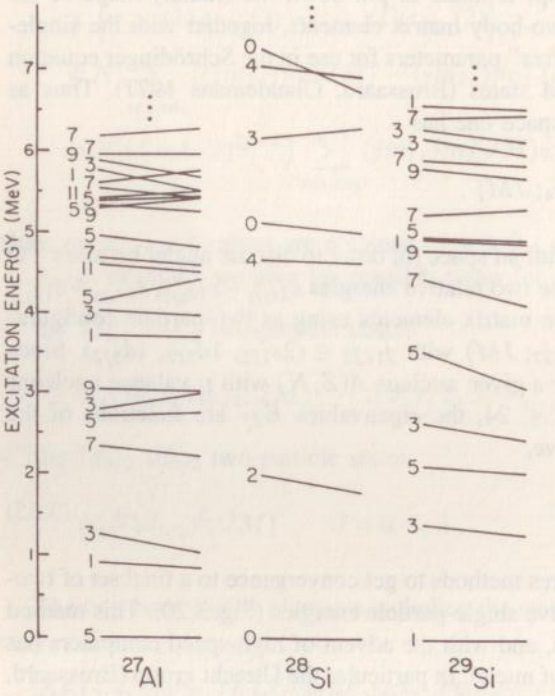


**Fig. 3.21.** Excited states for $^{27}$Al, $^{28}$Si and $^{29}$Si. The ground-state energies are set equal in the figure. The left-hand ending of each line contains the calculated number, the right-hand point the corresponding experimental number. In odd-mass nuclei, the level is characterized by the value $2J$. Known negative parity states have been left out from the data. All other data are given (up to the upper energy considered here) [taken from (Wildenthal 1985)]

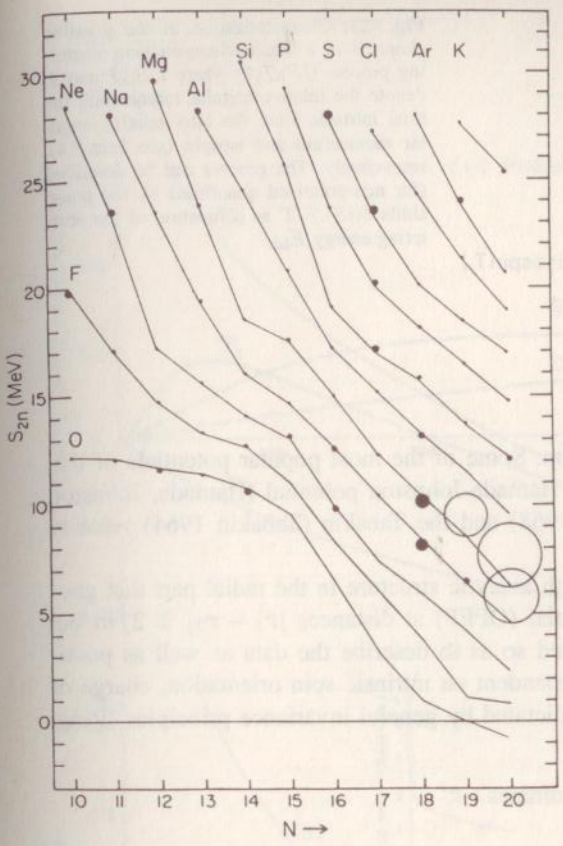


**Fig. 3.22.** Calculated and measured two-neutron separation energies $S_{2n}$ along sd-isotope chains. The lines connect the theoretical points. The data are indicated by dot, solid or open circles. The diameters and their placement relative to the lines indicate the *magnitude and directions* of the differences $S_{2n}$(th) − $S_{2n}$(exp) [taken from (Wildenthal 1985)]

### b) Realistic Interactions

In a completely different method, one tries to start from the free nucleon-nucleon interaction and to incorporate the necessary modifications to obtain the appropriate nuclear two-body interaction matrix elements. Pioneering work in this direction has been carried out by Brown and Kuo (Brown, Kuo 1967, Kuo, Brown 1966, Kuo et al. 1966).

Here we shall outline briefly how such "realistic" forces are determined, forces that are obtained by fitting to the free nucleon-nucleon scattering observables [phase shifts in all possible reaction channels $\delta(lS)\mathcal{J}$ ($E_{\text{lab}}$), polarization data, ...]. We illustrate in Fig. 3.23 those basic data in the $pp$, $nn$, $pn$ case (isospin $T = 1$ and $T = 0$ channels) for channels denoted by $^{2S+1}(l)\mathcal{J}$ quantum numbers ($l$: relative orbital angular momentum, $S$: relative intrinsic spin, $\mathcal{J}$: total relative angular momentum) (see also Fig. 3.24).

In general one describes processes up to $E_{\text{lab}} \lambda 350$ MeV. Thus the most important partial waves are $l = 0, 1, 2$ $S$, $P$ and $D$-waves (MacGregor et al. 1968a, b, Wright et al. 1967). At higher energies the concept of a non-relativistic scalar

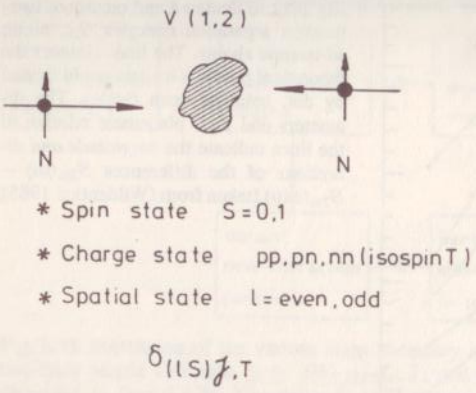


**Fig. 3.23.** Characterization of the possible channels in a free nucleon-nucleon scattering process $(lS)\mathcal{J},T$ where $l, S, \mathcal{J}$ and $T$ denote the relative angular momentum, the total intrinsic spin, the total relative angular momentum and isospin (see Sect. 3.4), respectively. The process can be described (for non-polarized quantities) by the phase shifts $\delta(lS)\mathcal{J},T$ as a function of the scattering energy $E_{\text{lab}}$

potential loses its precise definition. Some of the most popular potentials of this "realistic" type are the hard-core Hamada-Johnston potential (Hamada, Johnston 1962), the Reid soft-core (Reid 1968) and the Tabakin (Tabakin 1964) velocity dependent potentials.

One starts from a potential with analytic structure in the radial part that goes into the one-pion exchange potential (OPEP) at distances $|\boldsymbol{r}_1 - \boldsymbol{r}_2| \cong 2fm$ but with strengths that have to be fitted so as to describe the data as well as possible. These general shapes, also dependent on intrinsic spin orientation, charge of the interacting particles, etc., are dictated by general invariance principles (Ring, Schuck 1980):

i) under exchange of the coordinates,
ii) translation
iii) Galilean
iv) space reflection
v) time reversal
vi) rotational, in coordinate space
vii) rotational, in charge space.

Thus for local forces not depending on the velocity, the central force is the most important part:

$$V_C(1,2) = V_0(r) + V_\sigma(r)\boldsymbol{\sigma}_1 \cdot \boldsymbol{\sigma}_2 + V_\tau(r)\boldsymbol{\tau}_1 \cdot \boldsymbol{\tau}_2 + V_{\sigma\tau}(r)\boldsymbol{\sigma}_1 \cdot \boldsymbol{\sigma}_2\boldsymbol{\tau}_1 \cdot \boldsymbol{\tau}_2 \,. \tag{3.56}$$

(We shall discuss isospin where the $\tau$ operators occur in detail in Sect. 3.4.)

The remaining local part is of tensor character and given by

$$V_T(1,2) = \left[V_{T_0}(r) + V_{T_\tau}(r)\boldsymbol{\tau}_1 \cdot \boldsymbol{\tau}_2\right] S_{12}$$

with

$$S_{12} = \frac{3}{r^2}(\boldsymbol{\sigma}_1 \cdot \boldsymbol{r})(\boldsymbol{\sigma}_2 \cdot \boldsymbol{r}) - \boldsymbol{\sigma}_1 \cdot \boldsymbol{\sigma}_2 \,. \tag{3.57}$$

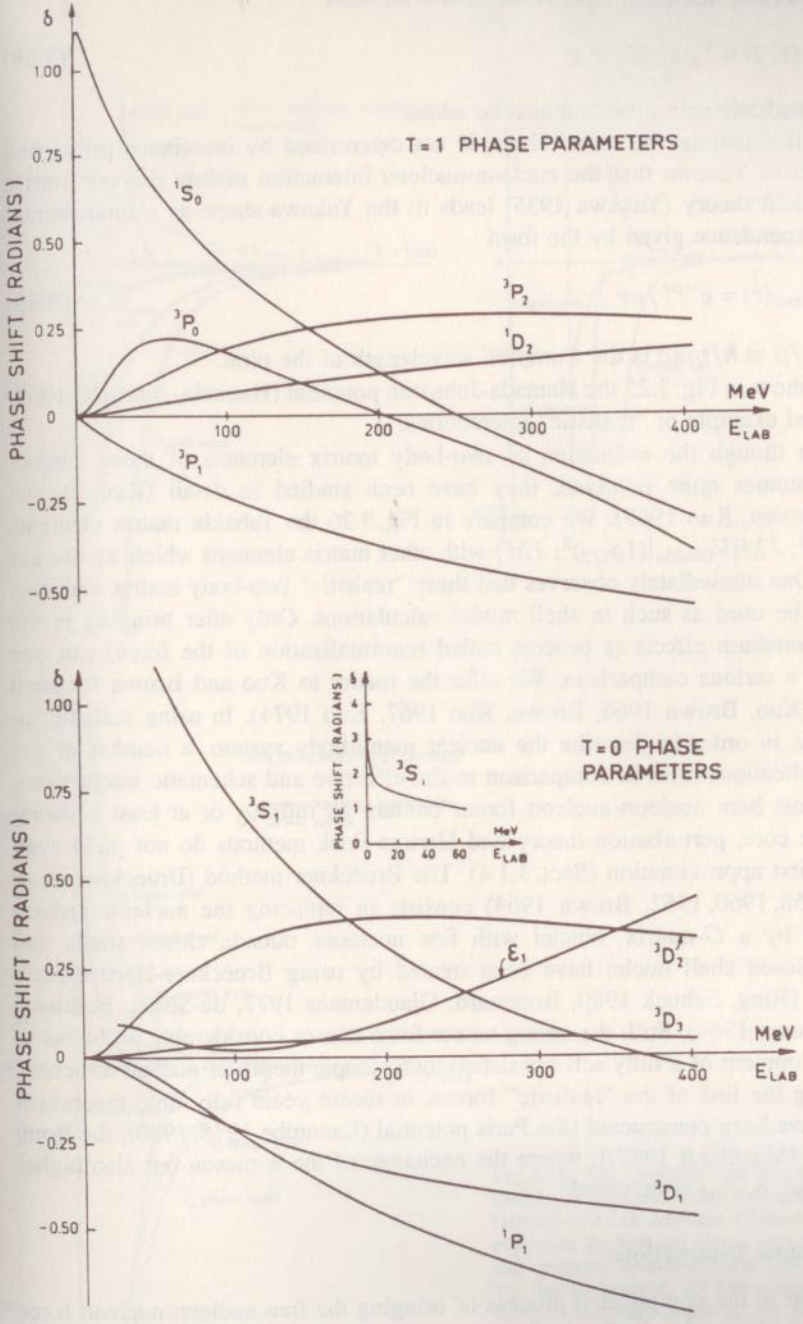


**Fig. 3.24.** The nuclear phase parameters for both the $T = 1$ and $T = 0$ channels and this for $S$, $P$ and $D$ channels, up to a laboratory energy of $E_{\text{lab}} = 400$ MeV. The low-energy behavior (insert) is determined by the effective-range parameters, the data for $E > 24$ have been taken from (Arndt 1966). Phase shifts are given in radians [taken from (Bohr, Mottelson 1969)]

The important non-local term is the spin-orbit term

$$V_{LS}(1,2) = V_{LS}(r)\boldsymbol{l}\cdot\boldsymbol{S}\,, \tag{3.58}$$

and a quadratic spin-orbit can also be added.

In all situations the radial shape is not determined by invariance principles. The idea of Yukawa that the nucleon-nucleon interaction mainly derives from a meson field theory (Yukawa 1935) leads to the Yukawa-shape as a fundamental radial dependence given by the form

$$V_{\text{Yukawa}}(r) = \mathrm{e}^{-\mu r}/\mu r\,, \tag{3.59}$$

where $1/\mu \equiv \hbar/m\pi c$ is the Compton wavelength of the pion.

We show in Fig. 3.25 the Hamada-Johnston potential (Hamada, Johnston 1962) as a good example of "realistic" interactions.

Even though the evaluation of two-body matrix elements of these interactions becomes quite involved, they have been studied in detail (Kuo, Brown 1966, Brown, Kuo 1967). We compare in Fig. 3.26 the Tabakin matrix elements $\langle(1g_{7/2})^2; JM|V_{\text{Tabakin}}|(1g_{7/2})^2; JM\rangle$ with other matrix elements which we discuss below. One immediately observes that these "realistic" two-body matrix elements can not be used as such in shell model calculations. Only after bringing in the nuclear medium effects (a process called renormalization of the force) can one perform a serious comparison. We refer the reader to Kuo and Brown for such studies (Kuo, Brown 1966, Brown, Kuo 1967, Kuo 1974). In using realistic interactions in order to describe the nuclear many-body system, a number of extra complications arise in comparison to the effective and schematic interactions. Since most bare nucleon-nucleon forces contain an infinite, or at least a strong repulsive core, perturbation theory and Hartree-Fock methods do not yield even a good first approximation (Sect. 3.1.4). The Brueckner method (Brueckner et al. 1955, 1958, 1960, 1962, Brown 1964) consists in replacing the nucleon-nucleon potential by a $G$-matrix. Nuclei with few nucleons outside closed shells and doubly-closed shell nuclei have been treated by using Brueckner-Hartree-Fock methods (Ring, Schuck 1980, Brussaard, Glaudemans 1977, de-Shalit, Feshbach 1974, Brown 1964). Still, the strong tensor force causes considerable problems in the development of a fully self-consistent microscopic theory of nuclear structure.

Along the line of the "realistic" forces, in recent years fully field-theoretical forces have been constructed [the Paris potential (Lacombe 1975, 1980), the Bonn potential (Machleidt 1987)], where the exchange of the $\pi$-meson but also higher mesons ($\omega$, $\varrho$, ...) is involved.

### c) Schematic Interactions

In contrast to the complicated process of bringing the free nucleon-nucleon force into the nucleus, simple forces have been used that are immediately useful in applications into a given mass region. One defines a simple radial shape leading to a numerically rather simple calculation and determines the strength(s) so that

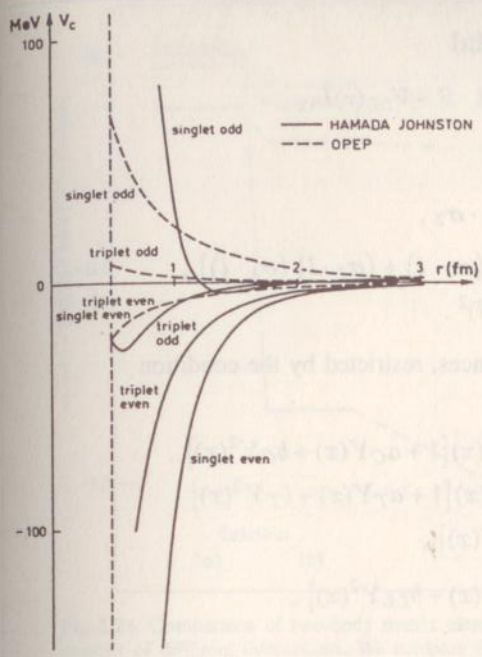


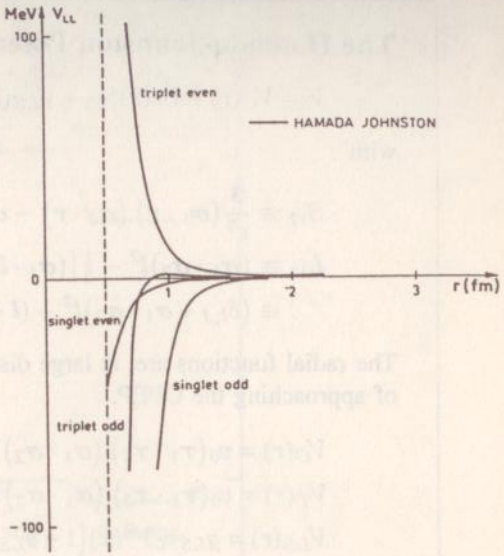


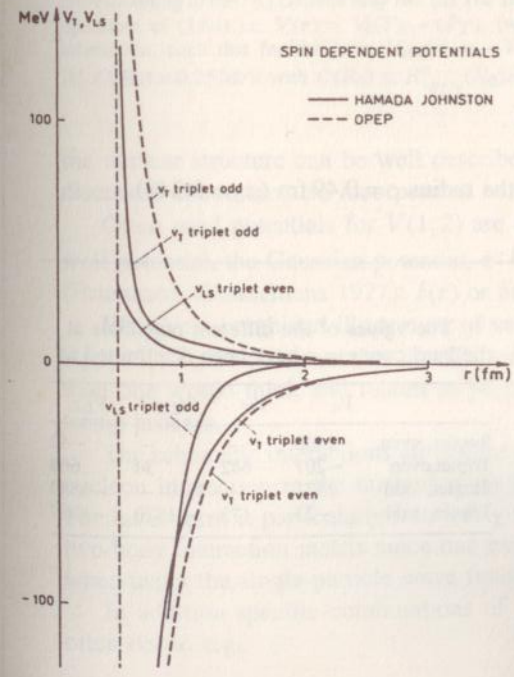


**Fig. 3.25.** The "realistic" nucleon-nucleon potentials as obtained from the analysis of T. Hamada and I.D. Johnston (Hamada 1962) are illustrated for both the central spin-orbit, tensor and quadratic spin-orbit parts [see (3.56–58)]. The dotted potentials (OPEP) correspond to the one-pion exchange potential. We give on p. 84 a box with the details of the Hamada-Johnston potential [taken from (Bohr, Mottelson 1969)]

## The Hamada-Johnston Potential

$$V = V_C(r) + V_T(r)S_{12} + V_{LS}(r)\boldsymbol{l}\cdot\boldsymbol{S} + V_{LL}(r)L_{12}\,,$$

with

$$S_{12} \equiv \frac{3}{r^2}(\boldsymbol{\sigma}_1\cdot\boldsymbol{r})\,(\boldsymbol{\sigma}_2\cdot\boldsymbol{r}) - \boldsymbol{\sigma}_1\cdot\boldsymbol{\sigma}_2\,,$$

$$L_{12} \equiv (\boldsymbol{\sigma}_1\cdot\boldsymbol{\sigma}_2)\boldsymbol{l}^2 - \tfrac{1}{2}\left[(\boldsymbol{\sigma}_1\cdot\boldsymbol{l})\,(\boldsymbol{\sigma}_2\cdot\boldsymbol{l}) + (\boldsymbol{\sigma}_2\cdot\boldsymbol{l})\,(\boldsymbol{\sigma}_1\cdot\boldsymbol{l})\right],$$

$$\equiv (\delta_{l,J} + \boldsymbol{\sigma}_1\cdot\boldsymbol{\sigma}_2)\boldsymbol{l}^2 - (\boldsymbol{l}\cdot\boldsymbol{S})^2\,.$$

The radial functions are, at large distances, restricted by the condition of approaching the OPEP.

$$V_C(r) = v_0(\boldsymbol{\tau}_1\cdot\boldsymbol{\tau}_2)\,(\boldsymbol{\sigma}_1\cdot\boldsymbol{\sigma}_2)Y(x)\left[1 + a_C Y(x) + b_C Y^2(x)\right],$$

$$V_T(r) = v_0(\boldsymbol{\tau}_1\cdot\boldsymbol{\tau}_2)\,(\boldsymbol{\sigma}_1\cdot\boldsymbol{\sigma}_2)Z(x)\left[1 + a_T Y(x) + b_T Y^2(x)\right],$$

$$V_{LS}(r) = g_{LS}v_0 Y^2(x)\left[1 + b_{LS}Y(x)\right],$$

$$V_{LL}(r) = g_{LL}v_0\frac{Z(x)}{x^2}\left[1 + a_{LL}Y(x) + b_{LL}Y^2(x)\right],$$

$$v_0 = \frac{1}{3}\frac{f^2}{\hbar c}m_\pi c^2 = 3.65\,\text{MeV}\,,$$

$$x = (m_\pi c)/\hbar\cdot r = r/1.43\,\text{fm}\,,$$

$$Y(x) = \frac{1}{x}\exp(-x)\,,$$

$$Z(x) = \left(1 + \frac{3}{x} + \frac{3}{x^2}\right)\cdot Y(x)\,.$$

In addition, an infinite repulsion at the radius $c = 0.49$ fm ($x_c = 0.343$), is assumed.

---

The optimum, adjusted parameters are given in the table.

| | Singlet even | Triplet even | Singlet odd | Triplet odd |
|---|---|---|---|---|
| $a_C$ | 8.7 | 6.0 | −8.0 | −9.07 |
| $b_C$ | 10.6 | −1.0 | 12.0 | 3.38 |
| $a_T$ | −. | −0.5 | −. | −1.29 |
| $b_T$ | −. | 0.2 | −. | 0.55 |
| $g_{LS}$ | −. | 2.77 | −. | 7.36 |
| $b_{LS}$ | −. | −0.1 | −. | −7.1 |
| $g_{LL}$ | −0.033 | 0.1 | −0.1 | −0.033 |
| $a_{LL}$ | 0.2 | 1.8 | 2.0 | −7.3 |
| $b_{LL}$ | −0.2 | −0.4 | 6.0 | 6.9 |

The values of the different potentials at the hard core $r = c$ have been determined as

| | $V_c$ | $V_T$ | $V_{LS}$ | $V_{LL}$ |
|---|---|---|---|---|
| Singlet, even | −1460 | – | – | −42 |
| Triplet,even | −207 | −642 | 34 | 668 |
| Singlet, odd | 2371 | – | – | −6683 |
| Triplet, odd | −23 | 173 | −1570 | −1087 |

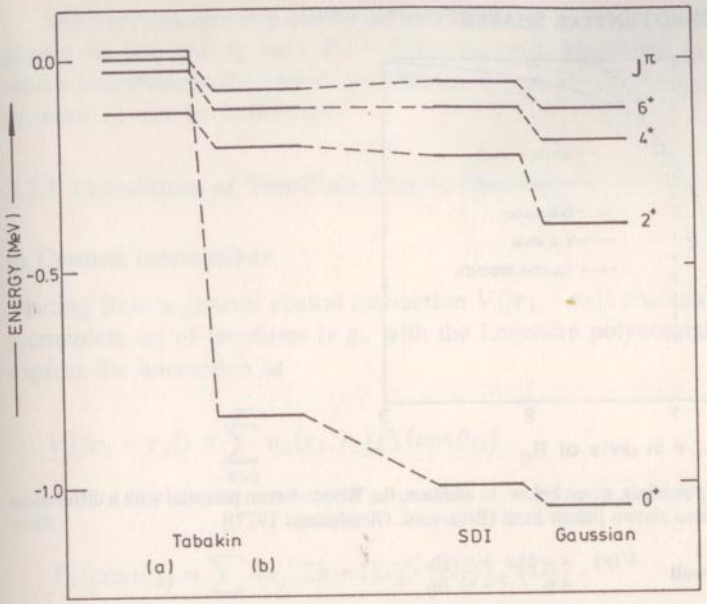


**Fig. 3.26.** Comparison of two-body matrix elements for the $(1g_{7/2})^2 J$ configuration according to a number of different interactions. We compare the surface-delta interaction (SDI) (see Appendix D), the Gaussian interaction and the realistic, velocity-dependent Tabakin interaction (Tabakin 1964). (i) For the Tabakin force, we give the total, bare matrix elements ($a$) and the Tabakin matrix elements corresponding to the $^1S_0$ channel only ($b$). (ii) The Gaussian interaction of Fig. 3.27, with the projection operators of (3.64) i.e. $V(r) = V_0(P_S + tP_T)$, (with $V_0 = -35$ MeV and $t = +0.2$). (iii) A SDI interaction, such that for the force $V_{\mathrm{SDI}}(r) = -4\pi A'_T \delta(\boldsymbol{r}_1 - \boldsymbol{r}_2)\delta(r_1 - R_0)$, the product $A_T = A'_T C(R_0) = 0.25$ MeV with $C(R_0) \equiv R^4_{1g_{7/2}}(R_0)R_0^2$

the nuclear structure can be well described. Eventually, the invariance principles discussed above are also incorporated to suit certain specific purposes.

Often used potentials for $V(1,2)$ are the Yukawa potential, $\mathrm{e}^{-\mu r}/\mu r$, square-well potential, the Gaussian potential, $\mathrm{e}^{-\mu r^2}$ and $\delta$ or surface-$\delta$ (SDI) interactions (Brussaard, Glaudemans 1977): $\delta(r)$ or $\delta(r)\delta(r_1 - R_0)$.

We give a combined illustration of various potentials in Fig. 3.27. In the brief Appendix D, we point out that the SDI interaction is actually much better founded than one would think and relates to properties of the nucleon-nucleon free scattering process.

The schematic interactions all illustrate the short-range aspects of the nucleon-nucleon interaction in the nucleus, with the $\delta$-function form as an extreme case. The latter form is particularly interesting to study the main features of the nuclear two-body interaction matrix since one can work out most results in analytic form when using the single-particle wave functions constructed in Sect. 3.1.

In addition specific combinations of the intrinsic spin and charge properties often occur, e.g.,

$$P_\sigma \equiv \tfrac{1}{2}\left(1 + \boldsymbol{\sigma}_1 \cdot \boldsymbol{\sigma}_2\right) . \tag{3.60}$$

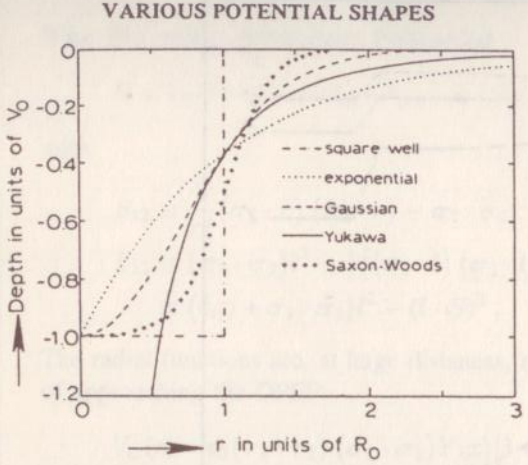


**Fig. 3.27.** Plots of the potentials, given below. In addition, the Woods-Saxon potential with a diffuseness parameter $a = 0.7$ is also shown [taken from (Brussaard, Glaudemans 1977)]

$$\text{Square well} \quad V(r) = \begin{cases} -V_0 & r \le R_0 \,, \\ 0 & r > R_0 \,, \end{cases}$$

$$\text{Exponential potential} \quad V(r) = -V_0 \exp(-r/R_0) \,,$$

$$\text{Gaussian potential} \quad V(r) = -V_0 \exp(-r^2/R_0^2) \,,$$

$$\text{Yukawa potential} \quad V(r) = -V_0 \exp(-r/R_0)/(r/R_0) \,.$$

This form is called the Bartlett term and is interesting for the following reason. If we add the intrinsic spins of the interacting nucleons

$$S = s_1 + s_2 \,, \tag{3.61}$$

we have

$$\sigma_1 \cdot \sigma_2 = 2\left[S^2 - s_1^2 - s_2^2\right] \,, \tag{3.62}$$

or for expectation value for an $S = 0$ or $S = 1$ state

$$\langle \sigma_1 \cdot \sigma_2 \rangle_S = 2S(S+1) - 3 \,. \tag{3.63}$$

Thus, the operator $P_\sigma$ is an exchange operator since

$$P_\sigma \psi_{S=1} = \psi_{S=1} \,,$$
$$P_\sigma \psi_{S=0} = -\psi_{S=0} \,,$$

and the two spin coordinates appear in a symmetric way in the $S = 1$ (parallel) state and in an antisymmetric way in the $S = 0$ (antiparallel) state. From the $P_\sigma$'s, projection operators for the $S = 1$ (triplet) and $S = 0$ (singlet) two-nucleon state can be defined:

$$\begin{aligned} P_S &\equiv \Pi_{S=0} = \tfrac{1}{2}\left(1 - P_\sigma\right) \,, \\ P_T &\equiv \Pi_{S=1} = \tfrac{1}{2}\left(1 + P_\sigma\right) \,. \end{aligned} \tag{3.64}$$

Similarly, an operator can be defined in charge space for the isospin operators, giving the Heisenberg term $P_\tau = \frac{1}{2}(1 + \tau_1 \cdot \tau_2)$. Moreover, the Majorana term which interchanges the spatial coordinates $r_1 - r_2 \to -(r_1 - r_2)$, induced by the operator $P_r$ can be introduced.

### 3.2.3 Calculation of Two-Body Matrix Elements

#### a) Central Interactions

Starting from a general central interaction $V(|r_1 - r_2|)$ one can expand it within a complete set of functions (e.g., with the Legendre polynomials). Thus, we can express the interaction as

$$V(|r_1 - r_2|) = \sum_{k=0}^{\infty} v_k(r_1, r_2) P_k(\cos\theta_{12}) \,, \tag{3.65}$$

with

$$P_k(\cos\theta_{12}) = \sum_{\kappa} 4\pi/(2k+1) Y_k^{\kappa^*}(\Omega_1) Y_k^{\kappa}(\Omega_2) \,. \tag{3.66}$$

From the normalized, antisymmetric two-particle wave functions constructed in Sect. 3.2.1, we obtain for the diagonal matrix element

$$\begin{aligned}\langle j_1 j_2; JM|V_{12}|j_1 j_2; JM\rangle_{\text{nas}} &= \langle j_1 j_2; JM|V_{12}|j_1 j_2; JM\rangle_{\text{dir}} \\ &- (-1)^{j_1+j_2-J}\langle j_1 j_2; JM|V_{12}|j_2 j_1; JM\rangle_{\text{exch}} \,,\end{aligned} \tag{3.67}$$

with a direct and an exchange term. We carry out the calculation in some detail, for both the direct and the exchange term:

The direct term can be written

$$\langle j_1 j_2; JM|V_{12}|j_1 j_2; JM\rangle_{\text{dir}} = \sum_k f_k F^k \,, \tag{3.68}$$

with

$$f_k = 4\pi/(2k+1)\langle j_1 j_2; JM|\boldsymbol{Y}_k(\Omega_1) \cdot \boldsymbol{Y}_k(\Omega_2)|j_1 j_2; JM\rangle \,, \tag{3.69}$$

and

$$\begin{aligned}F^k &= F^k(n_1 l_1, n_2 l_2) \\ &= \int |u_{n_1 l_1}(r_1) u_{n_2 l_2}(r_2)|^2 v_k(r_1, r_2)\, dr_1\, dr_2 \,.\end{aligned} \tag{3.70}$$

The expression for $f_k$ can be evaluated using the reduction rule I from Chap. 2, and yields

$$\begin{aligned}f_k = &4\pi/(2k+1) \cdot (-1)^{j_2+j_1+J} \begin{Bmatrix} j_1 & j_2 & J \\ j_2 & j_1 & k \end{Bmatrix} \\ &\times \langle j_1 \| \boldsymbol{Y}_k \| j_1 \rangle \langle j_2 \| \boldsymbol{Y}_k \| j_2 \rangle \,.\end{aligned} \tag{3.71}$$

For the exchange matrix element we get, analogously

$$\langle j_1 j_2; JM|V_{12}|j_2 j_1; JM\rangle_{\text{exch}} = \sum_{k=0}^{\infty} g_k G^k \,, \tag{3.72}$$

with

$$g_k = 4\pi/(2k+1)\cdot(-1)^{1+J}\begin{Bmatrix} j_1 & j_2 & J \\ j_1 & j_2 & k \end{Bmatrix} \times \langle j_1\|\boldsymbol{Y}_k\|j_2\rangle\langle j_2\|\boldsymbol{Y}_k\|j_1\rangle \,, \tag{3.73}$$

and

$$G^k = G^k(n_1 l_1, n_2 l_2) \equiv \int u_{n_1 l_1}(r_1) u_{n_2 l_2}(r_2) u_{n_1 l_1}(r_2) \times u_{n_2 l_2}(r_1) v_k(r_1, r_2)\, dr_1\, dr_2 \,. \tag{3.74}$$

Thus the total matrix element becomes for

i) $j_1 \neq j_2$

$$\Delta E_{j_1 j_2, J} = \sum_k f_k F^k - (-1)^{j_1+j_2-J} \sum_k g_k G^k \,, \tag{3.75}$$

and

ii) $j_1 = j_2$

$$\Delta E_{j^2, J} = \sum_k f_k F^k \,. \tag{3.76}$$

For a general central interaction when the $v_k(r_1, r_2)$ are determined, in most cases one has to evaluate the Slater integrals $G^k$ and $F^k$ numerically. If one chooses a simpler schematic force like the $\delta(\boldsymbol{r}_1 - \boldsymbol{r}_2)$ or the SDI $\delta(\boldsymbol{r}_1 - \boldsymbol{r}_2)\delta(r_1 - R_0)$ force, the integrals simplify significantly.

In Appendix F, we bring together the necessary Racah algebra expressions needed to carry out the calculation of the $\langle j\|\boldsymbol{Y}_k\|j'\rangle$ reduced matrix elements as well as the sums in (3.75, 76). We derive in Appendix E the multipole expansion for a zero-range $\delta(\boldsymbol{r}_1 - \boldsymbol{r}_2)$ interaction.

The result is

$$\delta(\boldsymbol{r}_1 - \boldsymbol{r}_2) = \sum_k \delta(r_1 - r_2)/(r_1 r_2)\cdot(2k+1)/4\pi \cdot P_k(\cos\theta_{12}) \,, \tag{3.77}$$

and so we easily get the $v_k(r_1, r_2)$ coefficient as

$$v_k(r_1, r_2) = \delta(r_1 - r_2)/(r_1 r_2)(2k+1)/4\pi \,. \tag{3.78}$$

Thus, the above radial integrals $F^k$ and $G^k$ reduce to

$$F^k = \frac{2k+1}{4\pi}\int_0^\infty \frac{1}{r^2}\left[u_{n_1 l_1}(r)u_{n_2 l_2}(r)\right]^2 dr = (2k+1)F^0\,,$$
$$G^k = \frac{2k+1}{4\pi}\int_0^\infty \frac{1}{r^2}\left[u_{n_1 l_1}(r)u_{n_2 l_2}(r)\right]^2 dr = (2k+1)F^0\,. \tag{3.79}$$

Furthermore, we use the explicit expression for the reduced matrix element $\langle j\|\boldsymbol{Y}_k\|j\rangle$, which becomes (Appendix F) after using the reduction rule I of Chap. 2

$$\langle (1/2l)j\|\boldsymbol{Y}_k\|(1/2l')j'\rangle = (-1)^{j-1/2}\hat{j}\hat{j}'\hat{k}/\sqrt{4\pi} \times \begin{pmatrix} j & k & j' \\ -\frac{1}{2} & 0 & \frac{1}{2}\end{pmatrix}\frac{1}{2}\left(1+(-1)^{l+l'+k}\right). \tag{3.80}$$

Combining the above result with (3.71) we get the explicit form of the $f_k$ term

$$f_k = (-1)^{2(j_1+j_2)+J-1}(2j_1+1)(2j_2+1)\tfrac{1}{2}\left(1+(-1)^k\right) \times \begin{Bmatrix} j_1 & j_2 & J \\ j_2 & j_1 & k\end{Bmatrix}\begin{pmatrix} j_1 & k & j_1 \\ -\frac{1}{2} & 0 & \frac{1}{2}\end{pmatrix}\begin{pmatrix} j_2 & k & j_2 \\ -\frac{1}{2} & 0 & \frac{1}{2}\end{pmatrix}, \tag{3.81}$$

and the total direct contribution reads (3.79)

$$\sum_k f_k F^k = F^0(2j_1+1)(2j_2+1)\sum_k (-1)^{J-1}\frac{1}{2}\left(1+(-1)^k\right) \times (2k+1)\begin{Bmatrix} j_1 & j_2 & J \\ j_2 & j_1 & k\end{Bmatrix}\begin{pmatrix} j_1 & k & j_1 \\ -\frac{1}{2} & 0 & \frac{1}{2}\end{pmatrix}\begin{pmatrix} j_2 & k & j_2 \\ -\frac{1}{2} & 0 & \frac{1}{2}\end{pmatrix}. \tag{3.82}$$

Using the expressions of Appendix F where

$$\sum_k (2k+1)\begin{Bmatrix} j_a & j_b & J \\ j_d & j_c & k\end{Bmatrix}\begin{pmatrix} j_a & k & j_c \\ -\frac{1}{2} & 0 & \frac{1}{2}\end{pmatrix}\begin{pmatrix} j_b & k & j_d \\ -\frac{1}{2} & 0 & \frac{1}{2}\end{pmatrix} = (-1)^{j_b+j_d+J}\begin{pmatrix} j_b & j_a & J \\ -\frac{1}{2} & -\frac{1}{2} & 1\end{pmatrix}\begin{pmatrix} j_c & j_d & J \\ \frac{1}{2} & \frac{1}{2} & -1\end{pmatrix}, \tag{3.83}$$

$$\sum_k (2k+1)(-1)^k\begin{Bmatrix} j_a & j_b & J \\ j_d & j_c & k\end{Bmatrix}\begin{pmatrix} j_a & k & j_c \\ -\frac{1}{2} & 0 & \frac{1}{2}\end{pmatrix}\begin{pmatrix} j_b & k & j_d \\ -\frac{1}{2} & 0 & \frac{1}{2}\end{pmatrix} = (-1)^{J-2j_d}\begin{pmatrix} j_b & j_a & J \\ \frac{1}{2} & -\frac{1}{2} & 0\end{pmatrix}\begin{pmatrix} j_c & j_d & J \\ \frac{1}{2} & -\frac{1}{2} & 0\end{pmatrix}, \tag{3.84}$$

we get the direct term

$$\langle j_1 j_2; JM|V_{12}|j_1 j_2; JM\rangle_{\text{dir}} = F^0(2j_1+1)(2j_2+1)\tfrac{1}{2} \times \left[\begin{pmatrix} j_1 & j_2 & J \\ \frac{1}{2} & -\frac{1}{2} & 0\end{pmatrix}^2 + \begin{pmatrix} j_1 & j_2 & J \\ \frac{1}{2} & \frac{1}{2} & -1\end{pmatrix}^2\right]. \tag{3.85}$$

In a completely analogous way one can calculate the exchange term on which we give some intermediate results, i.e.,

$$g_k = (-1)^{J+j_1+j_2} \begin{Bmatrix} j_1 & j_2 & J \\ j_1 & j_2 & k \end{Bmatrix} (2j_1+1)(2j_2+1)$$
$$\times \begin{pmatrix} j_1 & k & j_2 \\ -\frac{1}{2} & 0 & \frac{1}{2} \end{pmatrix} \begin{pmatrix} j_2 & k & j_1 \\ -\frac{1}{2} & 0 & \frac{1}{2} \end{pmatrix} \frac{1}{2}\left(1+(-1)^{l_1+l_2+k}\right), \tag{3.86}$$

with the exchange matrix element

$$\sum_k g_k G^k = F^0 (2j_1+1)(2j_2+1)(-1)^{J+j_1+j_2}$$
$$\times \sum_k \tfrac{1}{2}\left(1+(-1)^{l_1+l_2+k}\right) \begin{Bmatrix} j_1 & j_2 & J \\ j_1 & j_2 & k \end{Bmatrix}$$
$$\times \begin{pmatrix} j_1 & k & j_2 \\ -\frac{1}{2} & 0 & \frac{1}{2} \end{pmatrix} \begin{pmatrix} j_2 & k & j_1 \\ -\frac{1}{2} & 0 & \frac{1}{2} \end{pmatrix} (2k+1)\,. \tag{3.87}$$

Again using (3.83, 84), the exchange matrix element finally becomes

$$\langle j_1 j_2; JM|V_{12}|j_2 j_1; JM\rangle_{\text{exch}} = F^0 (2j_1+1)(2j_2+1)$$
$$\times (-1)^{j_1+j_2+J} \frac{1}{2}\left[ \begin{pmatrix} j_1 & j_2 & J \\ \frac{1}{2} & \frac{1}{2} & -1 \end{pmatrix}^2 - (-1)^{l_1+l_2+J} \begin{pmatrix} j_2 & j_1 & J \\ \frac{1}{2} & -\frac{1}{2} & 0 \end{pmatrix}^2 \right]. \tag{3.88}$$

The sum gives now when $j_1 \neq j_2$,

$$\Delta E_{j_1 j_2, J} = F^0 (2j_1+1)(2j_2+1) \begin{pmatrix} j_1 & j_2 & J \\ \frac{1}{2} & -\frac{1}{2} & 0 \end{pmatrix}^2$$
$$\times \left(1+(-1)^{l_1+l_2+J}\right)/2\,. \tag{3.89}$$

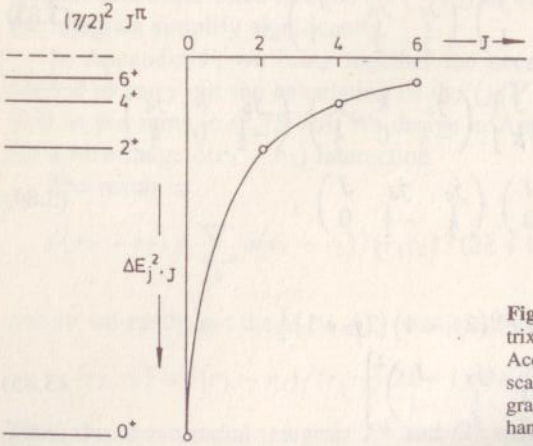


**Fig. 3.28.** Illustration of the two-particle matrix elements $\Delta E_{j^2,J}$ for the $j = \frac{7}{2}$ orbital. According to (3.90), the matrix elements are scaled with the corresponding Slater integrals $4F^0$. We also construct (on the right-hand side) the $\Delta E_{j^2,J}$ vs. $J$ plot

**Table 3.1.** The two-body matrix elements of (3.90) and this for a $j = \frac{7}{2}$ particle. The matrix elements are expressed in units $4F^0$ where $F^0$ denotes the corresponding Slater integral for the $j = \frac{7}{2}$ particle using a $\delta$-residual interaction

| $J$ | $\begin{pmatrix} j & j & J \\ \frac{1}{2} & -\frac{1}{2} & 0 \end{pmatrix}$ | $\Delta E_{j^2,J}/4F^0$ |
|---|---|---|
| 0 | $-\sqrt{\frac{1}{8}}$ | 1 |
| 2 | $\sqrt{\frac{5}{3.7.8}}$ | $\frac{5}{21} = 0.238$ |
| 4 | $-\sqrt{\frac{9}{8.7.11}}$ | $\frac{9}{77} = 0.117$ |
| 6 | $\sqrt{\frac{25}{3.8.11.13}}$ | $\frac{25}{429} = 0.058$ |

Using the same method as discussed above, for the specific case of $j_1 = j_2$, one obtains the result

$$\Delta E_{j^2,J} = \frac{F^0}{2}(2j+1)^2 \begin{pmatrix} j & j & J \\ \frac{1}{2} & -\frac{1}{2} & 0 \end{pmatrix}^2 . \tag{3.90}$$

As an example, we show this in Fig. 3.28 for a $j = 7/2$ particle, combining to a $J^\pi = 0^+, 2^+, 4^+$ and $6^+$ state (Table 3.1).

### b) Multipole Expansion

Instead of using the multipole summation relations from appendix $F$, as worked out explicitly in (3.83) and (3.84), the various multipole contributions to a particular two-body matrix element can be studied in more detail.

This sum over various multipoles, as depicted in (3.75) and (3.76), is restricted due to the angular momentum coupling conditions implied by the Wigner $6j$-symbol and Wigner $3j$-symbols which appear in (3.81) and (3.86). For the particular situation where $j_1 = j_2 = j$ i.e. evaluating diagonal two-body matrix elements, the above conditions imply that $0 \leq k \leq 2j$, with only even $k$ values contributing. The specific angular momentum ($J$) dependence in each give multipole contribution only comes from the Wigner $6j$-symbol $\begin{Bmatrix} j & j & J \\ j & j & k \end{Bmatrix}$ and has the following interesting properties:

i) for $k = 0$ (the monopole part), a constant contribution for all $J$-values results,
ii) for $k = 2$, the Wigner $6j$-symbol results in a quadratic expression in $J(J+1)$ (see also Fig. 3.29),
iii) for high-$k$ values (for $k \to \infty$), the contribution for the different $J$ values is very small compared to the $J = 0$ values. Therefore, it is often stated that the pairing properties in a given two-body force result from the highest multipole contributions.

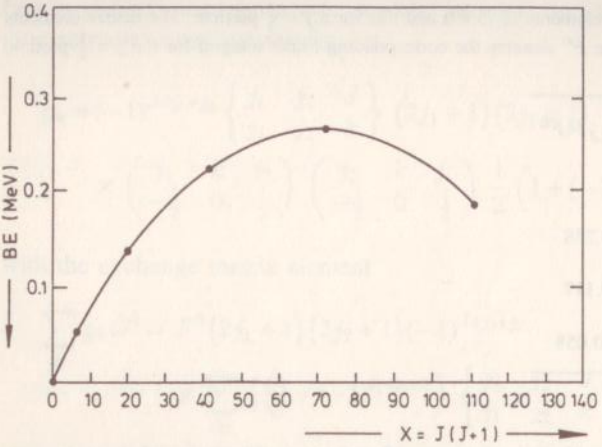


**Fig. 3.29.** Spin ($J$) dependence for the quadrupole ($k = 2$) component in the two-body matrix element for a $\langle j^2; JM|V|j^2; JM\rangle$ configuration with, in particular, $j = 1h_{11/2}$

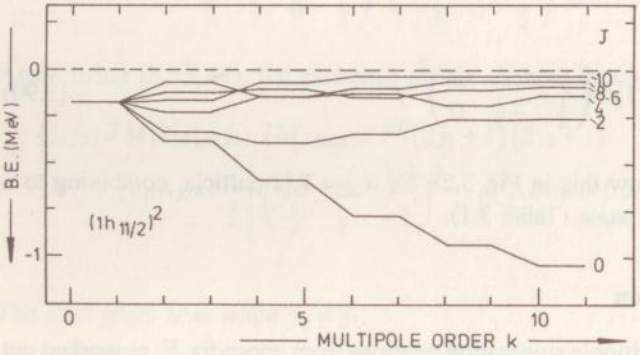


**Fig. 3.30.** Multipole decomposition ($0 \leq k \leq 10$) for the two-body matrix element $\langle (1h_{11/2})^2; JM|V|(1h_{11/2})^2; JM\rangle$, using a zero-range interaction

A full multipole decomposition is illustrated in Fig. 3.30 for a $(1h_{11/2})^2 J$ configuration. Here, only the multipoles $k = 0, 2, \ldots, 10$ contribute, with $k = 0$ giving the constant, monopole shift, $k = 2$ the quadrupole "parabolic" $J(J+1)$ dependence and with the high-$k$ values ($k = 8, 10$) exhibiting the pairing properties in the two-body matrix elements $\langle (1h_{11/2})^2; JM|V|(1h_{11/2})^2; JM\rangle$.

### c) Examples

In Chap. 9 we provide a computer program that calculates the two-body matrix elements in order to evaluate the $\delta$-function matrix elements. The Slater integrals for the $\delta$-interaction $F^0$ are calculated fully analytically. They are given together with the code.

We compare the two-body matrix elements for several nuclei:

i) $^{18}$O (Fig. 3.31): The $(1d_{5/2})^2 J$ matrix elements are compared with the experimental spectrum. The agreement is much improved when we also take more configurations into account ($2s_{1/2}$, $1d_{3/2}$) as well as the interactions among the different configurations. This we shall discuss in detail in Sect. 3.2.4.

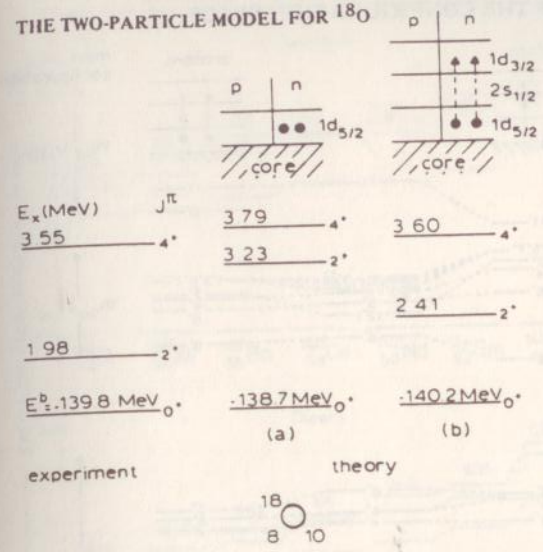


**Fig. 3.31.** A comparison between theory and experiment for both the binding energy and the excited states in $^{18}$O (**a**) the spectrum for the neutron $(1d_{5/2})^2$ configuration only and (**b**) the spectrum for two neutrons in the full $(1d_{5/2}\,2s_{1/2}\,1d_{3/2})$ space. In both cases, a MSDI interaction was used to calculate the spectra. The Modified SDI (MSDI) differs from the regular SDI force in the addition of terms $V_{\mathrm{MSDI}} = V_{\mathrm{SDI}} + B\boldsymbol{\tau}_1 \cdot \boldsymbol{\tau}_2$. For obtaining the spectra in (**a**) and (**b**), the values $A_{T=1} = B = 25\,\mathrm{MeV/A}$ were used [taken from (Brussaard, Glaudemans 1977)]

ii) $^{210}$Po (Fig. 3.32): Here we compare the effect of the possible configurations on the description of the energy spectrum and the effect of the model space on the strength of the two-body MSDI interaction [*M*odified *S*urface *D*elta *I*nteraction (Brussaard, Glaudemans 1977)]. In one case, we only take the $(1h_{9/2})^2 J$, $(1h_{9/2}\,2f_{7/2})J$ and $(1h_{9/2}\,1i_{13/2})J$ configurations into account, whereas in the other case, all two-body configurations within the full $(1h_{9/2},\ 2f_{7/2},\ 1i_{13/2})$ space are taken into account.

iii) We also make a comparison for the $N = 82$ single-closed shell nuclei $^{134}$Te-$^{146}$Gd (Fig. 3.33) where a two-quasi particle calculation was carried out. Full details of the quasi-particle excitations and the pairing degree of freedom will be discussed in Chap. 7. However, here one can clearly observe the typical features in the $0^+$-$2^+$-$4^+$-$6^+$ separation that show the short range correlations in the nucleon-nucleon residual interaction.

### d) Semi-Classical Interpretation

In comparing two-body matrix elements for many different mass regions, it is interesting to compare the matrix elements relative to the average matrix element (Fig. 3.34)

$$\bar{V} = \sum_J (2J+1)\langle (j_1)^2; JM|V_{12}|(j_1)^2; JM\rangle \Big/ \sum_J (2J+1)\,. \tag{3.91}$$

It is also possible to plot the matrix elements

$$\langle (j_1)^2; JM|V_{12}|(j_1)^2; JM\rangle/\bar{V}\,, \tag{3.92}$$

versus the angle between the classical orbits for the two valence nucleons $\theta_{12}$, which is defined as

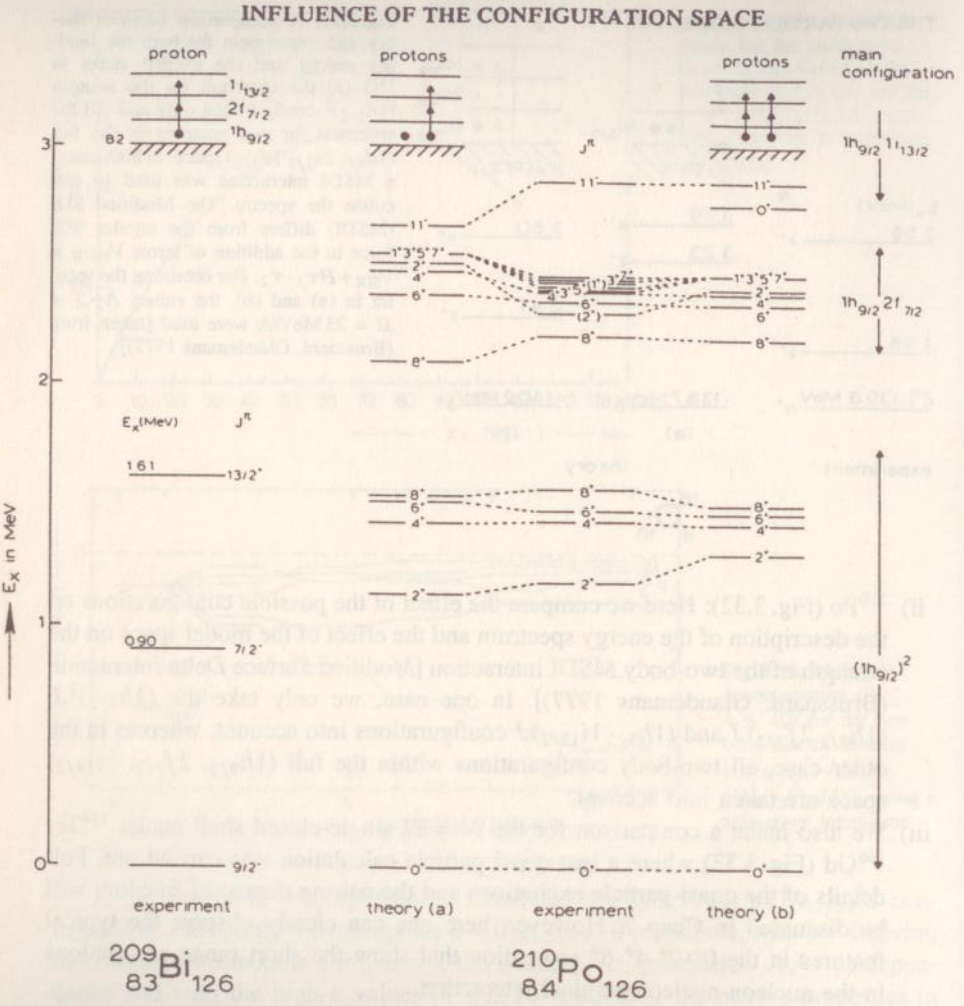


**Fig. 3.32.** The effect of the possible configurations on the spectrum and, in particular, on the MSDI parameter $A_{T=1}$ is illustrated for $^{210}_{84}Po_{126}$ (see also Sect. 3.2.4 for a detailed discussion on configuration mixing). In case (**a**) only the configurations $(1h_{9/2})^2$, $(1h_{9/2}\,2f_{7/2})$ and $(1h_{9/2}\,1i_{13/2})$ are considered with a value of $A_{T=1} = 0.33$ MeV. In case (**b**), both protons can be in the full space $(1h_{9/2}\,2f_{7/2}\,1i_{13/2})$ with now an optimum value of $A_{T=1} = 0.17$ MeV [taken from (Brussaard, Glaudemans 1977)]

$$\cos\theta_{12} = \frac{\boldsymbol{j}_1 \cdot \boldsymbol{j}_2}{|\boldsymbol{j}_1||\boldsymbol{j}_2|} = \frac{\boldsymbol{J}^2 - \boldsymbol{j}_1^2 - \boldsymbol{j}_2^2}{2|\boldsymbol{j}_1||\boldsymbol{j}_2|} \,. \tag{3.93}$$

This results in

$$\langle\cos\theta_{12}\rangle = \frac{J(J+1) - j_1(j_1+1) - j_2(j_2+1)}{2\sqrt{j_1(j_1+1)j_2(j_2+1)}} \,. \tag{3.94}$$

In such a way one measures the overlap of the orbitals. For $j_1 \cong j_2$ (large values) one obtains approximately $\theta_{12} \cong 0°$ for $J = j_1 + j_2$ and $\theta_{12} \cong 180°$ for $J = 0$

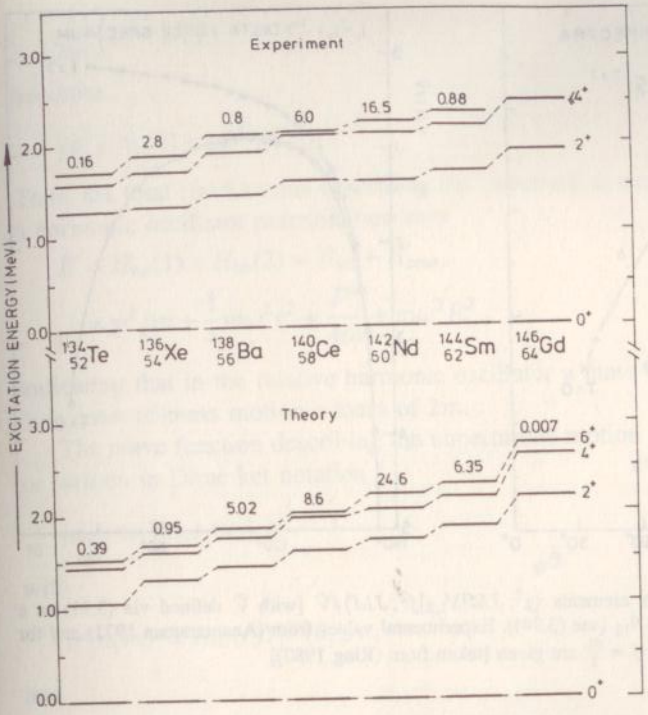


**Fig. 3.33.** We illustrate, for the $N = 82$ single closed-shell nuclei, the energy spectra in even-even nuclei $_{52}$Te, $_{54}$Xe, $_{56}$Ba, $_{58}$Ce, $_{60}$Nd, $_{62}$Sm and $_{64}$Gd. We show the lowest $2^+$, $4^+$, $6^+$ levels that are mainly formed from proton 2 quasi-particle ($2qp$) excitations (see Chap. 7 for a discussion on the theory of pairing among $n$ identical particles). The lifetime ($T_{1/2}$) for the $6^+$ level is indicated in units $\mu$s

(Fig. 3.35). The empirical results for a number of configurations $(1g_{9/2})^2$, $(1f_{7/2})^2$, $(2d_{3/2})^2$, $(2g_{9/2})^2$ do follow a single universal curve with the largest attractive matrix element at $\theta_{12} \cong 180°$ (antiparallel spins) (Fig. 3.34). It indeed follows that a $\delta$-interaction force, due to its short-range attractive characteristics, explains this experimental feature rather well.

### e) Moshinsky Transformation Method

In many cases of a central residual interaction depending only on the relative nucleon separation $r = |r_1 - r_2|$, a method exists to separate the relative from the center-of-mass coordinates when calculating the two-body matrix elements. When using harmonic oscillator radial wave functions, this method is extremely interesting.

If we consider harmonic oscillator potentials for the interacting nucleons, using the transformation

$$r = r_1 - r_2 \,, \quad R = \tfrac{1}{2}(r_1 + r_2) \,, \tag{3.95}$$

one can rewrite

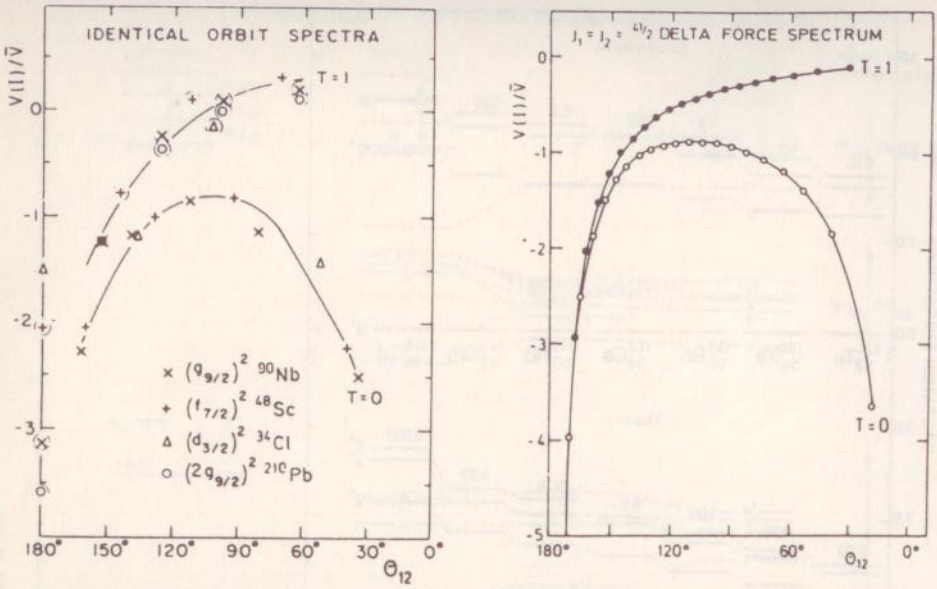


**Fig. 3.34.** The relative matrix elements $\langle j^2; JM|V_{1,2}|j^2; JM\rangle/\bar{V}$ [with $\bar{V}$ defined via (3.91) as a function of the overlap angle $\theta_{12}$ [see (3.94)]. Experimental values from (Anantaraman 1971) and for a pure $\delta$-force spectrum with $j = \frac{41}{2}$ are given [taken from (Ring 1980)]

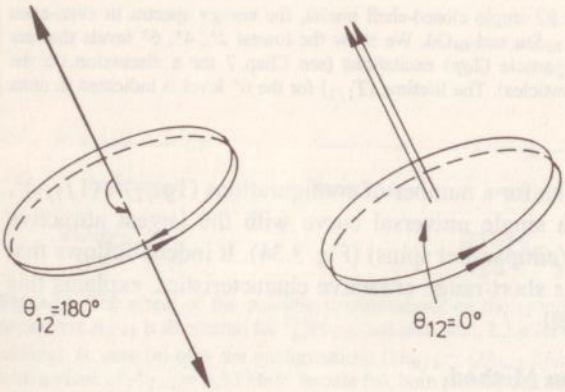


**Fig. 3.35.** The classical orbits for two particles coupled in the parallel ($\theta_{12} = 0°$) and antiparallel ($\theta_{12} = 180°$) way. The motion is, in a schematic way, presented by the arrow within the plane, perpendicular to the angular momentum vectors

$$\tfrac{1}{2}m\omega^2\left(r_1^2 + r_2^2\right), \tag{3.96}$$

as

$$\frac{1}{2}\left(\frac{m}{2}\right)\omega^2 r^2 + \frac{1}{2}(2m)\omega^2 R^2 . \tag{3.97}$$

Similarly, by transforming the momenta to a relative ($\boldsymbol{p}$) and center-of-mass total ($\boldsymbol{P}$) momentum, one can also rewrite the kinetic energy part such that

$$\frac{1}{2m}\left(\boldsymbol{p}_1^2+\boldsymbol{p}_2^2\right), \tag{3.98}$$

becomes

$$\tfrac{1}{2}\boldsymbol{p}^2/(m/2)+\tfrac{1}{2}\boldsymbol{P}^2/(2m). \tag{3.99}$$

Thus, the total Hamiltonian describing the unperturbed motion of two nucleons in a harmonic oscillator potential becomes

$$\begin{aligned} H &= H_{\text{ho}}(1)+H_{\text{ho}}(2)=H_{\text{rel}}+H_{\text{com}} \\ &= \boldsymbol{p}^2/m+\frac{1}{4}m\omega^2r^2+\frac{\boldsymbol{P}^2}{4m}+m\omega^2R^2, \end{aligned} \tag{3.100}$$

indicating that in the relative harmonic oscillator a mass of $m/2$ appears and for the center-of-mass motion a mass of $2m$.

The wave function describing the unperturbed motion of the two nucleons can be written in Dirac ket notation

$$|n_1l_1m_1\rangle|n_2l_2m_2\rangle, \tag{3.101}$$

with

$$\langle\boldsymbol{r}|nlm\rangle = R_{nl}(r)Y_l^m(\theta,\varphi), \tag{3.102}$$

and

$$R_{nl}(r)=N_{n,l}\cdot r^l\,\mathrm{e}^{-\nu r^2}L_{n-1}^{l+1/2}(2\nu r^2). \tag{3.103}$$

Here $\nu=m\omega/2\hbar$ and $n=k+1$.

Since the total Hamiltonian is also equal to the sum of a relative $(m/2)$ and center-of-mass $(2m)$ oscillator potential, the total two-particle wave function can also be written as

$$|nlm\rangle|N\Lambda M_\Lambda\rangle, \tag{3.104}$$

where $(n,l,m)$ and $(N,\Lambda,M_\Lambda)$ describe the quantum numbers of the relative and center-of-mass wave function. It is possible to transform between the two equivalent sets of basis functions (3.101, 104) by using the Moshinsky transformation (Brody, Moshinsky 1960). One writes

$$\begin{aligned} &|n_1l_1,n_2l_2;LM\rangle \\ &\quad=\sum_{n,l,N,\Lambda}\langle nl,N\Lambda;L|n_1l_1,n_2l_2;L\rangle|nl,N\Lambda;LM\rangle. \end{aligned} \tag{3.105}$$

One can easily prove that the transformation coefficients are independent of the projection quantum number $M$. During the transformation, a number of conservation laws hold:

$$\text{(i)}\quad \boldsymbol{l}_1+\boldsymbol{l}_2=\boldsymbol{L}=\boldsymbol{l}+\boldsymbol{\Lambda}, \tag{3.106}$$

$$\text{(ii)}\quad E_{n_1l_1}+E_{n_2l_2}=E_{nl}+E_{N\Lambda}, \tag{3.107}$$

or

$$2n_1 + l_1 + 2n_2 + l_2 = 2n + l + 2N + \Lambda \,. \tag{3.108}$$

We illustrate some of these transformation coefficients in Table 3.2. Applying this Moshinsky transformation to the calculation of the two-body matrix elements with a central force $V(r)$, we can evaluate

$$\begin{aligned} M &\equiv \langle n_1 l_1, n_2 l_2; LM | V(r) | n_1' l_1', n_2' l_2'; LM \rangle \\ &= \sum_{\substack{n,l,N,\Lambda \\ n',l',N',\Lambda'}} \langle n_1 l_1, n_2 l_2; L | nl, N\Lambda; L \rangle \\ &\quad \times \langle n_1' l_1', n_2' l_2'; L | n'l', N'\Lambda'; L \rangle \\ &\quad \langle nl, N\Lambda; LM | V(r) | n'l', N'\Lambda'; LM \rangle \,. \end{aligned} \tag{3.109}$$

In the radial integral part on the right-hand side of (3.109), the center-of-mass part of the wave function drops out; we get orthogonality conditions $\delta_{NN'}\delta_{\Lambda\Lambda'}$ and an extra factor $\delta_{ll'}$, since in the relative wave function $|nlm\rangle$, the angular part described by the $Y_l^m(\theta, \varphi)$ spherical harmonics, also drops out (to show this part of the calculation explicitly is left as an exercise). One then obtains

$$\begin{aligned} M = \sum_{n,n',l,N,\Lambda} & \langle n_1 l_1, n_2 l_2; L | nl, N\Lambda; L \rangle \\ & \times \langle n_1' l_1', n_2' l_2'; L | n'l, N\Lambda; L \rangle \\ & \times \langle nl | V(r) | n'l \rangle \,. \end{aligned} \tag{3.110}$$

Here, the radial integral $\langle nl|V(r)|n'l\rangle$ can be put explicitly, in coordinate space, as the integral

$$R \equiv \int R_{nl}(r) V(r) R_{n'l}(r) r^2 \, dr \,. \tag{3.111}$$

Using the explicit form of the Laguerre polynomials

$$L_{n-1}^{l+1/2}(x) = \sum_{k=0}^{n-1} a_k (-1)^k x^k \,, \tag{3.112}$$

and a Gaussian type of residual interaction

$$V(r) = V_0 \, \mathrm{e}^{-r^2/r_0^2} \,, \tag{3.113}$$

the radial integral can be evaluated as the double sum (note that $\nu \to \nu_{\mathrm{rel}} = \nu/2$)

$$\begin{aligned} R = N_{n,l} N_{n',l} & \sum_{k,k'=0}^{(n-1)(n'-1)} (-1)^{k+k'} a_k a_{k'} \\ & \times \int r^{2l} \, \mathrm{e}^{-\nu r^2} \, \mathrm{e}^{-r^2/r_0^2} \left(\nu r^2\right)^{k+k'} r^2 \, dr \,. \end{aligned} \tag{3.114}$$

**Table 3.2.** Illustration of transformation brackets from the product harmonic oscillator wave functions to a product basis of relative times centre-of-mass (c.o.m.) oscillator wave functions. The table lists coefficients $\langle n_1 l_1, n_2 l_2; L | nl, N\Lambda; L\rangle$ [taken from (Brody 1960)] with $n_1 = n_2 = 0$. Note that in the tables of Brody and Moshinsky, the total orbital angular momentum is denoted by $\lambda$, the c.o.m. angular momentum by $L$ and that the radial quantum number $n$ takes the values $n = 0, 1, 2, \ldots$

| $l_1$ | $l_2$ | $\lambda$ | $n$ | $l$ | $N$ | $L$ | $\varrho$ | $\langle\|\rangle$ | $\tau$ |
|---|---|---|---|---|---|---|---|---|---|
| 0 | 0 | 0 | 0 | 0 | 0 | 0 | | 1.00000000 | 1 |
| 0 | 1 | 1 | 0 | 0 | 0 | 1 | 1 | 0.70710678 | |
| | | | 0 | 1 | 0 | 0 | | −0.70710677 | 2 |
| 0 | 2 | 2 | 0 | 0 | 0 | 2 | 2 | 0.49999999 | |
| | | | 0 | 1 | 0 | 1 | | −0.70710679 | |
| | | | 0 | 2 | 0 | 0 | | 0.49999999 | 3 |
| 0 | 3 | 3 | 0 | 0 | 0 | 3 | 3 | 0.35355340 | |
| | | | 0 | 1 | 0 | 2 | | −0.61237245 | |
| | | | 0 | 2 | 0 | 1 | | 0.61237245 | |
| | | | 0 | 3 | 0 | 0 | | −0.35355340 | 4 |
| 0 | 4 | 4 | 0 | 0 | 0 | 4 | 4 | 0.24999999 | |
| | | | 0 | 1 | 0 | 3 | | −0.50000000 | |
| | | | 0 | 2 | 0 | 2 | | 0.61237245 | |
| | | | 0 | 3 | 0 | 1 | | −0.50000000 | |
| | | | 0 | 4 | 0 | 0 | | 0.24999999 | 5 |
| 0 | 5 | 5 | 0 | 0 | 0 | 5 | 5 | 0.17677670 | |
| | | | 0 | 1 | 0 | 4 | | −0.39528471 | |
| | | | 0 | 2 | 0 | 3 | | 0.55901700 | |
| | | | 0 | 3 | 0 | 2 | | −0.55901699 | |
| | | | 0 | 4 | 0 | 1 | | 0.39528471 | |
| | | | 0 | 5 | 0 | 0 | | −0.17677670 | 6 |
| 0 | 6 | 6 | 0 | 0 | 0 | 6 | 6 | 0.12500000 | |
| | | | 0 | 1 | 0 | 5 | | −0.30618623 | |
| | | | 0 | 2 | 0 | 4 | | 0.48412292 | |
| | | | 0 | 3 | 0 | 3 | | −0.55901699 | |
| | | | 0 | 4 | 0 | 2 | | 0.48412292 | |
| | | | 0 | 5 | 0 | 1 | | −0.30618622 | |
| | | | 0 | 6 | 0 | 0 | | 0.12500000 | |
| 1 | 1 | 0 | 0 | 0 | 1 | 0 | 2 | 0.70710679 | |
| | | | 0 | 1 | 0 | 1 | | 0.00000000 | |
| | | | 1 | 0 | 0 | 0 | | −0.70710679 | 3 |
| 1 | 1 | 1 | 0 | 1 | 0 | 1 | 2 | 0.99999999 | 1 |
| 1 | 1 | 2 | 0 | 0 | 0 | 2 | 2 | 0.70710678 | |
| | | | 0 | 1 | 0 | 1 | | 0.00000000 | |
| | | | 0 | 2 | 0 | 0 | | −0.70710678 | 3 |
| 1 | 2 | 1 | 0 | 0 | 1 | 1 | 3 | 0.40824829 | |
| | | | 0 | 1 | 0 | 2 | | 0.23570226 | |
| | | | 0 | 1 | 1 | 0 | | −0.52704628 | |
| | | | 0 | 2 | 0 | 1 | | 0.23570226 | |
| | | | 1 | 0 | 0 | 1 | | −0.52704628 | |
| | | | 1 | 1 | 0 | 0 | | 0.40824829 | 6 |
| 1 | 2 | 2 | 0 | 1 | 0 | 2 | 3 | 0.70710676 | |
| | | | 0 | 2 | 0 | 1 | | −0.70710676 | 2 |

| $l_1$ | $l_2$ | $\lambda$ | $n$ | $l$ | $N$ | $L$ | $\varrho$ | $\langle\|\rangle$ | $\tau$ |
|---|---|---|---|---|---|---|---|---|---|
| 1 | 2 | 3 | 0 | 0 | 0 | 3 | 3 | 0.61237245 | |
| | | | 0 | 1 | 0 | 2 | | −0.35355340 | |
| | | | 0 | 2 | 0 | 1 | | −0.35355340 | |
| | | | 0 | 3 | 0 | 0 | | 0.61237245 | 4 |
| 1 | 3 | 2 | 0 | 0 | 1 | 2 | 4 | 0.27386128 | |
| | | | 0 | 1 | 0 | 3 | | 0.20000000 | |
| | | | 0 | 1 | 1 | 1 | | −0.45825757 | |
| | | | 0 | 2 | 0 | 2 | | 0.00000000 | |
| | | | 0 | 2 | 1 | 0 | | 0.41833000 | |
| | | | 0 | 3 | 0 | 1 | | −0.20000000 | |
| | | | 1 | 0 | 0 | 2 | | −0.41833000 | |
| | | | 1 | 1 | 0 | 1 | | 0.45825757 | |
| | | | 1 | 2 | 0 | 0 | | −0.27386128 | 9 |
| 1 | 3 | 3 | 0 | 1 | 0 | 3 | 4 | 0.50000000 | |
| | | | 0 | 2 | 0 | 2 | | −0.70710677 | |
| | | | 0 | 3 | 0 | 1 | | 0.50000000 | 3 |
| 1 | 3 | 4 | 0 | 0 | 0 | 4 | 4 | 0.50000001 | |
| | | | 0 | 1 | 0 | 3 | | −0.49999999 | |
| | | | 0 | 2 | 0 | 2 | | −0.00000001 | |
| | | | 0 | 3 | 0 | 1 | | 0.49999999 | |
| | | | 0 | 4 | 0 | 0 | | −0.50000001 | 5 |
| 1 | 4 | 3 | 0 | 0 | 1 | 3 | 5 | 0.18898224 | |
| | | | 0 | 1 | 0 | 4 | | 0.15152288 | |
| | | | 0 | 1 | 1 | 2 | | −0.37115375 | |
| | | | 0 | 2 | 0 | 3 | | −0.05976143 | |
| | | | 0 | 2 | 1 | 1 | | 0.43915504 | |
| | | | 0 | 3 | 0 | 2 | | −0.05976143 | |
| | | | 0 | 3 | 1 | 0 | | −0.32732684 | |
| | | | 0 | 4 | 0 | 1 | | 0.15152288 | |
| | | | 1 | 0 | 0 | 3 | | −0.32732684 | |
| | | | 1 | 1 | 0 | 2 | | 0.43915504 | |
| | | | 1 | 2 | 0 | 1 | | −0.37115375 | |
| | | | 1 | 3 | 0 | 0 | | 0.18898224 | 12 |
| 1 | 4 | 4 | 0 | 1 | 0 | 4 | 5 | 0.35355339 | |
| | | | 0 | 2 | 0 | 3 | | −0.61237243 | |
| | | | 0 | 3 | 0 | 2 | | 0.61237243 | |
| | | | 0 | 4 | 0 | 1 | | −0.35355339 | 4 |
| 1 | 4 | 5 | 0 | 0 | 0 | 5 | 5 | 0.39528471 | |
| | | | 0 | 1 | 0 | 4 | | −0.53033006 | |
| | | | 0 | 2 | 0 | 3 | | 0.25000000 | |
| | | | 0 | 3 | 0 | 2 | | 0.24999999 | |
| | | | 0 | 4 | 0 | 1 | | −0.53033005 | |
| | | | 0 | 5 | 0 | 0 | | 0.39528471 | 6 |
| 1 | 5 | 4 | 0 | 0 | 1 | 4 | 6 | 0.13176157 | |
| | | | 0 | 1 | 0 | 5 | | 0.11111111 | |
| | | | 0 | 1 | 1 | 3 | | −0.29133579 | |
| | | | 0 | 2 | 0 | 4 | | −0.07273929 | |
| | | | 0 | 2 | 1 | 2 | | 0.40458680 | |
| | | | 0 | 3 | 0 | 3 | | 0.00000000 | |

| $l_1$ | $l_2$ | $\lambda$ | $n$ | $l$ | $N$ | $L$ | $\varrho$ | $\langle \vert \rangle$ | $\tau$ |
|---|---|---|---|---|---|---|---|---|---|
| | | | 0 | 3 | 1 | 1 | | −0.39086798 | |
| | | | 0 | 4 | 0 | 2 | | 0.07273929 | |
| | | | 0 | 4 | 1 | 0 | | 0.25230420 | |
| | | | 0 | 5 | 0 | 1 | | −0.11111111 | |
| | | | 1 | 0 | 0 | 4 | | −0.25230420 | |
| | | | 1 | 1 | 0 | 3 | | 0.39086798 | |
| | | | 1 | 2 | 0 | 2 | | −0.40458680 | |
| | | | 1 | 3 | 0 | 1 | | 0.29133579 | |
| | | | 1 | 4 | 0 | 0 | | −0.13176157 | 15 |
| 1 | 5 | 5 | 0 | 1 | 0 | 5 | 6 | 0.25000000 | |
| | | | 0 | 2 | 0 | 4 | | −0.50000000 | |
| | | | 0 | 3 | 0 | 3 | | 0.61237245 | |
| | | | 0 | 4 | 0 | 2 | | −0.50000001 | |
| | | | 0 | 5 | 0 | 1 | | 0.25000000 | 5 |

We define the dimensionless coordinate $x \equiv \nu^{1/2} r$, and obtain

$$R = N_{n,l} N_{n',l} \sum_p a_p \int x^{2p} \, \mathrm{e}^{-x^2} \, \mathrm{e}^{-x^2/(\nu r_0^2)} x^2 \, dx \,, \tag{3.115}$$

where $l \le p \le l + n + n' - 2$, $a_p = a_k a_{k'} (-1)^{k+k'} (\nu)^{-(l+3/2)}$.

Combining all intermediate results, the matrix element $M$ can be written in compact form

$$M = \sum_{\substack{n_1 n_1' l_1 \\ n_2 n_2' l_2 \\ N, \Lambda}} \langle n_1 l_1, n_2 l_2; L | n l, N \Lambda; L \rangle \langle n_1' l_1', n_2' l_2'; L | n' l, N \Lambda; L \rangle$$
$$\times N_{n,l} N_{n',l} \sum_p I_p \frac{a_p}{2} \Gamma\left(p + \tfrac{3}{2}\right) \,, \tag{3.116}$$

and where the Talmi integrals defined as $I_p$

$$I_p = \frac{2}{\Gamma\left(p + \frac{3}{2}\right)} \int x^{2(p+1)} \, \mathrm{e}^{-(1+\lambda^2) x^2} \, dx \,, \tag{3.117}$$

with $\lambda = (\nu^{1/2} r_0)^{-1}$, characterize the interaction. This Talmi integral can be evaluated in closed form and gives

$$I_p = \left(1 + \lambda^2\right)^{-p-3/2} \,. \tag{3.118}$$

In Fig. 3.36 we plot the Talmi integrals $I_p$ for the Gaussian interaction. This method is very general, and Talmi integrals for, e.g., the Yukawa shape $\mathrm{e}^{-\mu r}/\mu r$, the Coulomb shape $1/r$, or any other force depending on $r = |\boldsymbol{r}_1 - \boldsymbol{r}_2|$ can be obtained and evaluated (Talmi 1952).

In the above discussion we concentrated on the orbital part of the wave function. In actual situations, we calculate the two-body matrix elements

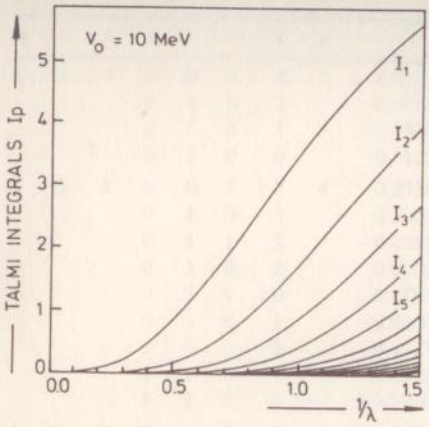


**Fig. 3.36.** The nuclear Talmi integrals [see (3.117) and (3.118)] for a residual interaction with a Gaussian shape. The abcissa is indicated by $1/\lambda$ where $\lambda = (\nu^{1/2} r_0)^{-1}$ with $\nu$ the harmonic oscillator parameter ($\nu = m\omega/2\hbar$) and $r_0$ the Gaussian shape parameter of $V(r) = V_0 \exp(-r^2/r_0^2)$. The values $I_1, \ldots, I_{13}$ are shown (in descending order). The strength of the Gaussian interaction $V_0 = 10\,\text{MeV}$ is taken

$\langle j_1 j_2; JM|V_{12}|j_3 j_4; JM\rangle$ where $j_1, \ldots, j_4$ are notations for a full single-particle wave function, containing besides the orbital part also the intrinsic spin part in a coupled form $(l\frac{1}{2})j$. In the problem set there is an exercise to go from the above two-body matrix elements into the relative integrals via the Moshinsky transformation brackets.

### 3.2.4 Configuration Mixing: Model Space and Model Interaction

In many cases when we consider nuclei with just two valence nucleons outside closed shells, it is not possible to single out one orbital $j$. Usually a number of valence shells are present in which the two nucleons can, in principle, move.

Let us consider the case of $^{18}$O with two neutrons outside the $^{16}$O core. In the most simple approach the two neutrons move in the energetically most favored orbital, i.e., in the $1d_{5/2}$ orbital (Fig. 3.37). Thus we can only form the $(2d_{5/2})^2\, 0^+, 2^+, 4^+$ configurations and then determine the strength of the residual interaction $V_{12}$ so that the theoretical $0^+$-$2^+$-$4^+$ spacing reproduces the experimental spacing as well as possible (Fig. 3.31). The next step is to consider the full *sd* model space with many more configurations for each $J^\pi$ value. For the $J^\pi = 0^+$ state, we have three configurations, i.e., the $(2d_{5/2})^2 0^+$, $(3s_{1/2})^2 0^+$ and the $(2d_{3/2})^2 0^+$ configurations. In the latter situation, the strength of the residual interaction $V_{12}$ will be different from the first model space where only the $(2d_{5/2})^2 0^+$ state was considered. Thus one generally concludes that the strength of the residual interaction depends on the model space chosen, that is, $V_{12} = V_{12}$ (model space) such that the larger the model space is, the smaller $V_{12}$ will become in order to get a similar overall agreement. In the larger model spaces, one will, in general, be able to describe the observed properties in the nucleus better than with the smaller model spaces. This argument only relates to effective forces using a given form, i.e., a Gaussian interaction, an $(M)$SDI interaction, etc. for which only the strength parameter determines the overall magnitude of the two-body matrix elements in a given finite dimensional model space. Thus one should not extrapolate to the full

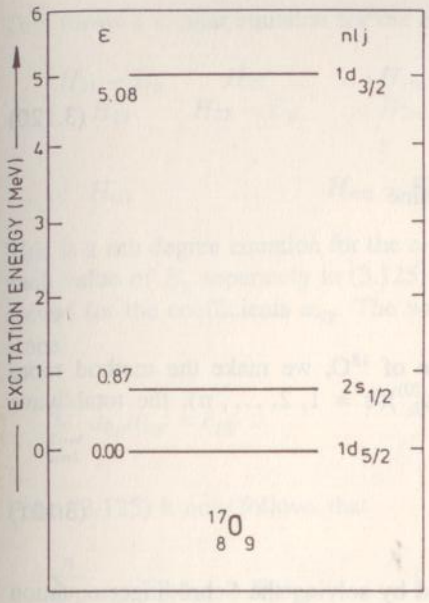


**Fig. 3.37.** The neutron single-particle energies in $^{17}_{8}O_9$ (relative to the $1d_{5/2}$ orbital) for $2s_{1/2}$ and $1d_{3/2}$ orbitals. The energies are taken from the experimental spectrum in $^{17}O$

(infinite dimensional initial) configuration space in which the bare nucleon-nucleon force would be acting.

Thus, in the case of $^{18}O$ where the $3s_{1/2}$ and $2d_{5/2}$ orbitals separate from the higher-lying $2d_{3/2}$ orbital, for the model spaces one has

$$
\begin{aligned}
J^\pi = 0^+ &\rightarrow \left(1d_{5/2}\right)^2_{0^+},\ \left(3s_{1/2}\right)^2_{0^+} \\
J^\pi = 2^+ &\rightarrow \left(1d_{5/2}\right)^2_{2^+},\ \left(1d_{5/2}2s_{1/2}\right)_{2^+} \\
J^\pi = 3^+ &\rightarrow \left(1d_{5/2}2s_{1/2}\right)_{3^+} \\
J^\pi = 4^+ &\rightarrow \left(1d_{5/2}\right)^2_{4^+}\ .
\end{aligned}
$$

The energy eigenvalues for the $J^\pi = 0^+$ states, for example, will be the corresponding eigenvalues for the eigenstates to the Hamiltonian

$$
\begin{aligned}
H &= H_0 + H_{\text{res}}\ , \\
&= \sum_{i=1}^{2} h_0(i) + V_{12}\ ,
\end{aligned}
\tag{3.119}
$$

where the core energy corresponding to the closed shell system $E_0$ is taken as the reference value.

The wave functions will, in general, be linear combinations of the possible basis functions. This means that for $J^\pi = 0^+$ we will get two eigenfunctions

$$|\Psi_{0^+;1}\rangle = \sum_{k=1}^{n} a_{k,1}|\psi_k^{(0)};0^+\rangle ,$$
$$|\Psi_{0^+;2}\rangle = \sum_{k=1}^{n} a_{k,2}|\psi_k^{(0)};0^+\rangle , \tag{3.120}$$

where for the particular case of $^{18}$O we define

$$|\psi_1^{(0)};0^+\rangle \equiv |\left(1d_{5/2}\right)^2;0^+\rangle ,$$
$$|\psi_2^{(0)};0^+\rangle \equiv |\left(2s_{1/2}\right)^2;0^+\rangle .$$

Before turning back to the particular case of $^{18}$O, we make the method more general. If the basis set is denoted by $|\psi_k^{(0)}\rangle (k = 1, 2, \ldots, n)$, the total wave function can be expanded as

$$|\Psi_p\rangle = \sum_{k=1}^{n} a_{kp}|\psi_k^{(0)}\rangle . \tag{3.121}$$

The coefficients $a_{kp}$ have to be determined by solving the Schrödinger equation for $|\Psi_p\rangle$, or

$$H|\Psi_p\rangle = E_p|\Psi_p\rangle . \tag{3.122}$$

In explicit form this becomes [using the Hamiltonian of (3.119)]

$$\left(H_0 + H_{\text{res}}\right)\sum_{k=1}^{n} a_{kp}|\psi_k^{(0)}\rangle = E_p\sum_{k=1}^{n} a_{kp}|\psi_k^{(0)}\rangle , \tag{3.123}$$

or

$$\sum_{k=1}^{n}\langle\psi_l^{(0)}|H_0 + H_{\text{res}}|\psi_k^{(0)}\rangle a_{kp} = E_p a_{lp} . \tag{3.124}$$

Since the basis functions $|\psi_k^{(0)}\rangle$ correspond to eigenfunctions of $H_0$ with eigenvalues (unperturbed energies) $E_k^{(0)}$, we can rewrite (3.124) in shorthand form as

$$\sum_{k=1}^{n} H_{lk}a_{kp} = E_p a_{lp} , \tag{3.125}$$

with

$$H_{lk} \equiv E_k^{(0)}\delta_{lk} + \langle\psi_l^{(0)}|H_{\text{res}}|\psi_k^{(0)}\rangle . \tag{3.126}$$

The eigenvalue equation becomes a matrix equation

$$[H][A] = [E][A] . \tag{3.127}$$

This forms a secular equation for the eigenvalues $E_p$ which are determined from

$$\begin{vmatrix} H_{11} - E_p & H_{12} & \dots & H_{1n} \\ H_{21} & H_{22} - E_p & \dots & H_{2n} \\ \vdots & \ddots & & \vdots \\ H_{n1} & \dots & & H_{nn} - E_p \end{vmatrix} = 0 \,. \tag{3.128}$$

This is a $n$th degree equation for the $n$-roots $E_p$ ($p = 1, 2, \dots, n$). Substitution of each value of $E_p$ separately in (3.125) gives a set of linear equations that can be solved for the coefficients $a_{kp}$. The wave functions $|\Psi_p\rangle$ can be orthonormalized since

$$\sum_{k=1}^{n} a_{kp} a_{kp'} = \delta_{pp'} \,. \tag{3.129}$$

From (3.125) it now follows that

$$\sum_{l,k=1}^{n} a_{lp'} H_{lk} a_{kp} = E_p \delta_{pp'} \,, \tag{3.130}$$

or, in matrix form

$$[\widetilde{A}][H][A] = [E] \,, \tag{3.131}$$

with

$$[\widetilde{A}] = [A]^{-1} \,.$$

Equation (3.131) indicates a similarity transformation to a new basis that makes $[H]$ diagonal and thus produces the $n$ energy eigenvalues. In practical situations ($n$ large), this process needs high-speed computers. A number of algorithms exist for $[H]$ (hermitian, real in most cases) matrix diagonalization which we do not discuss here (Wilkinson 1965): the Jacobi method (small $n$ or $n\lambda 50$), the Householder method ($50 < n < 200$), the Lanczos algorithm ($n\gamma 1000$, requiring the calculation of only a small number of eigenvalues, normally the lowest lying ones). In cases where the non-diagonal matrix elements $|H_{ij}|$ are of the order of the unperturbed energy differences $|E_i^{(0)} - E_j^{(0)}|$, large configuration mixing will result and the final energy eigenvalues $E_p$ can be very different from the unperturbed spectrum of eigenvalues $E_p^{(0)}$. If, on the other hand, the $|H_{ij}|$ are small compared to $|E_i^{(0)} - E_j^{(0)}|$, energy shifts will be small and even perturbation theory might be applied.

Now to make these general considerations more specific, we discuss the case of $J^\pi = 0^+$ levels in $^{18}$O for the $(1d_{5/2}2s_{1/2})$ model space. As shown before, the model space reduces to a two-dimensional space $n = 2$ (3.120) and the $2 \times 2$ energy matrix can be written out as

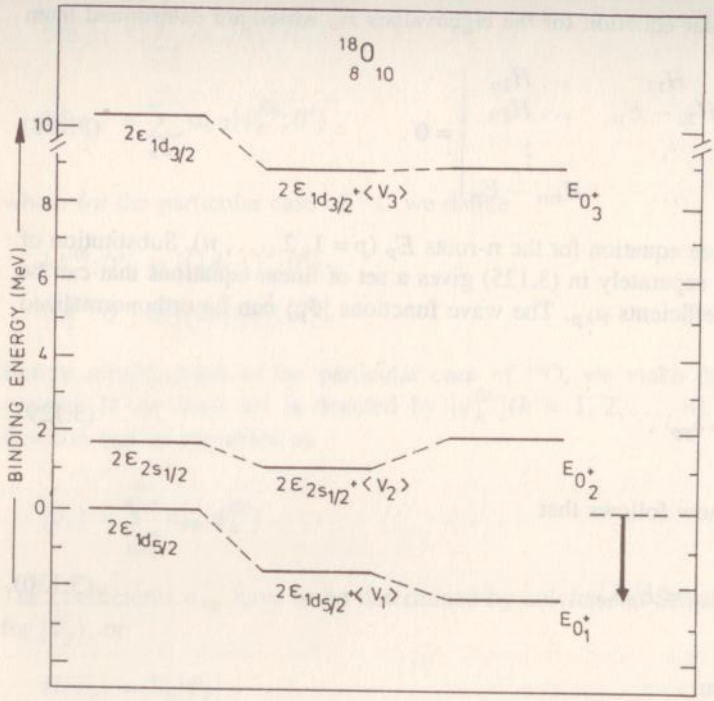


**Fig. 3.38.** The solution of the secular equation for $0^+$ states in $^{18}O$, shown in a diagrammatic way. On the extreme left we show the unperturbed two-neutron single-particle energies $2\varepsilon_j$. In the middle part the diagonal interaction matrix elements $\langle j^2; J^\pi = 0^+|V_{1,2}|j^2; J^\pi = 0^+\rangle$ for the three configurations are added and denoted by $\langle V_1\rangle$, $\langle V_2\rangle$, $\langle V_3\rangle$, respectively. On the right-hand side, the resulting energy eigenvalues $E_{0^+_i}$ $(i = 1, 2, 3)$ from diagonalizing the energy matrix (3.132) are shown

$$H = \begin{bmatrix} 2\varepsilon_{1d_{5/2}} + \langle \left(1d_{5/2}\right)^2; 0^+|V_{12}|\left(1d_{5/2}\right)^2; 0^+\rangle & \langle \left(1d_{5/2}\right)^2; 0^+|V_{12}|\left(2s_{1/2}\right)^2; 0^+\rangle \\ \langle \left(2s_{1/2}\right)^2; 0^+|V_{12}|\left(1d_{5/2}\right)^2; 0^+\rangle & 2\varepsilon_{2s_{1/2}} + \langle \left(2s_{1/2}\right)^2; 0^+|V_{12}|\left(2s_{1/2}\right)^2; 0^+\rangle \end{bmatrix} \tag{3.132}$$

These diagonal elements yield the first correction to the unperturbed single-particle energies $2\varepsilon_{1d_{5/2}}$ and $2\varepsilon_{2s_{1/2}}$, respectively (the diagonal two-body interaction matrix elements $H_{11}$ and $H_{22}$, Fig. 3.38). The energy matrix is Hermitian (for a real matrix this means symmetric and $H_{12} = H_{21}$) and, in shorthand notation gives the secular equation

$$\begin{bmatrix} H_{11} - \lambda & H_{12} \\ H_{12} & H_{22} - \lambda \end{bmatrix} = 0 \,. \tag{3.133}$$

We can solve this easily since we get a quadratic equation in $\lambda$

$$\lambda^2 - \lambda(H_{11} + H_{22}) - H_{12}^2 + H_{11}H_{22} = 0 \tag{3.134}$$

with the roots

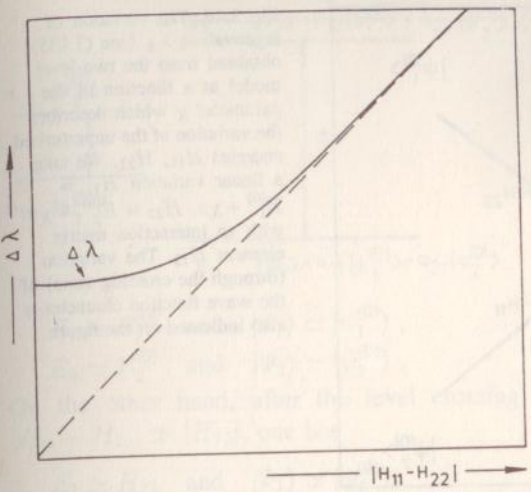


**Fig. 3.39.** The variation of the difference of eigenvalues $\Delta\lambda \equiv \lambda_+ - \lambda_-$ for the two-level model of (3.133) and (3.136) as a function of the energy difference between the unperturbed states $\Delta H \equiv |H_{11} - H_{22}|$

$$\lambda_\pm = \frac{H_{11}+H_{22}}{2} \pm \frac{1}{2}\left[(H_{11}-H_{22})^2 + 4H_{12}^2\right]^{1/2} . \tag{3.135}$$

The difference $\Delta\lambda \equiv \lambda_+ - \lambda_-$ then becomes

$$\Delta\lambda = \left[(H_{11}-H_{22})^2 + 4H_{12}^2\right]^{1/2} , \tag{3.136}$$

and is shown in Fig. 3.39. Even for $H_{11} = H_{22}$, the degenerate situation for the two basis states, a difference of $\Delta\lambda = 2H_{12}$ results. It is as if the two levels are repelled over a distance of $H_{12}$. Thus $2H_{12}$ is the minimal energy difference. In the limit of $|H_{11} - H_{22}| \gg |H_{12}|$, the energy difference $\Delta\lambda$ becomes asymptotically equal to $\Delta H \equiv H_{11} - H_{22}$.

The equation for $\lambda_\pm$ given in (3.135) is interesting with respect to perturbation theory.

i) If we consider the case $|H_{11} - H_{22}| \gg |H_{12}|$, then we see that one can obtain by expanding the square root around $H_{11} = H_{22}$

$$\begin{aligned} \lambda_1 &= H_{11} + \frac{H_{12}^2}{H_{11}-H_{22}} + \dots , \\ \lambda_2 &= H_{22} + \frac{H_{12}^2}{H_{22}-H_{11}} + \dots . \end{aligned} \tag{3.137}$$

[We use the expansion $(1+x)^{1/2} \cong 1 + \frac{1}{2}x + \dots$.)

ii) One can show that if the perturbation expansion does not converge easily, one has to sum the full perturbation series up to infinity. The final result of this sum can be shown to be equal to the square root expression of (3.135) (see Problem set).

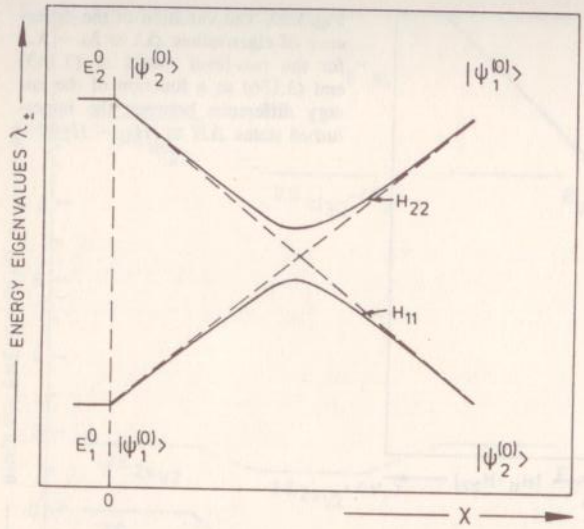


**Fig. 3.40.** The variation of eigenvalues $\lambda_\pm$ [see (3.135)] obtained from the two-level model as a function of the parameter $\chi$ which describes the variation of the unperturbed energies $H_{11}$, $H_{22}$. We take a linear variation $H_{11} = E_1^{(0)} + \chi a$, $H_{22} = E_2^{(0)} - \chi b$ with an interaction matrix element $H_{12}$. The variation (through the crossing zone) of the wave function character is also indicated on the figure

It is also interesting to study (3.135) with a constant interaction matrix element $H_{12}$ when the unperturbed energies $H_{11}$, $H_{22}$ vary linearly, i.e., $H_{11} = E_1^{(0)} + \chi a$ and $H_{22} = E_2^{(0)} - \chi b$ (Fig. 3.40). There will be a crossing point for the unperturbed energies at a certain value of $\chi = \chi_{\text{crossing}}$. However, the eigenvalues $E_1$, $E_2$ will first approach the crossing but then change direction (no-crossing rule). The wave functions are also interesting. First of all, we study the wave functions analytically (the coefficients $a_{kp}$).

We get

$$|\Psi_1\rangle = a_{11}|\psi_1^{(0)}\rangle + a_{21}|\psi_2^{(0)}\rangle$$
$$|\Psi_2\rangle = a_{12}|\psi_1^{(0)}\rangle + a_{22}|\psi_2^{(0)}\rangle \,. \tag{3.138}$$

If we use one of the eigenvalues, say $\lambda_1$, the coefficients follow from

$$(H_{11} - \lambda_1)a_{11} + H_{12}a_{21} = 0 \,, \tag{3.139}$$

or

$$\frac{a_{11}}{a_{21}} = \frac{-H_{12}}{H_{11} - \lambda_1} \,. \tag{3.140}$$

The normalizing condition $a_{11}^2 + a_{21}^2 = 1$ then gives

$$a_{21} = \left(1/\left(1 + \left(H_{12}/\left(H_{11} - \lambda\right)\right)^2\right)\right)^{1/2} \,, \tag{3.141}$$

and similar results for the other coefficients. In the situation that $H_{11} = H_{22}$, the absolute values of the coefficients $a_{11}$, $a_{12}$, $a_{21}$ and $a_{22}$ all have absolute value $1/\sqrt{2}$. These coefficients then also determine the wave functions of Fig. 3.41 at the crossing point. One can see in Fig. 3.40 that for the case of $\chi = 0$, one has

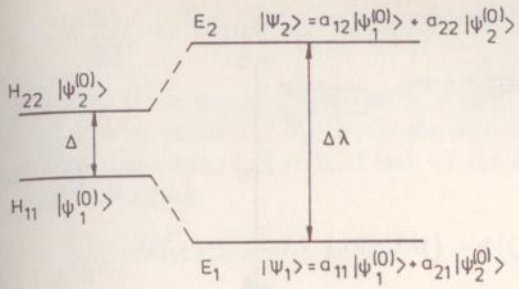


**Fig. 3.41.** The change in energy separation $\Delta$ ($\Delta \equiv H_{22} - H_{11}$) to $\Delta\lambda$ ($\equiv E_2 - E_1$) from unperturbed to perturbed spectrum in a two-level model. The specific form of the wave functions $|\Psi_1\rangle$ and $|\Psi_2\rangle$ is also given using the basis functions $|\psi_1^{(0)}\rangle$, $|\psi_2^{(0)}\rangle$

$$E_1 \simeq E_1^{(0)} \quad \text{and} \quad |\Psi_1\rangle \simeq |\psi_1^{(0)}\rangle \,,$$
$$E_2 \simeq E_2^{(0)} \quad \text{and} \quad |\Psi_2\rangle \simeq |\psi_2^{(0)}\rangle \,.$$

On the other hand, after the level crossing and in the region where again $|H_{11} - H_{22}| \gg |H_{12}|$, one has

$$E_1 \simeq H_{22} \quad \text{and} \quad |\Psi_1\rangle \simeq |\psi_2^{(0)}\rangle \,,$$
$$E_2 \simeq H_{11} \quad \text{and} \quad |\Psi_2\rangle \simeq |\psi_1^{(0)}\rangle \,,$$

so that one can conclude that the "character" of the states has been interchanged in the crossing region, although the levels never actually cross!

In the realistic situations of $^{18}$O and $^{210}$Po (Figs. 3.31 and 3.32) (Brussaard, Glaudemans 1977), the results are now the results of configuration mixing: in $^{18}$O (the $1d_{5/2}$ and full $1d_{5/2}$, $2s_{1/2}$, $1d_{3/2}$ spaces, respectively) and for $^{210}$Po [using the $(1h_{9/2})^2$, $1h_{9/2}\,2f_{7/2}$, $1h_{9/2}\,1i_{13/2}$ and the full $(1h_{9/2}, 2f_{7/2}, 1i_{13/2})$ spaces, respectively]. In the case of $^{18}$O, one observes a net improvement for the larger model space when comparing with the data. Also, for $^{210}$Po some improvement can be observed for the larger model space. In both cases ($^{18}$O, $^{210}$Po) one needs to reduce the MSDI force strength when going to the larger space.

The above method of configuration mixing was discussed and worked out in detail for the two-level model (as applied) to the lowest $0^+$ levels in $^{18}$O. If we restrict ourselves to the full *sd*-shell, the complete two-neutron configuration space can be constructed for all possible $J^\pi$ values, as was done for the $0^+$ state shown in Fig. 3.38. According to the specific neutron single-particle spacings as deduced from the experimental spectrum of $^{17}$O, we construct the full unperturbed two-particle spectrum on the extreme left-hand side of Fig. 3.42. At the same time (second column of levels), all possible $J^\pi$ values are shown. Subsequently, the various diagonal two-body matrix elements (using a zero-range interaction) $\langle j_1 j_2; JM|V|j_1 j_2; JM\rangle$, which already split the original degeneracy to a large extent, are added. The results of diagonalizing the various energy matrices ($J^\pi = 0^+, 1^+, \ldots, 4^+$) are given separately and, finally, at the extreme right-hand side, the full theoretical two-particle spectrum for $^{18}$O is obtained. The global binding energy of the 0 ground-state configuration is also indicated, relative to the unperturbed energy of $2\varepsilon_{1d_{5/2}}$. In this figure, the full details of how such a calculation within a two-particle space is carried out, is clearly illustrated. The above method can now also be applied to any other nucleus containing either a two-particle or a two-hole configuration.

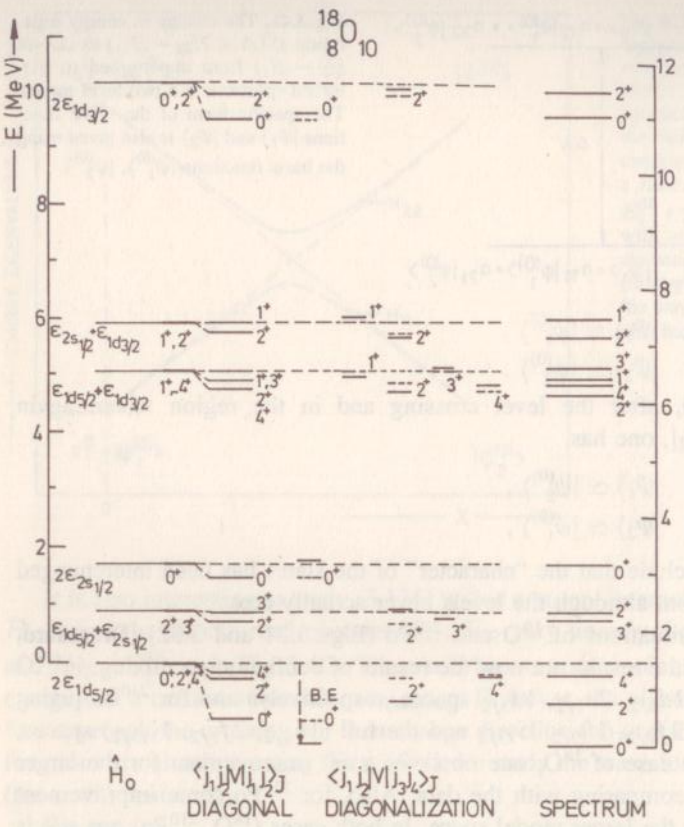


**Fig. 3.42.** Energy spectrum for $^{18}$O with two neutrons occupying the full ($sd$) model space. Besides the unperturbed energy spectrum and the various diagonal contributions, the results of diagonalizing the variou $J^\pi = 0^+, \ldots, 4^+$ matrices as well as the total spectrum are illustrated

## 3.3 Three-particle Systems and Beyond

It is our purpose to construct fully antisymmetric and normalized many-particle wave functions in order to be able, using the methods as outlined in Sect. 3.2, to obtain energy spectra and wave functions for the many-particle nuclear Schrödinger equation. We first start from the three-particle system to show the general methods before extending to the $n$-particle system.

### 3.3.1 Three-particle Wave Functions

First of all, we consider three-particle systems with the nucleons moving in the orbitals $j_a$, $j_b$ and $j_c$ [remember we use the notation $j \equiv (n, l, j)$].

i) We consider the simplest situation of $j_a \neq j_b \neq j_c$. The antisymmetrized, normalized wave function is constructed in a straightforward way as

$$\mathcal{N}\sum_P (-1)^P \psi\big((j_a(1)j_b(2))J_{12}, j_c(3); JM\big)\,, \tag{3.142}$$

where $\mathcal{N}$ is the normalization and $\sum$ means a sum over all permutations of the particle coordinates 1, 2 and 3 over the orbitals $j_a, j_b$ and $j_c$ with $(-1)^P = +1$ for an even permutation of $(1,2,3)$ and $-1$ for an odd permutation of $(1,2,3)$. So, (3.142) becomes

$$\begin{aligned}\frac{1}{\sqrt{6}}\Big\{ &\psi\big((j_a(1)j_b(2))J_{12}, j_c(3); JM\big) - \psi\big((j_a(2)j_b(1))J_{12}, j_c(3); JM\big)\\ &+\psi\big((j_a(2)j_b(3))J_{12}, j_c(1); JM\big) - \psi\big((j_a(3)j_b(2))J_{12}, j_c(1); JM\big)\\ &+\psi\big((j_a(3)j_b(1))J_{12}, j_c(2); JM\big) - \psi\big((j_a(1)j_b(3))J_{12}, j_c(2); JM\big)\Big\}\,.\end{aligned} \tag{3.143}$$

ii) We consider the case $(j_a = j_b = j) \neq j_c$. In this case, the two-particle wave function where $j_a$ and $j_b$ in (3.143) show up now contains two identical orbitals $j$. Thus, the six terms are reduced to only three terms because of the symmetry condition

$$\begin{aligned}&\psi\big((j(2)j(1))J_{12}, j_c(3); JM\big)\\ &\quad = (-1)^{2j-J_{12}}\psi\big((j(1)j(2))J_{12}, j_c(3); JM\big)\,,\end{aligned} \tag{3.144}$$

with $J_{12}$ even and $(-1)^{2j} = -1$. Thus the total wave function of (3.143) reduces to

$$\begin{aligned}\frac{1}{\sqrt{3}}\Big\{ &\psi\big((j^2(12))J_{12}, j_c(3); JM\big) - \psi\big((j^2(13))J_{12}, j_c(2); JM\big)\\ &+\psi\big((j^2(23))J_{12}, j_c(1); JM\big)\Big\}\,.\end{aligned} \tag{3.145}$$

iii) The case where all three angular momenta become equal $j_a = j_b = j_c = j$ is the most interesting one. It is possible to recouple the angular momenta in (3.145) such that the particle coordinates in the three terms always come in the sequence $1,2,3$ and in increasing order. In this case, the standard rules of angular momentum algebra when calculating matrix elements are applicable. We try to bring the second and third term in (3.145) in the order of the first term by recoupling

$$\begin{aligned}&\psi\big((j^2(23))J_{12}, j(1); JM\big)\\ &\quad = \sum_{J'_{12}} (-1)^{J_{12}} \hat{J}_{12}\hat{J}'_{12} \begin{Bmatrix} j & j & J_{12}\\ J & j & J'_{12}\end{Bmatrix} \psi\big((j^2(12))J'_{12}, j(3); JM\big)\,,\end{aligned}$$

and

$$\begin{aligned}&\psi\big((j^2(13))J_{12}, j(2); JM\big)\\ &\quad = \sum_{J'_{12}} (-1)^{J_{12}+J'_{12}+1} \hat{J}_{12}\hat{J}'_{12} \begin{Bmatrix} j & j & J_{12}\\ J & j & J'_{12}\end{Bmatrix}\\ &\qquad \times \psi\big((j^2(12))J'_{12}, j(3); JM\big)\,.\end{aligned} \tag{3.146}$$

By bringing these terms together with the first term in (3.145) we always have the particles in the order (1, 2, 3). Thus we can actually leave out the nucleon coordinates. The state thus constructed is an antisymmetric state of three particles moving in a $j$-orbital and coupled to angular momentum $J$, denoted as $\psi(j^3; JM)_{\text{as}}$. Written explicitly,

$$\psi(j^3; JM)_{\text{nas}} = \mathcal{N}' \sum_{J'_{12}\ (\text{even})} \left[ \delta_{J_{12}J'_{12}} + 2\hat{J}_{12}\hat{J}'_{12} \times \begin{Bmatrix} j & j & J_{12} \\ J & j & J'_{12} \end{Bmatrix} \right] \psi\left( (j^2(12))J'_{12}, j(3); JM \right) . \tag{3.147}$$

The expansion on the right-hand side goes over all states $J'_{12}$ where one couples a third particle $j(3)$ to an antisymmetric state of two particles in a single $j$-shell $j^2(12)J'_{12}$. The latter basis, a basis of three-particle wave functions antisymmetrized in particle coordinates 1 and 2 but not in particle coordinate 3, is much larger than the basis of three-particle states antisymmetric in all three particle coordinates. In (3.147) one writes the $\psi(j^3; JM)_{\text{nas}}$ by calculating the overlap with all states $\psi((j^2(12))J_{12}, j(3); JM)$, i.e., we project onto the subspace $\psi(j^3; JM)_{\text{nas}}$. The expansion (projection) coefficients [...] do not form a unitary transformation, therefore a special notation is used for the coefficients:

$$\psi(j^3; JM)_{\text{nas}} = \sum_{\substack{J_1 \\ \text{even}}} \left[ j^2(J_1) j J | \} j^3 J \right] \psi\left( j^2(J_1), j; JM \right) , \tag{3.148}$$

and the coefficient $[j^2(J_1)jJ|\}j^3J]$ is the cfp coefficient (coefficient of fractional parentage) giving the projection of the state $\psi(j^3; JM)_{\text{nas}}$ on the basis $\psi\left(j^2(J_1)j; JM\right)$. In the latter wave functions we leave out of the right-hand side the nucleon coordinates since they are ordered in the sequence 1, 2, 3.

As an example we discuss the case of the $(d_{5/2})^3 J$ configurations.

In making the two-particle configurations first, we have $(d_{5/2})^2$ $0^+$, $2^+$, $4^+$ configurations. Next we couple a third $d_{5/2}$ particle by just using angular momentum coupling, thereby constructing the basis $|(d_{5/2})^2 J_{12}(d_{5/2}); JM\rangle$, i.e., we have

$$\begin{aligned} &|(d_{5/2})^2_{0^+},\ d_{5/2};\ 5/2^+\rangle \\ &|(d_{5/2})^2_{2^+},\ d_{5/2};\ 1/2^+, \ldots, 9/2^+\rangle \\ &|(d_{5/2})^2_{4^+},\ d_{5/2};\ 3/2^+, \ldots, 13/2^+\rangle \end{aligned} .$$

This space has 12 states. Now using (3.147) to explicitly calculate the three-particle cfp's for the $(d_{5/2})^3 J$ configurations, for all $J_{12}$ intermediate values one keeps just 3 fully antisymmetric states with $J^\pi = 3/2^+, 5/2^+, 9/2^+$. If we call the first space $A$ (12 states) and the latter space $B$ (3 states), then $B$ is entirely within space $A$ and the states in $B$ can be expanded using the projection coefficients of the fully antisymmetric states on the basis spanning space $A$ (Fig. 3.43). Making this explicit for $(d_{5/2})^3 J$, we have

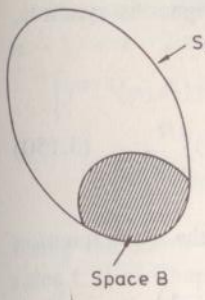


**Fig. 3.43.** Example for the construction of antisymmetric three-particle states in the $(d_{5/2})^3$ configuration. We indicate space $A$: the larger space of states $|(d_{5/2})^2 J_1,\ (d_{5/2}); JM\rangle$ antisymmetric in two-particles only and the smaller space $B$: the space $|(d_{5/2})^3; JM\rangle$ of antisymmetrized three-particle configurations. Space $(B)$ is a subspace of space $(A)$ and can be obtained via a projection

$$|(d_{5/2})^3;\ J=\tfrac{5}{2}\rangle = -\frac{\sqrt{2}}{3}|(d_{5/2})^2_{0^+},\ d_{5/2};\ 5/2^+\rangle + \frac{\sqrt{5}}{3\sqrt{2}}|(d_{5/2})^2_{2^+},\ d_{5/2};\ 5/2^+\rangle + \frac{1}{\sqrt{2}}|(d_{5/2})^2_{4^+},\ d_{5/2};\ 5/2^+\rangle\ ,$$

$$|(d_{5/2})^3;\ J=\tfrac{3}{2}\rangle = -\frac{\sqrt{5}}{\sqrt{7}}|(d_{5/2})^2_{2^+},\ d_{5/2};\ 3/2^+\rangle + \frac{\sqrt{2}}{\sqrt{7}}|(d_{5/2})^2_{4^+},\ d_{5/2};\ 3/2^+\rangle\ ,$$

$$|(d_{5/2})^3;\ J=\tfrac{9}{2}\rangle = \frac{\sqrt{3}}{\sqrt{14}}|(d_{5/2})^2_{2^+},\ d_{5/2};\ 9/2^+\rangle - \frac{\sqrt{11}}{\sqrt{14}}|(d_{5/2})^2_{4^+},\ d_{5/2};\ 9/2^+\rangle\ .$$

In describing the fully antisymmetric three-particle states as in (3.148), in most cases more than just one $J$ state can be made from the $j^3$ configuration: an extra quantum number $\alpha$ will be needed to characterize the state uniquely.

If only *one* state can be formed, $\alpha$ is not necessary. In the latter case, the wave function should be unique (except for an eventual overall phase factor) and independent of the initial two-particle spin $J_{12}$ [see (3.147)]. In making the discussion somewhat more detailed, we first normalize the states $\psi(j^3; JM)$ leading to normalized cfp coefficients

$$\left[j^2(J_1)jJ|\}j^3J\right] = \left[\delta_{J_1,J_{12}} + 2\hat{J}_1\hat{J}_{12} \begin{Bmatrix} j & j & J_1 \\ J & j & J_{12} \end{Bmatrix}\right]\left[3+6(2J_{12}+1)\begin{Bmatrix} j & j & J_{12} \\ J & j & J_{12} \end{Bmatrix}\right]^{-1/2}\ . \tag{3.149}$$

In the case $J = j$, we can start from the choice $J_{12} = 0$. For $j \leq \frac{7}{2}$ there is only one antisymmetric state $\psi(j^3;\ J = j)$ (by construction). For $j > \frac{7}{2}$, this is no longer the case.

If we now put $J_{12} = 0$, and fill in the explicit values of the Wigner $6j$-symbols, we get

$$\left[j^2(0)j\ J = j|\}j^3 J = j\right] = \left((2j-1)/\left(3(2j+1)\right)\right)^{1/2},$$
$$\left[j^2(J_1)j\ J = j|\}j^3 J = j\right] = -2\left((2J_1+1)/\left(3(2j-1)(2j+1)\right)\right)^{1/2}, \qquad (3.150)$$

with $J_1 > 0$, even.

For the case of $(d_{5/2})^3$, these expressions (3.150) reduce to the wave function

$$\psi\left((d_{5/2})^3\,(J_{12}=0),\ J=\tfrac{5}{2}\right) = \frac{\sqrt{2}}{3}\psi\left((d_{5/2})^2 J_1 = 0,\ d_{5/2};\ J=\tfrac{5}{2}\right)$$
$$-\frac{1}{3}\frac{\sqrt{5}}{\sqrt{2}}\psi\left((d_{5/2})^2 J_1 = 2,\ d_{5/2};\ J=\tfrac{5}{2}\right)$$
$$-\frac{1}{\sqrt{2}}\psi\left((d_{5/2})^2 J_1 = 4,\ d_{5/2};\ J=\tfrac{5}{2}\right). \qquad (3.151)$$

Here, we include $J_{12} = 0$ on the left-hand side to point out that we have antisymmetrized starting from the $J_{12} = 0$ two-particle state. One can now verify that starting from other states $J_{12} = 2, 4$ leads to the same wave function (3.151) multiplied by a phase of $-1$. This will no longer be the case for $j = \frac{9}{2}$ in the $(9/2)^3$ configuration where different wave functions (cfp coefficients) result when starting from $J_{12} = 0$ or from $J_{12} = 2$. In these cases, one has to construct orthonormalized states explicitly.

### 3.3.2 Extension to $n$-particle Wave Functions

Using the discussion in Sect. 3.3.1, by using the building up principle one can construct consecutively more complicated states, ending up with $n$-particle states

$$\psi(j^n\alpha; JM)_{\text{nas}} = \sum_{\alpha_1, J_1}\left[j^{n-1}(\alpha_1 J_1)jJ|\}j^n\alpha J\right]$$
$$\times\,\psi\left(j^{n-1}(\alpha_1 J_1)j; JM\right), \qquad (3.152)$$

where cfp coefficients are used to project from the fully antisymmetric $n$-particle wave functions onto the space of wave functions antisymmetric in the first $(n-1)$ particles, coupled to the $n$th particle with the use of angular momentum coupling. Thus, this is a $2 \to 3 \to \ldots\ n-1 \to n$ building up principle. One can also carry out the process by using two-particle cfp coefficients where the $\psi(j^n\alpha; JM)_{\text{nas}}$ wave functions are constructed from an antisymmetrized $(n-2)$ and an antisymmetrized 2 particle wave function. This leads to an expression of the form

$$\psi(j^n\alpha; JM)_{\text{nas}} = \sum_{\alpha_1, J_1, J_2}\left[j^{n-2}(\alpha_1 J_1)j^2(J_2)J|\}j^n\alpha J\right]$$
$$\times\,\psi\left(j^{n-2}(\alpha_1 J_1)j^2(J_2); JM\right). \qquad (3.153)$$

Here the $n \to n-2$ cfp can be expressed in terms of $n \to n-1$ and $n-1 \to n-2$ one particle cfp coefficients (see problem set) with as a result

$$\left[j^{n-2}(\alpha_1 J_1) j^2(J_2) J|\}j^n \alpha J\right] = \sum_{\alpha_1', J_1'} \left[j^{n-2}(\alpha_1 J_1) j J_1'|\}j^{n-1}\alpha_1' J_1'\right]$$

$$\times \left[j^{n-1}(\alpha_1' J_1') j J|\}j^n \alpha J\right] \hat{J}_2 \hat{J}_1' (-1)^{2j+J+J_1} \begin{Bmatrix} J_1 & j & J_1' \\ j & J & J_2 \end{Bmatrix} . \tag{3.154}$$

Using the above wave functions, we are now in a position (using the reduction rules I, II of Chap. 2 to calculate matrix elements of spherical tensor operators) to evaluate all matrix elements necessary to set up a $n$-particle energy matrix and, later on, to calculate one-body operator expectation or transition matrix elements to test the wave functions against observable nuclear properties (electromagnetic moments and transition rates, beta-decay transition probabilities, etc.).

**i) One-Body Matrix Elements.** Here, the general one-body operator for an $n$-particle system reads

$$F_\kappa^{(k)} = \sum_{i=1}^{n} f_\kappa^{(k)}(i) , \tag{3.155}$$

where $i$ denotes the particle coordinates $(\boldsymbol{r}_i, \boldsymbol{\sigma}_i, \ldots)$. We wish to evaluate the reduced $n$-particle matrix element

$$\langle j^n \alpha J \| \boldsymbol{F}^{(k)} \| j^n \alpha' J' \rangle \tag{3.156}$$

which is related to the normal matrix element $\langle j^n \alpha; JM | F_\kappa^{(k)} | j^n \alpha'; J'M' \rangle$ via the Wigner-Eckart theorem. Since $F_\kappa^{(k)}$ is a sum over $n$ particles and since $\psi(j^n \alpha; JM)$ and $\psi(j^n \alpha'; J'M')$ are antisymmetrized wave functions, one can write that

$$\begin{aligned} &\langle j^n \alpha; JM | f_\kappa^{(k)}(1) | j^n \alpha'; J'M' \rangle + \langle j^n \alpha; JM | f_\kappa^{(k)}(2) | j^n \alpha'; J'M' \rangle \\ &\quad + \ldots + \langle j^n \alpha; JM | f_\kappa^{(k)}(n) | j^n \alpha'; J'M' \rangle \\ &\quad = n \langle j^n \alpha; JM | f_\kappa^{(k)}(n) | j^n \alpha'; J'M' \rangle . \end{aligned} \tag{3.157}$$

Using the $n \to n-1$ cfp coefficients, one can separate the $(n-1)$ particle part out of the wave function and after some simple algebra obtain for the reduced matrix element of (3.156)

$$\begin{aligned} \langle j^n \alpha J \| \boldsymbol{F}^{(k)} \| j^n \alpha' J' \rangle = n \sum_{\alpha_1, J_1} &\left[j^{n-1}(\alpha_1 J_1) j J|\}j^n \alpha J\right] \\ &\times \left[j^{n-1}(\alpha_1 J_1) j J'|\}j^n \alpha' J'\right] (-1)^{J_1+j+J+k} \hat{J} \hat{J}' \\ &\times \begin{Bmatrix} j & J & J_1 \\ J' & j & k \end{Bmatrix} \langle j \| \boldsymbol{f}^{(k)} \| j \rangle . \end{aligned} \tag{3.158}$$

Thus, the $n$-particle matrix elements are expressed in terms of the one-body matrix elements $\langle j \| \boldsymbol{f}^{(k)} \| j \rangle$ only. This is an important result which we shall discuss later in some detail.

**ii) Two-Body Matrix Elements.** Here, a general two-body operator is

$$V = \sum_{i<k=1}^{n} V(i,k) \,.$$

The nuclear two-body interaction has this structure and we shall need these operators in evaluating the energy for an $n$-particle system $\langle j^n\alpha; JM|V|j^n\alpha; JM\rangle$ or calculating the matrix elements needed to solve the $n$-particle secular equation.

Using similar arguments as under (i), since the two-body operator $V = V(1,2) + V(1,3) + \ldots V(2,3) + \ldots V(n-1,n)$, is symmetric in the coordinates of the interacting nucleons and since the wave functions are antisymmetric in the interchange of the coordinates of any two nucleons, one has

$$\langle j^n\alpha; JM|V|j^n\alpha; JM\rangle = \frac{n(n-1)}{2}\langle j^n\alpha; JM|V(n-1,n)|j^n\alpha; JM\rangle \,. \quad (3.159)$$

Now, using the $n \to n-2$ cfp coefficients, (3.159) can be reduced to

$$\langle j^n\alpha; JM|V|j^n\alpha; JM\rangle = \frac{n(n-1)}{2} \sum_{\alpha_2 J_2, J'} \left[j^{n-2}(\alpha_2 J_2)j^2(J')J|\}j^n\alpha J\right]^2 \times \langle j^2; J'M'|V|j^2; J'M'\rangle \,, \quad (3.160)$$

where a reduction of the $n$-particle interaction matrix element is obtained as a linear combination of two-body matrix elements only. If we now use the total Hamiltonian for the $n$-particle system

$$H = H_0 + H_{\text{res}} = \sum_{i=1}^{n} h_0(i) + \sum_{i<j=1}^{n} V(i,j) \,, \quad (3.161)$$

the expectation value of the energy becomes

$$\langle j^n\alpha; JM|H|j^n\alpha; JM\rangle = n\varepsilon_j + \frac{n(n-1)}{2} \sum_{\alpha_2 J_2, J'} \left[j^{n-2}(\alpha_2 J_2)j^2(J')J|\}j^n\alpha J\right]^2 \langle j^2; J'M'|V|j^2; J'M'\rangle \,. \quad (3.162)$$

As we conclude this section, before discussing some applications, it becomes clear that once we know the "basic" constituents: the single-particle matrix elements $\varepsilon_j = \langle jm|h_0(i)|jm\rangle$, $\langle j\|f^{(k)}\|j\rangle$ for a general operator $f_\kappa^{(k)}$ and the two-body interaction matrix elements $\langle j^2; J'M'|V|j^2; J'M'\rangle$, by using (3.158, 162), the related $n$-particle matrix elements can be obtained in order to study $n$-particle nucleon systems when the cfp coefficients are known. Thus one can test, e.g., the consistency of the nuclear observables in the $1f_{7/2}$ shell model orbital (excitation energies, transition rates): nuclei between $^{40}_{20}\text{Ca}_{20}$ and $^{56}_{28}\text{Ni}_{28}$ starting from a single set of two-body matrix elements $\langle (1f_{7/2})^2; JM|V|(1f_{7/2})^2; JM\rangle$ and the one-body matrix elements $\langle 1f_{7/2}\|f^{(k)}\|1f_{7/2}\rangle$. This process is schematically given in Fig. 3.44.

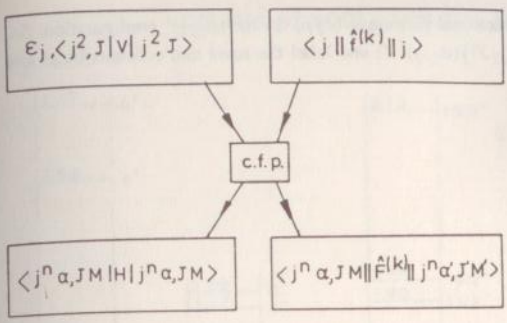


**Fig. 3.44.** Schematic illustration of how the $n$-particle properties (energy matrix elements and transition matrix elements) are related to the one- and two-body properties $\varepsilon_j$, $\langle j^2; JM|V_{1,2}|j^2; JM\rangle$ and $\langle j\|\boldsymbol{f}^{(k)}\|j\rangle$ using the cfp coefficients for a $n \to n-1 \to n-2 \to \ldots \to 2$ decomposition

**iii) Fitting One- and Two-Body Matrix Elements.** In the light of the above discussion, it is clear that (see (3.159)) two-body matrix elements in a $j^n$ configuration depend quadratically on $n$, and that one-body matrix elements (see (3.158)) in a $j^n$ configuration only depend linearly on the particle number $n$.

In order to deduce, using a fit between theoretical and experimental energies, two-body matrix elements and single-particle energies in a given mass region (the $1f_{7/2}$ shell for the Ca nuclei, the full $sd$-shell between $^{16}$O and $^{40}$Ca, ...) as precisely as possible, it is important to pay special attention to those energies in nuclei with a large number of valence nucleons $n$. On the contrary, if two-body matrix elements are fixed by the two-particle spectra in two-particle configuration only, even small deviations from the optimal values will 'propagate' through a multiplicative factor of $n^2$ in proceeding towards nuclei with a large number of valence nucleons outside of the closed shells.

### 3.3.3 Some Applications: Three-particle Systems

Starting from the discussion at the end of Sect. 3.3.2, we are now able to calculate spectra in nuclei having three particles outside a closed shell configuration. The first application, of course, is the case where only a single configuration $j$ is important.

In this case,

$$\langle j^3\alpha; JM|H|j^3\alpha; JM\rangle = 3\varepsilon_j + 3\sum_{J'}\left[j^2(J')jJ|\}j^3J\right]^2 A_{J'}\,, \tag{3.163}$$

(with $A_{J'} \equiv \langle j^2; J'M|V|j^2; J'M\rangle$), the unperturbed energy $3\varepsilon_j$ can be left out as a constant energy shift. For a $(d_{5/2})^3$ configuration, one has $J = \frac{3}{2}, \frac{5}{2}, \frac{9}{2}$ and $A_0$, $A_2$ and $A_4$. The corresponding cfp coefficients are given in Table 3.3.

Using these cfp, we obtain

$$\begin{aligned} J = \tfrac{5}{2} \quad &\to \quad \tfrac{2}{3}A_0 + \tfrac{5}{6}A_2 + \tfrac{3}{2}A_4\,, \\ J = \tfrac{3}{2} \quad &\to \quad \tfrac{15}{7}A_2 + \tfrac{6}{7}A_4\,, \\ J = \tfrac{9}{2} \quad &\to \quad \tfrac{9}{14}A_2 + \tfrac{33}{14}A_4\,. \end{aligned} \tag{3.164}$$

**Table 3.3.** The one-particle coefficients of fractional parentage ($cfp$) for the $(d_{5/2})^3$ configuration. So, we denote the coefficients as $[(d_{5/2})^2 J'\ d_{5/2} J] \{(d_{5/2})^3 J]$ and label the rows and columns by $J$ and $J'$, respectively

| $J$ \ $J'$ | 0 | 2 | 4 |
|---|---|---|---|
| $\frac{5}{2}$ | $-\frac{\sqrt{2}}{3}$ | $\frac{\sqrt{5}}{(3\sqrt{2})}$ | $\frac{1}{\sqrt{2}}$ |
| $\frac{3}{2}$ | | $-\frac{\sqrt{5}}{\sqrt{7}}$ | $\frac{\sqrt{2}}{\sqrt{7}}$ |
| $\frac{9}{2}$ | | $\frac{\sqrt{3}}{\sqrt{14}}$ | $-\frac{\sqrt{11}}{\sqrt{14}}$ |

Now, by using a residual $\delta$-interaction the two-particle matrix elements can be obtained, using (3.90) as

$$A_0 = F_0'/2\,;\ A_2 = 8/35\left(F_0'/2\right)\,;\ A_4 = 2/21\left(F_0'/2\right)\,,$$

with

$$F_0' = (2j+1)F^0 = 6F^0\,.$$

This then leads to the interaction matrix elements

$$\begin{aligned} J = \tfrac{5}{2} \quad &\rightarrow \quad F_0'/2\,, \\ J = \tfrac{3}{2} \quad &\rightarrow \quad \tfrac{4}{7}\left(F_0'/2\right)\,, \\ J = \tfrac{9}{2} \quad &\rightarrow \quad \tfrac{13}{35}\left(F_0'/2\right)\,. \end{aligned} \tag{3.165}$$

The result is shown in Fig. 3.45.

It is now possible to use the expressions (3.164) in a slightly different way. If one knows the experimental $2^+$ and $4^+$ states and their excitation energy in the nucleus with a two-particle $(d_{5/2})^2$ configuration, then one can use (3.164), but

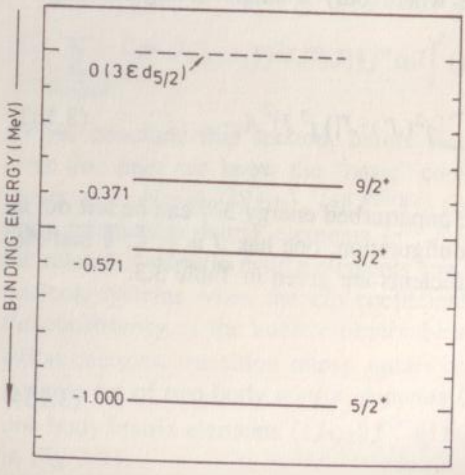


**Fig. 3.45.** The three-particle spectrum $(d_{5/2})^3$ $J^\pi$ ($J^\pi = 5/2^+,\ 3/2^+,\ 9/2^+$ expressed in terms of the two-body properties. The equations (3.165) are used with $F^0$ the Slater integral for the $\delta$-interaction. Relative to the unperturbed energy $3\varepsilon d_{5/2}$, the energies are given in units $F_0'/2$ [with $F_0' = (2j+1)F^0$]

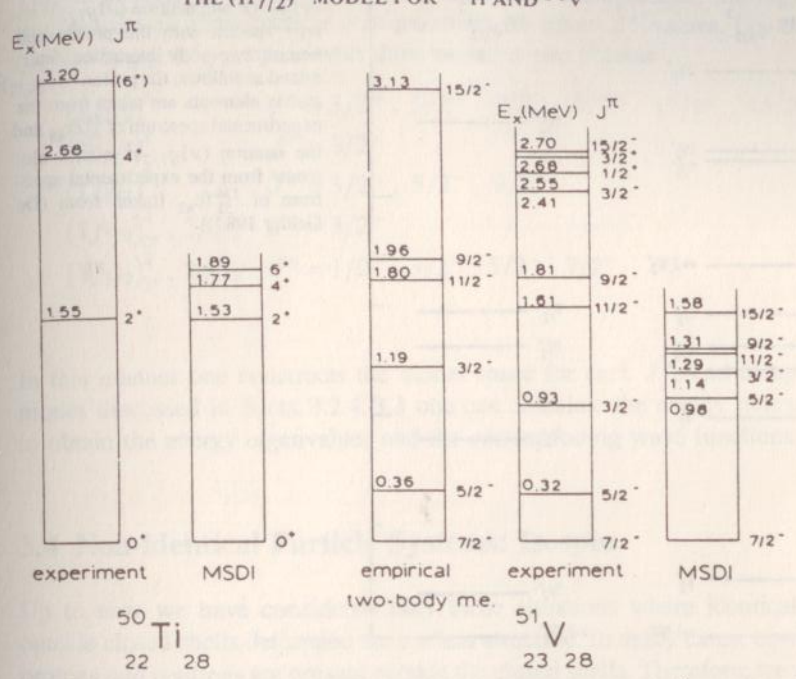


**Fig. 3.46.** The spectra of $^{50}_{22}Ti_{28}$ and $^{51}_{23}V_{28}$ for the configurations $(1f_{7/2})^2$ and $(1f_{7/2})^3$. Both the MSDI interaction (using a value of $A_{T=1} = 25/A$ MeV) and the case of two-body empirical matrix elements (taken from the experimental spectrum of $^{50}$Ti itself) are illustrated [taken from (Brussaard, Glaudemans 1977)]

now interpreting the matrix elements $A_J$ as differences from matrix elements, i.e., $A_{J'} \equiv A_J - A_0$ ($A_0$ can not be determined from experiment but the $A_{J'}$ are the relative or excitation energies for the corresponding $J$ states). Thus one obtains the relative energies in the three-particle case from the relative energies in the two-particle case (see problem set).

We illustrate this for the relation $^{50}_{22}Ti_{28} \rightarrow ^{51}_{23}V_{28}$ (Fig. 3.46) where (Brussaard, Glaudemans 1977)

i) We use theoretical values (MSDI-matrix elements $A_0, \ldots A_6$) obtained from a fit to the $^{50}_{22}$Ti spectrum in order to evaluate the $^{53}_{23}$V spectrum. Agreement is not very good.

ii) Now, using the empirical method where relative matrix elements $A'_2, \ldots A'_6$ are taken from the $^{50}_{22}$Ti experimental spectrum, agreement becomes rather good. This latter point proves that the spectra in $^{50}$Ti-$^{51}$V are rather consistent with a single $1f_{7/2}$ shell model configuration using an empirical set of two-body matrix elements.

This discussion illustrates very well the methods discussed in Sect. 3.2.2.

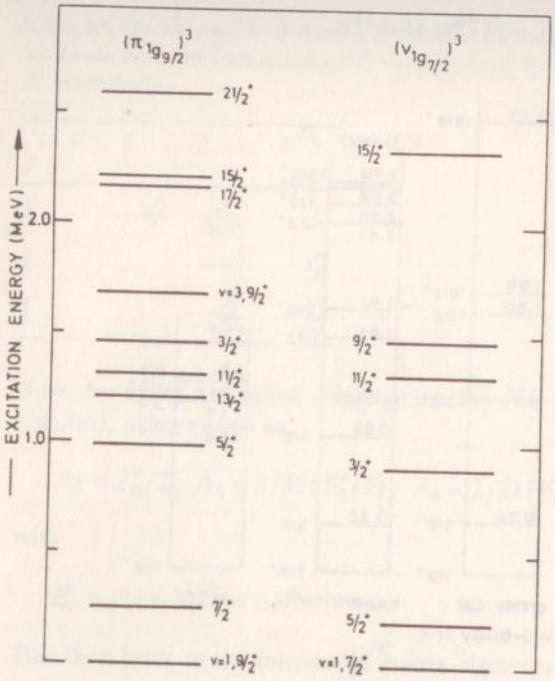


**Fig. 3.47.** We show the proton $(\pi 1g_{9/2})^3$ and neutron $(\nu 1g_{7/2})^3$ energy spectra with the proton and neutron two-body interaction determined as follows: the proton $(\pi 1g_{9/2})^2$ matrix elements are taken from the experimental spectrum of $^{88}_{40}Zr_{48}$ and the neutron $(\nu 1g_{7/2})^2$ matrix elements from the experimental spectrum of $^{134}_{52}Te_{82}$ [taken from (De Gelder 1980)]

**Table 3.4.** The $cfp$ coefficients $[(f_{7/2})^2 J'\ f_{7/2} J|](f_{7/2})^3 J]$ for the three particle configurations. We denote the rows and columns by $J$ and $J'$, respectively [taken from (Brussaard, Glaudemans 1977)]

| $J$ | $J'=0$ | $J'=2$ | $J'=4$ | $J'=6$ |
|---|---|---|---|---|
| $\frac{3}{2}$ | 0 | 0.463 | −0.886 | 0.000 |
| $\frac{5}{2}$ | 0 | 0.782 | 0.246 | −0.573 |
| $\frac{7}{2}$ | 0.500 | −0.373 | −0.500 | −0.601 |
| $\frac{9}{2}$ | 0 | 0.321 | −0.806 | 0.497 |
| $\frac{11}{2}$ | 0 | 0.527 | −0.444 | −0.725 |
| $\frac{15}{2}$ | 0 | 0.000 | 0.477 | −0.879 |

We further illustrate three-particle spectra for some higher $j$ orbitals: the proton $(1g_{9/2})^3$ spectrum and the neutron $(1g_{7/2})^3$ spectrum (Fig. 3.47), (Table 3.4) (De Gelder et al. 1980).

From all the above illustrations, it is clear that the lowest-lying state is always the $(j)^3 J = j$ state. This is easily explained since only for this $J = j$ state does the cfp for the intermediate two-particle $0^+$ state occur. Now, the $0^+$ two-particle matrix elements are by far the largest attractive matrix elements and still appear in the three-particle spectra via the cfp coefficients.

In the above situation, if we consider besides the $1f_{7/2}$ orbital also the relatively close-lying $2p_{3/2}$ and $1f_{5/2}$ orbitals, a more complicated situation results.

This is because as in the two-particle case with configuration mixing, we have to construct all three-particle configurations for given $J^\pi$ values. For the present $(1f_{7/2}, 2p_{3/2}, 1f_{5/2})$ space with three particles one obtains

$$
\begin{array}{ll}
(1f_{7/2})^3 & J^\pi = 3/2^-,\ 5/2^-,\ 7/2^-,\ 9/2^-,\ 11/2^-,\ 15/2^- \\
(2p_{3/2})^3 & J^\pi = 3/2^- \\
(1f_{5/2})^3 & J^\pi = 3/2^-,\ 5/2^-,\ 9/2^- \\
(1f_{7/2})^2_{0^+},\ 2p_{3/2} & J^\pi = 3/2^- \\
(1f_{7/2})^2_{2^+},\ 2p_{3/2} & J^\pi = 1/2^-,\ 3/2^-,\ 5/2^-,\ 7/2^- \\
\vdots &
\end{array}
$$

In this manner one constructs the model space for each $J^\pi$, and using the techniques discussed in Sects. 3.2.4, 3.3 one can calculate the energy matrix in order to obtain the energy eigenvalues and the corresponding wave functions.

## 3.4 Non-identical Particle Systems: Isospin

Up to now we have considered only those situations where identical nucleons outside closed shells determine the nuclear structure. In many cases, however, both protons *and* neutrons are present outside the closed shells. Therefore, we would like to construct an extension of the methods outlined above so that the same general structure remains. We shall introduce the concept of "charge" quantum number or "isospin" quantum number, depending on which nuclei we are treating. Before constructing the nuclear wave functions including this new quantum number, we shall point out the evidence that exists in nuclear properties to introduce the concept of isospin as a valuable quantum number.

### 3.4.1 Isospin: Introduction and Concepts

Protons and neutrons have almost identical mass ($\Delta m/m \cong 1.4 \times 10^{-3}$). In addition, they show an almost identical behavior in their nuclear interactions. In 1932, Heisenberg proposed to consider protons and neutrons as two distinct forms of "nucleons", by using a double-valued variable called isospin that distinguishes between the "proton" state (described by a projection quantum number $t_z = -\frac{1}{2}$) and a "neutron" state (described by a projection quantum number $t_z = +\frac{1}{2}$) (Heisenberg 1932). The isospin (or isotopic spin) formalism can now be duplicated from the properties we studied in Chaps. 1, 2 on intrinsic spin ($s$) of the proton and the neutron. We first present some of the experimental evidence for the equivalence of protons and neutrons in their nuclear interactions.

i) Low energy $np$ scattering and $pp$ scattering below $E < 5\,\text{MeV}$, after correcting for Coulomb effects, is equal within a few percent in the $^1S$ scattering channel (Arndt, MacGregor 1966, Wright et al. 1967, MacGregor et al. 1968a, b).

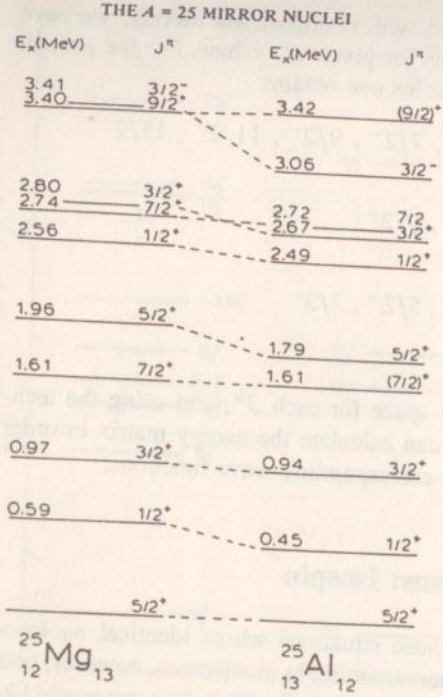


**Fig. 3.48.** A comparison of the level schemes of the $A = 25$ ($^{25}$Mg-$^{25}$Al) mirror nuclei shows the close similarity of the excitation energies for the states with identical $J^\pi$ values [taken from (Brussaard, Glaudemans 1977)]

ii) Energy spectra in "mirror" nuclei are almost identical (Fig. 3.48). The small differences are both a consequence of the difference in the Coulomb interaction energy and of specific nuclear wave functions. From this observation one concluded that the exchange of protons and neutrons gives no modification of the nuclear interaction energy or, that the substitution $n - n \Leftrightarrow p - p$; $n - p \Leftrightarrow p - n$ does not modify the interaction energy. This observation implies the concept of *charge symmetry* in nuclear forces.

iii) Further information on how the $n - n$, $p - p$ forces relate to the $n - p$ force cannot be deduced from mirror nuclei. If we, therefore, study the triplet of nuclei, e.g., $^{30}_{14}\mathrm{Si}_{16}$, $^{30}_{15}\mathrm{P}_{15}$, $^{30}_{16}\mathrm{S}_{14}$, it is immediately clear that within a number of states $(0^+, 2^+)$ (after correcting for Coulomb energies) the nuclear binding energies are equal in all three nuclei. From this observation a new characteristic of the nuclear forces can be deduced. Taking as a core $^{28}_{14}\mathrm{Si}_{14}$, the data show that the residual interaction energies due to $n-n$, $p-p$ and $n-p$ interactions are equal in a number of states (Fig. 3.49). The above leads to an even more stringent condition than obtained from (ii), i.e., *charge independence* in nuclear configurations that are possible in an $n-n$, $n-p$ and $p-p$ interacting system. A number of states in $^{30}$P do not find a partner in the $^{30}$Si, $^{30}$S nuclei. This follows from the Pauli principle that excludes the realization of a number of configurations in identical nucleon systems $(n - n, p - p)$ compared to the $n - p$ (non-identical nucleons) system. Thus the Pauli principle explains the large number of extra states in $^{30}$P, as shown in Fig. 3.49.

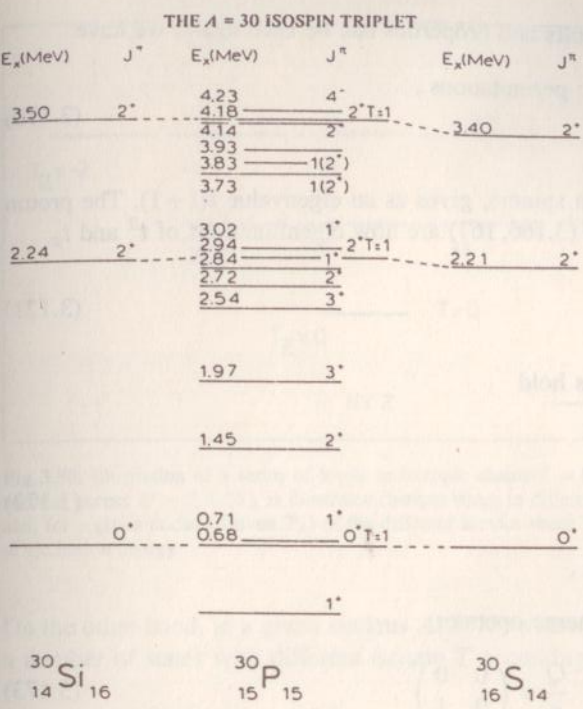


**Fig. 3.49.** The level spacings between the $T = 1$ isospin states in the mass $A = 30$ chain ($^{30}$Si-$^{30}$P-$^{30}$S) are very similar to the corresponding spacings in $^{30}$Si, $^{30}$P and $^{30}$S. The states in $^{30}$P where isospin is not given are the isospin $T = 0$ states [taken from (Brussaard, Glaudemans 1977)]

### 3.4.2 Isospin Formalism

#### a) General Properties of Isospin

We describe the neutron and proton by using a two-valued quantity just like the intrinsic spin, but now in isospin space:

$$\varphi_n(\boldsymbol{r}) = \varphi(\boldsymbol{r}) \begin{pmatrix} 1 \\ 0 \end{pmatrix} , \tag{3.166}$$

$$\varphi_p(\boldsymbol{r}) = \varphi(\boldsymbol{r}) \begin{pmatrix} 0 \\ 1 \end{pmatrix} , \tag{3.167}$$

where $\varphi(\boldsymbol{r})$ describes the spatial wave function which is the same for the proton and the neutron in the present case.

As for intrinsic spin, we can introduce Pauli isospin matrices $\boldsymbol{\tau}(\tau_x, \tau_y, \tau_z)$

$$\tau_x = \begin{pmatrix} 0 & 1 \\ 1 & 0 \end{pmatrix} ; \tau_y = \begin{pmatrix} 0 & -\mathrm{i} \\ \mathrm{i} & 0 \end{pmatrix} ; \tau_z = \begin{pmatrix} 1 & 0 \\ 0 & -1 \end{pmatrix} , \tag{3.168}$$

and define the isospin ($t = \frac{1}{2}$) operator as

$$\boldsymbol{t} = \frac{\boldsymbol{\tau}}{2} . \tag{3.169}$$

All other spin $\frac{1}{2}$ algebra results and properties can be used again: we have

$$\begin{aligned} &[t_x, t_y] = it_z, \text{ and cyclic permutations}, \\ &[\boldsymbol{t}^2, t_i] = 0, \; i = x, y, z, \end{aligned} \tag{3.170}$$

and $\boldsymbol{t}^2$, acting on the isospin spinors, gives as an eigenvalue $t(t+1)$. The proton and neutron wave functions (3.166, 167) are now eigenfunctions of $\boldsymbol{t}^2$ and $t_z$

$$\begin{aligned} t_z\varphi_p(\boldsymbol{r}) &= -\tfrac{1}{2}\varphi_p(\boldsymbol{r}), \\ t_z\varphi_n(\boldsymbol{r}) &= \tfrac{1}{2}\varphi_n(\boldsymbol{r}). \end{aligned} \tag{3.171}$$

Now, the following relations hold

$$\begin{aligned} &\tfrac{1}{2}(1-\tau_z)\varphi_p(\boldsymbol{r}) = \varphi_p(\boldsymbol{r}), \\ &\tfrac{1}{2}(1+\tau_z)\varphi_p(\boldsymbol{r}) = 0, \\ &\tfrac{1}{2}(1-\tau_z)\varphi_n(\boldsymbol{r}) = 0, \\ &\tfrac{1}{2}(1+\tau_z)\varphi_n(\boldsymbol{r}) = \varphi_n(\boldsymbol{r}), \end{aligned} \tag{3.172}$$

and we can introduce the charge operator

$$\frac{Q}{e} \equiv \frac{1}{2}(1-\tau_z) \quad \text{with} \quad \frac{Q}{e} = \begin{pmatrix} 0 & 0 \\ 0 & 1 \end{pmatrix}. \tag{3.173}$$

The ladder operator properties hold here, too, and change proton into neutron states ($t_+$) or neutron into proton states ($t_-$), respectively:

$$\begin{aligned} t_+\varphi_p(\boldsymbol{r}) &= \varphi_n(\boldsymbol{r}), \\ t_+\varphi_n(\boldsymbol{r}) &= 0, \\ t_-\varphi_n(\boldsymbol{r}) &= \varphi_p(\boldsymbol{r}), \\ t_-\varphi_p(\boldsymbol{r}) &= 0. \end{aligned} \tag{3.174}$$

Extending to a many-nucleon system, the total isospin operators are constructed according to the methods of adding angular momenta (Chap. 2) and we obtain

$$\begin{aligned} \boldsymbol{T} &= \sum_{i=1}^{A} \boldsymbol{t}_i \\ T_z &= \sum_{i=1}^{A} t_{z,i}. \end{aligned} \tag{3.175}$$

Acting on a many-nucleon eigenstate, the eigenvalues of $\boldsymbol{T}^2$ are $T(T+1)$ with $-T \leq T_z \leq +T$. The total isospin will be integer or half-integer according to whether $A$ is even or odd. For each $T$ value, there exists an isospin multiplet with $2T+1$ members, characterized by the $z$-component $T_z$ since $T_z$ varies from $-T$ to $+T$. The eigenvalue of $T_z$ according to its definition in (3.175) becomes $\frac{1}{2}(N-Z)$.

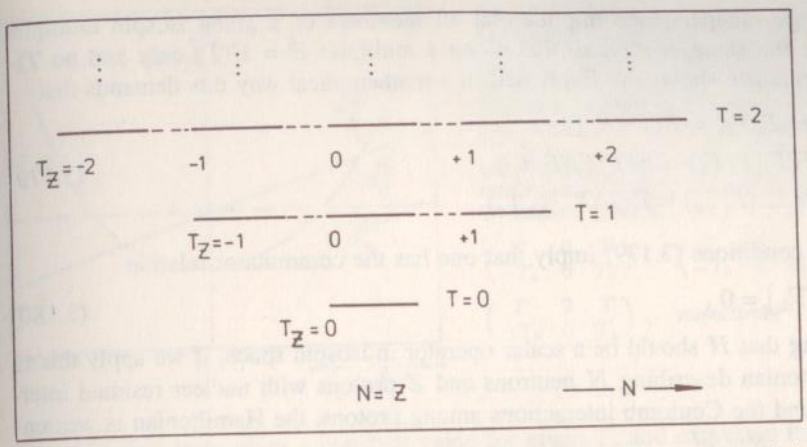


**Fig. 3.50.** Illustration of a series of levels in isotopic chains $T = 0, 1, 2, \ldots$ . The variation with the neutron excess $N - Z = 2T_z$ is illustrated (isospin states in different nuclei of a given mass $A$ chain) and, for a given nucleus (given $T_z$) of the different isospin states $T$ ($|T_z| \leq T \leq A/2$) as a function of excitation energy

On the other hand, in a given nucleus $A(Z, N)$ with a given $T_z$ value one can find a number of states with different isospin $T$ according to the conditions

$$T = |T_z|\,,\ |T_z| + 1\,,\ \ldots\,,\ \frac{A}{2}\,.$$

This multiplet structure is illustrated in Fig. 3.50 for a number of nuclei. The different members of an isospin multiplet denoted by the eigenvector $|T, T_z\rangle$ are connected via the ladder operators

$$T_\pm = T_x \pm \mathrm{i}T_y = \sum_{i=1}^{A} t_\pm(i)\,, \tag{3.176}$$

and give as a result

$$T_\pm |T, T_z\rangle = \left[T(T+1) - T_z(T_z \pm 1)\right]^{1/2} |T, T_z \pm 1\rangle\,. \tag{3.177}$$

Consecutive action of $T_\pm$ changes $T_z$ but does not affect the isospin $T$. This means that within an isospin multiplet the spin-spatial wave function remains constant; only the charge part changes as is expressed in the $|T, T_z\rangle$ eigenvectors.

We now try to express the charge symmetry and charge independence properties of the nuclear interactions in a more formal way.

i) Conservation of charge implies

$$[H, T_z] = 0\,, \tag{3.178}$$

ii) Charge independence implies that all members of a given isospin multiplet have the same energy, so that along a multiplet $E = E(T)$ only and no $T_z$-dependence shows up. Expressed in a mathematical way this demands that

$$\begin{aligned} H|T,T_z\rangle &= E(T)|T,T_z\rangle\,, \\ HT_+|T,T_z\rangle &= E(T)T_+|T,T_z\rangle\,, \\ HT_-|T,T_z\rangle &= E(T)T_-|T,T_z\rangle\,. \end{aligned} \tag{3.179}$$

The conditions (3.179) imply that one has the commutator relation

$$[H,T_\pm] = 0\,, \tag{3.180}$$

indicating that $H$ should be a scalar operator in isospin space. If we apply this to a Hamiltonian describing $N$ neutrons and $Z$ protons with nuclear residual interactions and the Coulomb interactions among protons, the Hamiltonian is written

$$\begin{aligned} H = &-\sum_{i=1}^{N}\frac{\hbar^2}{2m_n}\Delta(n) - \sum_{i=N+1}^{A}\frac{\hbar^2}{2m_p}\Delta(p) \\ &+\frac{1}{2}\sum_{i,j=1}^{A}V(i,j) + \sum_{i<k=1}^{Z}\frac{e^2}{|\boldsymbol{r}_i-\boldsymbol{r}_j|} \end{aligned} \tag{3.181}$$

$$\begin{aligned} H \cong &-\sum_{i=1}^{A}\frac{\hbar^2}{2m}\Delta_i + \sum_{i=1}^{A}\frac{\hbar^2}{m^2}t_z(i)\cdot\Delta m\Delta_i + \frac{1}{2}\sum_{i,j=1}^{A}V(i,j) \\ &+\sum_{i<j=1}^{A}\frac{e^2}{4|\boldsymbol{r}_i-\boldsymbol{r}_j|} - \sum_{i<j=1}^{A}\frac{e^2}{2}\big(t_z(i)+t_z(j)\big)/|\boldsymbol{r}_i-\boldsymbol{r}_j| \\ &+\sum_{i<j=1}^{A}e^2t_z(i)t_z(j)/|\boldsymbol{r}_i-\boldsymbol{r}_j|\,. \end{aligned} \tag{3.182}$$

In the second expression $m = (m_n + m_p)/2$ and $\Delta m$ is the difference $\Delta m = |m_n - m| = |m_p - m|$. Here one observes that the Hamilton operator is not a scalar in isospin space but contains terms that are the $T_z = 0$ component of an isospin vector (rank 1) and of an isospin tensor (rank 2), indicating that the actual many nucleon Hamiltonian is not fully charge independent. In shorthand,

$$H = H_0^{(2)} + H_0^{(1)} + H_0^{(0)}\,, \tag{3.183}$$

in rank (2) (1) (0) with $T_z = 0$ in each case.

From this general Hamiltonian, an energy expression can easily be obtained as

$$\begin{aligned} \langle T,T_z|H|T,T_z\rangle = &(-1)^{T-T_z}\begin{pmatrix} T & 0 & T \\ -T_z & 0 & T_z \end{pmatrix}\langle T\|\boldsymbol{H}^{(0)}\|T\rangle \\ &+(-1)^{T-T_z}\begin{pmatrix} T & 1 & T \\ -T_z & 0 & T_z \end{pmatrix}\langle T\|\boldsymbol{H}^{(1)}\|T\rangle \\ &+(-1)^{T-T_z}\begin{pmatrix} T & 2 & T \\ -T_z & 0 & T_z \end{pmatrix}\langle T\|\boldsymbol{H}^{(2)}\|T\rangle\,. \end{aligned} \tag{3.184}$$

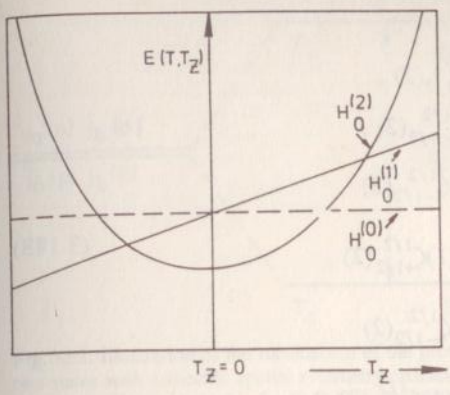


**Fig. 3.51.** Variation of the energy $E(T,T_z) \equiv \langle T,T_z|H|T,T_z\rangle$ with $T_z\,(=(N-Z)/2)$. The different contributions from (3.184) are illustrated: the constant energy coming from the $H_0^{(0)}$ part (isoscalar contribution), the linear term coming from the $H_0^{(1)}$ (isovector) term and the quadratic term coming from the $H_0^{(2)}$ (tensor of rank 2) term. The dependence on $T_z$ (for a given $T$) values is given by

$$\begin{pmatrix} T & 0 & T \\ -T_z & 0 & T_z \end{pmatrix}, \quad \begin{pmatrix} T & 1 & T \\ -T_z & 0 & T_z \end{pmatrix},$$

$$\begin{pmatrix} T & 2 & T \\ -T_z & 0 & T_z \end{pmatrix}, \quad \text{respectively}$$

Here, the first term gives a constant value for given $T$, and expresses the charge independent part of $H$. The second term (coming from the mass difference in the kinetic energies of protons and neutrons and from the Coulomb term) induces a linear dependence on $T_z$, and the third term (Coulomb effect) introduces a quadratic $T_z$ dependence. The total dependence is shown schematically in Fig. 3.51 for $(T,T_z)$.

Taking into account the explicit values of the different Wigner $3j$-symbols appearing in (3.184), an energy formula results for the different $|T,T_z\rangle$ members of an isospin multiplet as

$$\begin{aligned} E(T,T_z) &= \langle T,T_z|H|T,T_z\rangle\,, \\ &= a(T) + b(T)T_z + c(T)T_z^2\,. \end{aligned} \tag{3.185}$$

The coefficients $a(T)$, $b(T)$ and $c(T)$ are specific for a given $T$-value and the full expression of $E(T,T_z)$ is a quadratic function in $T_z$. More examples of such simple energy or mass relations have also been obtained in other domains of physics (Gell-Mann (1962), Okubo (1962)) and will be discussed as realizations of a given dynamical symmetry that is present in the Hamiltonian describing the interacting fermion (boson) $A$-body system (see discussion in Chap. 7).

### b) Isospin Wave Functions

We first construct the two-nucleon isospin wave functions by using

$$\begin{aligned} \varphi_n(\boldsymbol{r}) &= \zeta_{+1/2}^{1/2} \cdot \varphi(\boldsymbol{r}) \\ \varphi_p(\boldsymbol{r}) &= \zeta_{-1/2}^{1/2} \cdot \varphi(\boldsymbol{r})\,, \end{aligned} \tag{3.186}$$

with $\zeta_{t_z}^{1/2}$ the isospin spinors formally corresponding to the spin eigenvectors $\chi_{m_s}^{1/2}$.

For the two-nucleon isospin eigenvectors, we construct

$$\zeta\left(\tfrac{1}{2}\,\tfrac{1}{2}\,;TT_z\right) = \sum_{t_z,t_z'} \langle \tfrac{1}{2}t_z,\ \tfrac{1}{2}t_z'|TT_z\rangle \zeta_{t_z}^{1/2}(1)\zeta_{tz'}^{1/2}(2)\,, \tag{3.187}$$

or

$$\begin{aligned}
\zeta\left(\tfrac{1}{2}\,\tfrac{1}{2}\,;T=1,T_z=+1\right) &= \zeta^{1/2}_{+1/2}(1)\zeta^{1/2}_{+1/2}(2)\,,\\
\zeta\left(\tfrac{1}{2}\,\tfrac{1}{2}\,;T=1,T_z=-1\right) &= \zeta^{1/2}_{-1/2}(1)\zeta^{1/2}_{-1/2}(2)\,,\\
\zeta\left(\tfrac{1}{2}\,\tfrac{1}{2}\,;T=1,T_z=0\right) &= \frac{1}{\sqrt{2}}\zeta^{1/2}_{+1/2}(1)\zeta^{1/2}_{-1/2}(2)\\
&\quad+\frac{1}{\sqrt{2}}\zeta^{1/2}_{-1/2}(1)\zeta^{1/2}_{+1/2}(2)\,,\\
\zeta\left(\tfrac{1}{2}\,\tfrac{1}{2}\,;T=0,T_z=0\right) &= \frac{1}{\sqrt{2}}\zeta^{1/2}_{+1/2}(1)\zeta^{1/2}_{-1/2}(2)\\
&\quad-\frac{1}{\sqrt{2}}\zeta^{1/2}_{-1/2}(1)\zeta^{1/2}_{+1/2}(2)\,,
\end{aligned} \tag{3.188}$$

written explicitly. The first gives a two-neutron, the second a two-proton wave function. The other two are linear combinations for a proton-neutron wave function, however, with a specific symmetry for the interchange of the quantum numbers of the nucleons: $T = 1$ symmetric and $T = 0$ antisymmetric.

Consider now the more general case of a proton moving in the orbital $(j_a, m_a)$ and a neutron moving in the orbital $(j_b, m_b)$. The wave function describing this particular situation reads

$$\psi_{pn}(j_a j_b; JM) = \sum_{m_a,m_b} \langle j_a m_a, j_b m_b | JM\rangle \varphi_{j_a m_a}(\boldsymbol{r}_p)\varphi_{j_b m_b}(\boldsymbol{r}_n)\,. \tag{3.189}$$

In the nuclear potential (in particular for light and for medium heavy nuclei) the situation with a proton moving in the orbital $(j_b, m_b)$ and a neutron in the orbital $(j_a, m_a)$ is almost degenerate in the former case. This tells us that the two configurations,

$$\begin{aligned}
&\psi_{pn}(j_a j_b; JM)\,,\\
&\psi_{np}(j_a j_b; JM)\,,
\end{aligned} \tag{3.190}$$

are almost degenerate in energy. If we now diagonalize the residual proton-neutron interaction $V_{pn}$, the degeneracy in (3.190) will be lifted and we get two states with given symmetry $\psi^{\pm}_{pn}(j_a j_b; JM)$

$$\begin{aligned}
\psi^{\pm}_{pn}(j_a j_b; JM) &= N \sum_{m_a,m_b} \langle j_a m_a, j_b m_b | JM\rangle\\
&\times \left\{\varphi_{j_a m_a}(\boldsymbol{r}_p)\varphi_{j_b m_b}(\boldsymbol{r}_n) \pm \varphi_{j_a m_a}(\boldsymbol{r}_n)\varphi_{j_b m_b}(\boldsymbol{r}_p)\right\}\,,
\end{aligned} \tag{3.191}$$

and we can also evaluate the energy shift between the states with different symmetry $\Delta E^{\pm}_J$ (Fig. 3.52). In (3.191), in contrast to (3.189) and (3.190), the index $pn$ of the wave function $\Psi^{\pm}_{pn}(j_a j_b; JM)$ simply indicates that we are still describing a proton and a neutron, but the information regarding a precize localization in a given single-particle orbital is lost through the diagonalization process. One calls

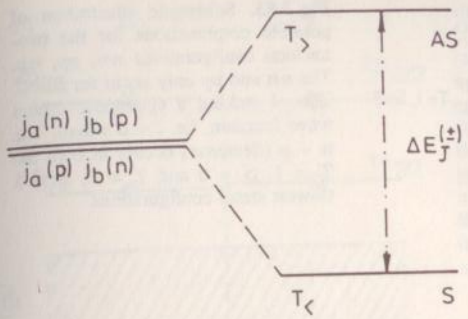


**Fig. 3.52.** Illustration of the mechanism of the proton-neutron interaction establishing the formation of two states with a specific spatial symmetry character. Starting from the *two* unperturbed configurations $\psi_{\mathrm{pn}}(j_a j_b; JM)$ and $\psi_{\mathrm{np}}(j_a j_b; JM)$ [see (3.190)], the proton-neutron force generates a symmetric (S) and antisymmetric (AS) state [see (3.191)]. The lower, symmetric state corresponds to the isospin $T_<$ (lower isospin, $T = 0$ for two-particle state) and the upper, antisymmetric state corresponds to the isospin $T_>$ (upper isospin, $T = 1$ for two-particle state). The energy separation is denoted by $\Delta E_J^{(\pm)}$

the low-lying state with the spatial symmetric wave function the $T_<$ state (lower isospin; $T = 0$ for a two-particle system) and the high-lying state with the spatial antisymmetric wave function the $T_>$ state (upper isospin; $T = 1$ for a two-particle system). Using now the two-particle isospin wave functions of (3.188), one can rewrite (3.191) as

$$
\begin{aligned}
& N \sum_{m_a, m_b} \langle j_a m_a, j_b m_b | JM \rangle \\
& \quad \times \Big( \varphi_{j_a m_a}(1) \varphi_{j_b m_b}(2) \\
& \quad \pm \varphi_{j_a m_a}(2) \varphi_{j_b m_b}(1) \Big) \zeta_{-1/2}^{1/2}(1) \zeta_{+1/2}^{1/2}(2) \, .
\end{aligned}
\tag{3.192}
$$

If we now exchange the coordinates of particles 1 and 2 in (3.192), the physical content of the wave function remains identical. Thus we get extra information that can be removed by making linear combinations of (3.192), and (3.192) with $1 \Leftrightarrow 2$ interchanged. We make linear combinations such that the final wave functions obey a generalized exclusion principle: antisymmetry with respect to *all* (spatial, spin, isospin) coordinates. Remember that this is *not* an extra assumption but just a convenient formalism that allows us to handle $n - n$, $p - p$ and $n - p$ systems consistently. The above combinations are now constructed as (using $a \equiv j_a, m_a, \ldots$)

$$
\begin{aligned}
\psi_{\mathrm{pn}}^{+}(j_a j_b; JM) &= \frac{N}{\sqrt{2}} \sum \langle \ldots | \ldots \rangle \\
&\quad \times \big( \varphi_a(1) \varphi_b(2) + \varphi_a(2) \varphi_b(1) \big) \zeta\big(T = 0, T_z = 0\big) \, , \\
\psi_{\mathrm{pn}}^{-}(j_a j_b; JM) &= \frac{N}{\sqrt{2}} \sum \langle \ldots | \ldots \rangle \\
&\quad \times \big( \varphi_a(1) \varphi_b(2) - \varphi_a(2) \varphi_b(1) \big) \zeta\big(T = 1, T_z = 0\big) \, ,
\end{aligned}
\tag{3.193}
$$

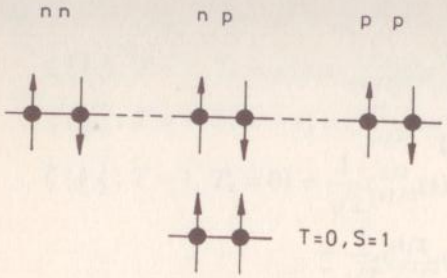


**Fig. 3.53.** Schematic illustration of possible combinations for the two-nucleon configurations $nn$, $pp$, $np$. The $nn$ and $pp$ only occur for $S = 0$, $T = 1$ (taking a symmetric orbital wave function, i.e. $l = 0$ wave). The $n - p$ (deuteron) occurs in both the $T = 1$, $S = 0$ and $T = 0$, $S = 1$ (lowest state) configurations

$$\psi_{\mathrm{pp}}(j_a j_b; JM) = \frac{N}{\sqrt{2}} \sum \langle \ldots | \ldots \rangle$$
$$\times \left(\varphi_a(1)\varphi_b(2) - \varphi_a(2)\varphi_b(1)\right)\zeta\left(T = 1,\, T_z = -1\right),$$
$$\psi_{\mathrm{nn}}(j_a j_b; JM) = \frac{N}{\sqrt{2}} \sum \langle \ldots | \ldots \rangle$$
$$\times \left(\varphi_a(1)\varphi_b(2) - \varphi_a(2)\varphi_b(1)\right)\zeta\left(T = 1,\, T_z = 1\right).$$

In the above, we have either a symmetric spatial-spin function ($S$) and an antisymmetric isospin function $\zeta(T = 0,\, T_z = 0)$ or an antisymmetric spatial-spin function ($AS$) and a symmetric isospin function $\zeta(T = 1,\, T_z)$ (see Fig. 3.53 for application to the deuteron). Note once again that we could have studied nuclei without using the generalized Pauli principle with isospin, but simply by using the charge quantum numbers.

The outcome of constructing *all* basis configurations according to the proton-neutron valence numbers, is, however, in line with the isospin results.

To illustrate, we take the example of a light nucleus $^{42}_{21}\mathrm{Sc}_{21}$ where we consider possible proton-neutron configurations (Fig. 3.54). Besides the $1f_{7/2}(p)\ 2p_{3/2}(n)$ basis state, we shall also have to take the $1f_{7/2}(n)\ 2p_{3/2}(p)$ basis state into account. In this small model space diagonalizing the nucleon-nucleon force, one ends up with two classes of states: one set with a symmetric wave function in the interchange of the charge coordinates, ($T = 1$) states that are high in energy, and another set with antisymmetric wave functions ($T = 0$) that are low in energy. Thus, if $\varepsilon_{1f_{7/2}}(p) = \varepsilon_{1f_{7/2}}(n)$, $\varepsilon_{2p_{3/2}}(p) = \varepsilon_{2p_{3/2}}(n)$ and all matrix elements are exactly charge independent, the coefficients in the $S$ and $AS$ combination will be equal to $1/\sqrt{2}$, thus again forming the isospin structure. Slight differences in the above conditions will induce some isospin mixing and thus, depending on whether one likes charge-quantum numbers or isospin, constitutes a convenient basis for obtaining the same physics.

If we now move to heavy nuclei with a neutron excess, the underlying principles in constructing isospin cannot be used easily since configurations $\psi_{\mathrm{pn}}(j_a j_b; JM)$ and $\psi_{\mathrm{np}}(j_a j_b; JM)$ are not at *all* degenerate any more: it costs a lot of energy to create the "exchanged" state and isospin can be heavily broken for low-lying states (Fig. 3.55). Here, one should better use a charge quantum number formalism. It is, however, possible to define certain states that correspond to a good isospin, i.e., configurations with two valence protons in orbitals that

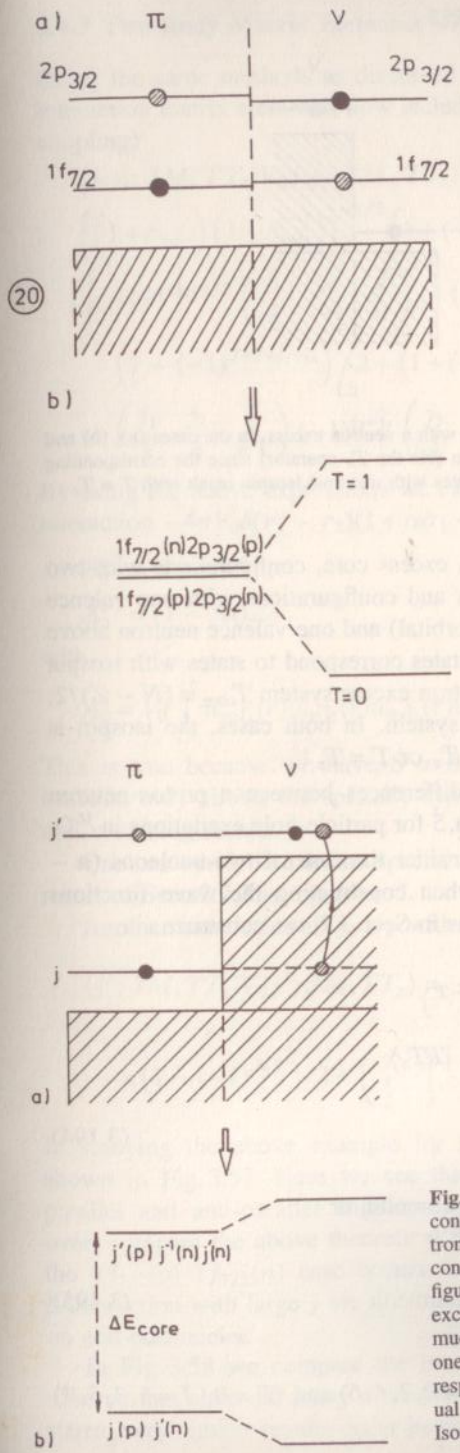


**Fig. 3.54a, b.** Illustration how, for a nucleus like $^{42}_{21}Sc_{21}$, the isospin $T = 0$ and $T = 1$ states can be realized for the $1f_{7/2}\,2p_{3/2}$ configuration. **(a)** In the upper part we show the two possible, almost degenerate proton-neutron configurations $\pi 1f_{7/2}\ \nu 2p_{3/2}$ (•) and $\nu 1f_{7/2}\ \pi 2p_{3/2}$ (⊘) configurations. **(b)** In the lower part, we indicate how the two, nearly degenerate configurations form specific linear combinations when diagonalizing $V_{p,n}$. The lowest state, the $T = 0$ state, gives a symmetric spatial state, the upper one, the $T = 1$ state, corresponds to an antisymmetric spatial state

**Fig. 3.55.** Construction, as in Fig. 3.54, for proton-neutron configurations, but now for heavy nuclei with a large neutron excess **(a)**. In the upper part, we have the $\pi j\ \nu j'$ configuration. Due to the neutron excess, the $\nu j\ \pi j'$ configuration does not exist, instead we have to make a core excited state $(\nu j)^{-1}\,(\nu j')\,\pi j'$. The latter state occurs at a much higher excitation energy compared with the former one. In the lower part **(b)** we illustrate these two states corresponding to a large energy difference $\Delta E_{\text{core}}$. The residual interaction $V_{p,n}$ will only induce minor admixtures. Isospin is not needed to be introduced

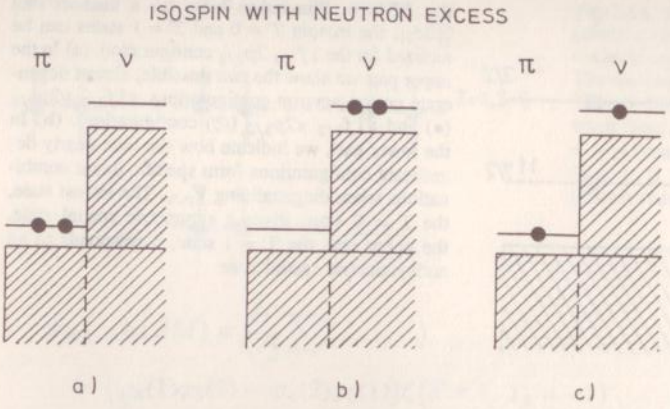


**Fig. 3.56.** States with fixed isospin $T = T_z$ for nuclei with a neutron excess. In the cases (**a**), (**b**) and (**c**), it is impossible to change a proton into a neutron (via the $T_+$ operator) since the corresponding neutron orbitals are fully occupied in the core. So, states with maximal isospin result with $T = T_z$

correspond to filled orbitals in the neutron excess core, configurations with two valence neutrons above the neutron excess and configurations with one valence proton (corresponding to a neutron excess orbital) and one valence neutron above the neutron excess (Fig. 3.56). The above states correspond to states with isospin obtained by coupling the isospin of the neutron excess system $T_{\text{core}} = (N - Z)/2$, to the isospin $T = 1$ of the two-particle system. In both cases, the isospin is *maximal* and corresponds to the projection $T_z$ or $T = T_z$ !

We shall illustrate the analogies and differences between a proton-neutron formalism versus isospin formalism in Chap. 5 for particle-hole excitations in $^{16}$O.

To finish the present discussion, we consider the case of two-nucleons ($n - n$, $p - p$ or $p - n$) in a single $j$-shell when constructing the wave functions $\psi\left(j^2; JM, TT_z\right)$. Using the same method as in Sect. 3.2, we construct

$$\begin{aligned}\psi\left(j^2; JM, TT_z\right) &= N'\left(1 - (-1)^{2j-J+1-T}\right) \\ &\times \sum_{m,m'} \langle jm, jm' | JM\rangle \sum_{t_z, t'_z} \langle \tfrac{1}{2} t_z, \tfrac{1}{2} t'_z, | TT_z\rangle \\ &\times \varphi_{jm}(1)\varphi_{jm'}(2)\zeta^{1/2}_{t_z}(1)\zeta^{1/2}_{t'_z}(2)\,. \end{aligned} \tag{3.194}$$

These functions disappear except when $J + T =$ odd, or

$$\begin{aligned} &T = 1\,, \quad J = \text{even} = 0, 2, \ldots, 2j - 1\,, \\ &T = 0\,, \quad J = \text{odd} = 1, 3, \ldots, 2j\,, \end{aligned} \tag{3.195}$$

with, as an example, the $(1f_{7/2})^2$ ($T = 1$, $J = 0, 2, 4, 6$) and ($T = 0$, $J = 1, 3, 5, 7$) configurations.

### 3.4.3 Two-Body Matrix Elements with Isospin

Using the same methods as discussed in Sect. 3.2.3, one can evaluate two-body interaction matrix elements, now including isospin, with the result (using $\boldsymbol{l}+\boldsymbol{s}=\boldsymbol{j}$ coupling)

$$\langle j_1 j_2; JM, TT_z|V|j_3 j_4; JM, TT_z\rangle = -A_0^{(T)}\hat{j}_1\,\hat{j}_2\,\hat{j}_3\,\hat{j}_4 \cdot$$
$$\left[\left(1+\delta_{j_1 j_2}\right)\left(1+\delta_{j_3 j_4}\right)\right]^{-1/2}\left(1+(-1)^{l_1+l_2+l_3+l_4}\right)/2 \cdot$$
$$\left[(-1)^{j_1+l_2+1/2}\begin{pmatrix} j_1 & j_2 & J \\ \frac{1}{2} & -\frac{1}{2} & 0\end{pmatrix}(-1)^{j_3+l_4+1/2}\begin{pmatrix} j_3 & j_4 & J \\ \frac{1}{2} & -\frac{1}{2} & 0\end{pmatrix}\right.$$
$$\left(1-(-1)^{J+T+l_3+l_4}\right)/2+\left(1+(-1)^T\right)/2(-1)^{j_1+j_2}$$
$$\left.\begin{pmatrix} j_1 & j_2 & J \\ \frac{1}{2} & \frac{1}{2} & -1\end{pmatrix}(-1)^{j_3+j_4}\begin{pmatrix} j_3 & j_4 & J \\ \frac{1}{2} & \frac{1}{2} & -1\end{pmatrix}\right] . \tag{3.196}$$

By using the above expressions we can also evaluate the matrix elements of the interaction $-4\pi V_0\delta(\boldsymbol{r}_1-\boldsymbol{r}_2)(1+\alpha\boldsymbol{\sigma}_1\cdot\boldsymbol{\sigma}_2)$ by the concordance

$$\begin{aligned} A_0^{(0)} &= (1+\alpha)A_0 \,, \\ A_0^{(1)} &= (1-3\alpha)A_0 \,, \end{aligned} \tag{3.197}$$

with

$$A_0 = V_0\int u_{n_1 l_1}(r)u_{n_2 l_2}(r)u_{n_3 l_3}(r)u_{n_4 l_4}(r)\frac{1}{r^2}dr \,.$$

This is true because we have $S=0$, $T=1$ and $S=1$, $T=0$ since the $\delta$-function only allows the spatially symmetric ($L$ = even) wave functions to give non-vanishing results.

One can verify that in the special case of $\alpha=0$, $j_1=j_3$, $j_2=j_4$, $j_1\neq j_2$, the result of Sect. 3.2.3 is reproduced.

Another case is for all $j_i=j$ with

$$\langle j^2; JM, TT_z|V|j^2; JM, TT_z\rangle = -A_0^{(T)}(2j+1)^2\frac{1}{2}\left[\begin{pmatrix} j & j & J \\ \frac{1}{2} & -\frac{1}{2} & 0\end{pmatrix}^2\right.$$
$$\left.\times\left(1-(-1)^{J+T}\right)/2+\begin{pmatrix} j & j & J \\ \frac{1}{2} & \frac{1}{2} & -1\end{pmatrix}^2\left(1+(-1)^T\right)/2\right] . \tag{3.198}$$

In studying the above example for $(1f_{7/2})^2_{T=0}$ states, we obtain the spectrum shown in Fig. 3.57. Here we see that the interaction is most attractive in the parallel and anti-parallel angular momenta for $T=0$ states. We can, moreover, compare the above theoretical results with the $^{42}_{21}$Sc nucleus where indeed, the $1f_{7/2}(p)\ 1f_{7/2}(n)$ case occurs. In Sect. 3.2.3, the results for $T=0$ for a $\delta$-interaction with large $j$ are illustrated and compare well with experimental data on odd-odd nuclei.

In Fig. 3.58 we compare the low-lying spectra for $^{42}_{20}$Ca$_{22}$ with $^{42}_{21}$Sc$_{21}$, and observe that although many more states occur in $^{42}$Sc, for the $(1f_{7/2})^2_{T=1;\,J=0,2,4,6}$ states, very similar results occur because of charge independence.

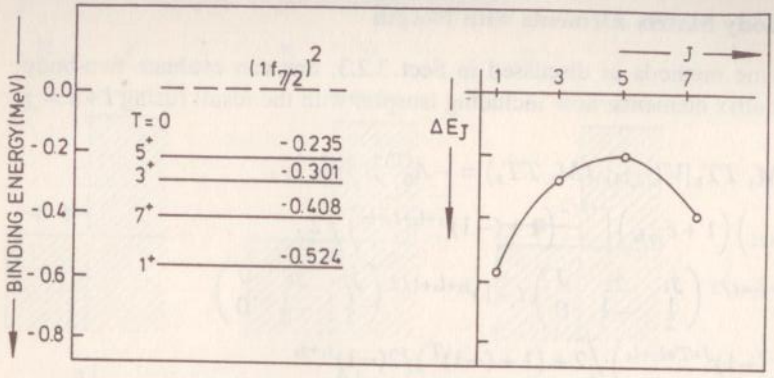


**Fig. 3.57.** Isospin $T = 0$ two-body matrix elements for two particles in the $1f_{7/2}$ orbital. The matrix elements are expressed as $\Delta E_J \equiv \langle j^2; JM, T = 0|V_{1,2}|j^2; JM, T = 0\rangle / 4A_0^{(0)}$. On the right-hand side, a corresponding $\Delta E_J$ vs. $J$ plot has been made

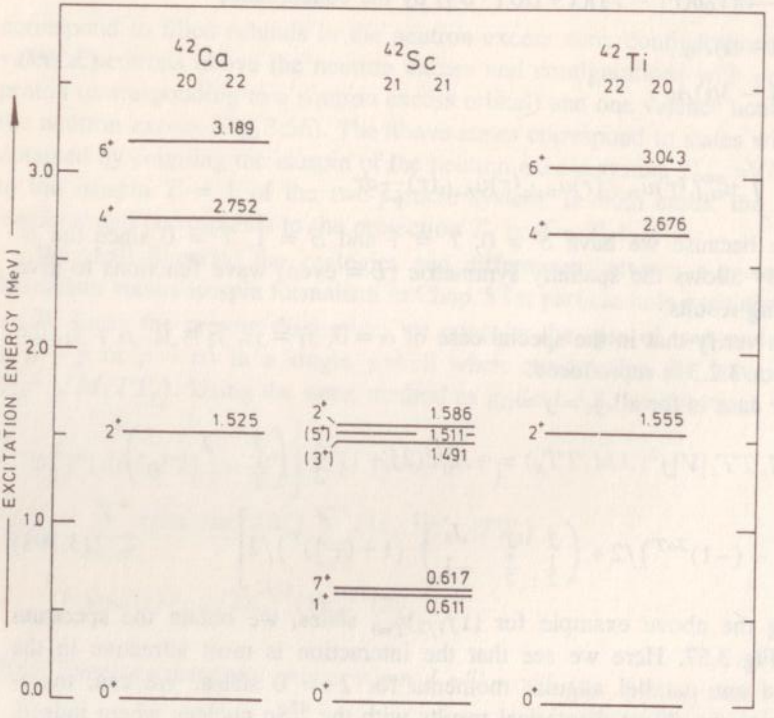


**Fig. 3.58.** Comparison of the data in $^{42}$Ca, $^{42}$Sc and $^{42}$Ti. We compare the $T = 1$ and $T = 0$ $(1f_{7/2})^2$ states. The conditions of charge independence are well followed when comparing $^{42}$Ca and $^{42}$Ti. In $^{42}$Sc, the extra states $1^+$, $7^+$, $(3^+)$, $(5^+)$ are also given. In the case of $^{42}$Ca and $^{42}$Ti, some low-lying levels $(0^+, 2^+)$ have been left out since they do not correspond to the $(1f_{7/2})^2$ configuration

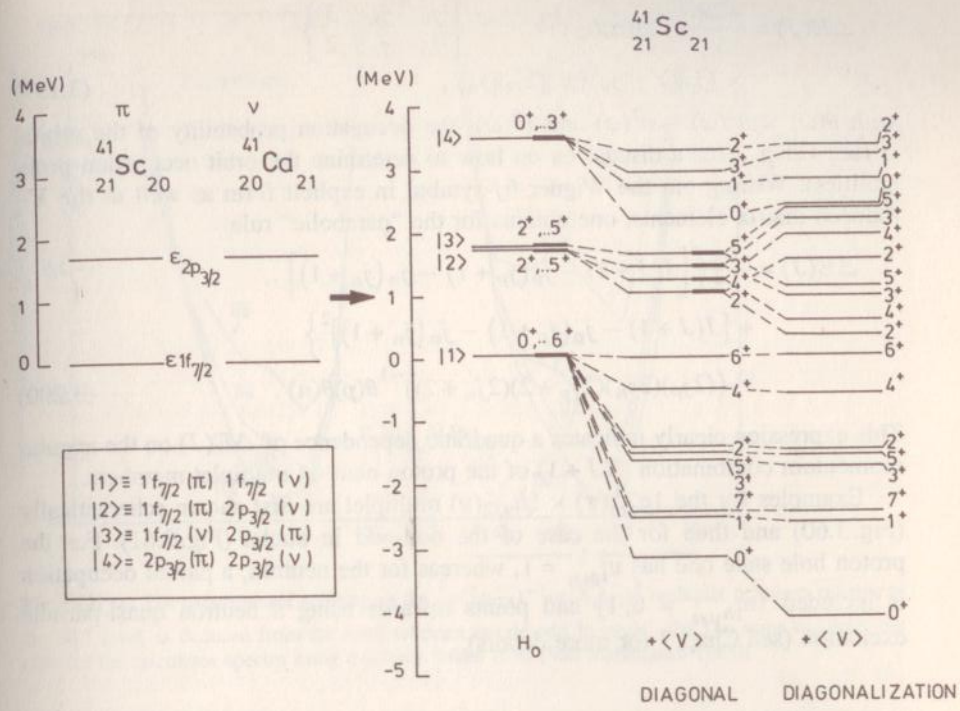


**Fig. 3.59.** Spectrum for the doubly-odd nucleus $^{42}$Sc with a proton and a neutron occupying the $1f_{7/2}$ and $2p_{3/2}$ orbitals. On the left-hand side, the unperturbed energies are given. The energy spectrum is decomposed in to the unperturbed spectrum, the spectrum after adding diagonal terms and, finally, the full result after diagonalizing the residual interactions

Starting from a knowledge of the isospin $T = 0$ and $T = 1$ splitting that is obtained for the two-fold degeneracy resulting in a proton-neutron system, the full spectrum of the nucleus $^{42}_{21}$Sc$_{21}$ can then be obtained when we constrain the separate proton and neutron single-particle space to the $1f_{7/2}$ and the $2p_{3/2}$ orbitals. Taking the single-particle energies to be degenerate (left-hand side of Fig. 3.59), the states combined from the $|1f_{7/2}(p)1f_{7/2}(n); JM\rangle$; $|1f_{7/2}(p)2p_{3/2}(n); JM\rangle$; $|1f_{7/2}(n)2p_{3/2}(p); JM\rangle$ and the $|2p_{3/2}(p)2p_{3/2}(n); JM\rangle$ configurations are given on the right-hand side. Then, subsequently adding the two-particle diagonal matrix elements and, on the extreme right, taking into account the results of diagonalization in the above model space, a rather good approximation to the full $(J, T)$ structure of the energy spectrum in an odd-odd nucleus such as $^{42}_{21}$Sc$_{21}$ can be reached.

The above particle-particle spectra in odd-odd nuclei are remarkably consistent with a parabolic behavior. This works throughout the whole nuclear mass region (In nuclei, $N = 81$ and $N = 83$ nuclei) and is known as the parabolic rule (Paar 1979, Van Maldeghem, Heyde 1985, Van Maldeghem 1988). Although somewhat outside the scope of the present discussion, it has been shown that such a parabolic dependence on spin $J$ can be derived (Van Maldeghem 1988):

$$\Delta E(J) = \frac{-2\pi}{5}\theta(p)\theta(n)(-1)^{j_p+j_n+J}\begin{Bmatrix} j_p & j_n & J \\ j_n & j_p & 2 \end{Bmatrix} \times \langle j_p \| \boldsymbol{Y}_2 \| j_p \rangle \langle j_n \| \boldsymbol{Y}_2 \| j_n \rangle \,, \tag{3.199}$$

with $\theta(\omega) = u^2(\omega) - v^2(\omega)$ and $v^2(\omega)$, the occupation probability of the orbital $\omega$ (see Chap. 7 for a discussion on how to determine the orbit occupation probabilities). Writing out the Wigner $6j$-symbol in explicit form as well as the $\boldsymbol{Y}_2$ reduced matrix elements, one obtains for the "parabolic" rule

$$\Delta E(J) = -\tfrac{3}{4}\Big\{\big[J(J+1) - j_p(j_p+1) - j_n(j_n+1)\big] + \big[J(J+1) - j_p(j_p+1) - j_n(j_n+1)\big]^2\Big\} \times \big((2j_p)(2j_n)(2j_p+2)(2j_n+2)\big)^{-1}\theta(p)\theta(n) \,. \tag{3.200}$$

This expression clearly indicates a quadratic dependence of $\Delta E(J)$ on the angular momentum combination $J(J+1)$ of the proton-neutron multiplet members.

Examples for the $1g_{9/2}^{-1}(\pi) \times 1h_{9/2}(\nu)$ multiplet are first shown schematically (Fig. 3.60) and then for the case of the odd-odd In nuclei (Fig. 3.61). For the proton hole state one has $v^2_{1g_{9/2}} = 1$, whereas for the neutron, a partial occupation is included $\left(v^2_{1h_{11/2}} \neq 0, 1\right)$ and points towards using a neutron quasi-particle excitation (see Chap. 7 for more details).

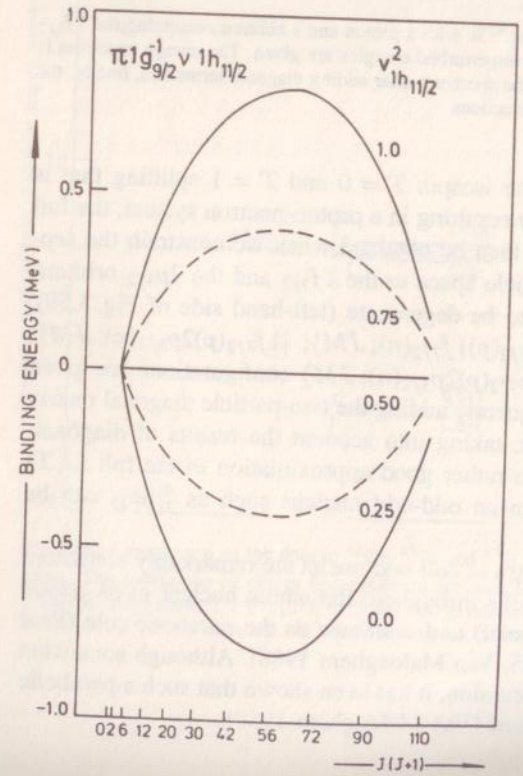


**Fig. 3.60.** Schematic illustration of the $[\pi(1g_{9/2})^{-1}\,\nu(1h_{11/2})]$ proton-neutron multiplet members, according to the parabolic rule of (3.200). It is the pairing factor (see Chap. 7) that causes a turn-over of the parabola from convex to concave in shape. Here, the notation $\pi(\nu)$ is used for proton (neutron) orbitals

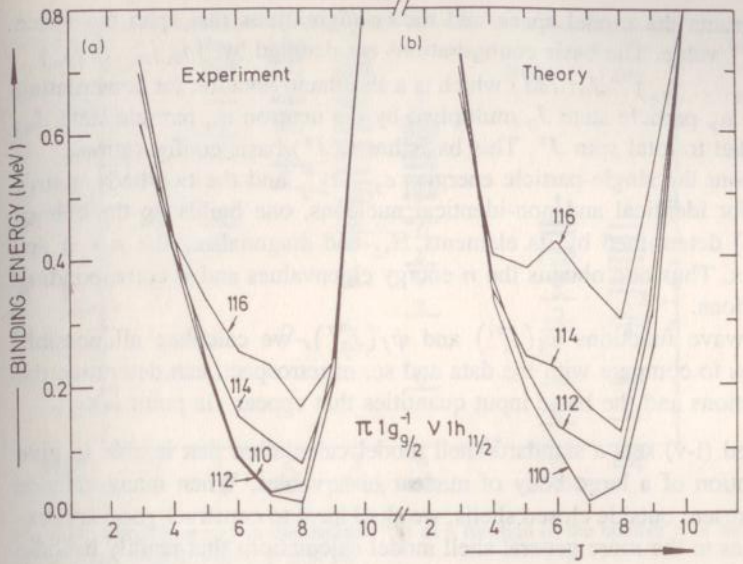


**Fig. 3.61.** (**a**) The experimental splitting of the $\left[\pi(1g_{9/2})^{-1}\nu(1h_{11/2})\right]$ multiplet members relative to the $10^-$ level as deduced from the level schemes in odd-odd In nuclei. (**b**) The same multiplet but now for the calculated spectra using a $\delta$-force [taken from (Van Maldeghem 1985)]

## 3.5 Large-Scale Shell-Model Calculations

In this chapter we have learned how to study nuclei where the number of nucleons outside closed shells is not too large to allow for an exact shell model treatment. We have discussed methods of calculating the matrix elements needed to set up the secular equation for the energy eigenvalues both for identical and non-identical nucleons. We have also shown, once the wave functions are known, how to calculate one-body expectation values that determine the nuclear observables (half-lives of nuclear excited states, decay rates, moments, etc.). In particular, the evaluation of these observables for electric and magnetic transitions and moments will be outlined in Chap. 4.

Here we summarize the above procedure and philosophy for the study of a given nucleus $(N, Z)$.

i) One determines the nearby closed shells given by $Z_{\rm cl}$ and $N_{\rm cl}$ so as to fix the number of valence protons and neutrons.
ii) The number of active particles becomes $n_p = (Z - Z_{\rm cl})$ and $n_n = (N - N_{\rm cl})$ where $n_p$ and $n_n$ are the valence number of proton (neutron) particles (or holes). Through (i) one can fix the single-particle orbitals $j_{p_1}, j_{p_2}, \ldots$ and $j_{n_1}, j_{n_2}, \ldots$ that determine the properties at low energy when constructing the model space.

iii) One constructs the model space and the configurations that span the space for each $J^\pi$ value. The basis configurations are denoted by $|(j_{p_1} j_{p_2} \cdots j_{p_n})^{n_p} J_p, (j_{n_1} j_{n_2} \cdots j_{n_n})^{n_n} J_n; JM\rangle$ which is a shorthand notation for constructing the proton $n_p$ particle state $J_p$ multiplied by the neutron $n_n$ particle state $J_n$, both coupled to total spin $J^\pi$. This basis has $n(J^\pi)$ basis configurations.

iv) Starting from the single-particle energies $\varepsilon_{j_{p_i}}, \varepsilon_{j_{n_j}}$ and the two-body matrix elements for identical and non-identical nucleons, one builds up the energy matrix $[H]$ determined by its elements $H_{ij}$ and diagonalizes the $n \times n$ energy matrix. Thus one obtains the $n$ energy eigenvalues and $n$ corresponding eigenfunctions.

v) With the wave functions $\psi_i(J_i^{\pi_i})$ and $\psi_f(J_f^{\pi_f})$, we calculate all possible observables to compare with the data and so, in retrospect, can determine the wave functions and the basic input quantities that appear via point iv).

This method (i-v) sets a standard shell model calculation that is able to give a good description of a large body of nuclear observables. When many valence nucleons are present outside closed shells, we shall have to construct good approximation schemes to the more general shell model calculations that readily become unfeasible. Such approximation schemes will be discussed in Chap. 6 and Chap. 7 in detail.

With the advent of large and fast computing facilities, however, shell-model calculations using very big shell-model configuration spaces have become possible. One of the most thoroughly investigated regions in that respect is formed by the full *sd*-shell-model region spanning the various nuclei between $^{16}$O and $^{40}$Ca. Here, a maximum of 24 particles can fill up the proton and neutron $1d_{5/2}$, $2s_{1/2}$ and $1d_{3/2}$ orbitals. For a given number of valence proton particles ($n_\pi$) and neutron particles ($n_\nu$), either a proton-neutron or an isospin basis can be used to construct the energy matrices. Because the proton and neutron single-particle energies are not fully identical, one could start from a basis which is a product state of proton and neutron basis configurations. The separate charge configurations then become

$$\psi_\pi \left[ \left(1d_{5/2}\right)^{n_1}_{\alpha_1 J_1} \left(2s_{1/2}\right)^{n_2}_{\alpha_2 J_2} \left(1d_{3/2}\right)^{n_3}_{\alpha_3 J_3} \right] J_\pi^{n_\pi} \tag{3.201}$$

and

$$\psi_\nu \left[ \left(1d_{5/2}\right)^{n_1'}_{\alpha_1' J_1'} \left(2s_{1/2}\right)^{n_2'}_{\alpha_2' J_2'} \left(1d_{3/2}\right)^{n_3'}_{\alpha_3' J_3'} \right] J_\nu^{n_\nu} \tag{3.202}$$

with $n_\pi = n_1 + n_2 + n_3$; $n_\nu = n_1' + n_2' + n_3'$ and $\alpha_i, J_i(\alpha_i', J_i')$ the proton (neutron) quantum numbers needed to specify the internal configurations in an unique way.

As an example, in $^{28}$Si, the 12-particle state with $M = 0$ and $T_z = 0$ has a dimension 93,710 in the $m$-scheme and, in the $(J, T)$ scheme, the $J = 3$, $T = 1$ 12 particle basis has a dimension 6,706. We also illustrate the case of $^{28}$Si, in particular, for the binding energy of the $(1d_{5/2})^{12}(2s_{1/2})^0(1d_{3/2})^0$ closed sub-shell configuration, in Fig. 3.62. In increasing the number of particles excited from the $1d_{5/2}$ into the $2s_{1/2}$ and $1d_{3/2}$ orbitals (excitation order 1 to 12), the full configuration space rapidly 'explodes'. Only after all possible partitions of the 12

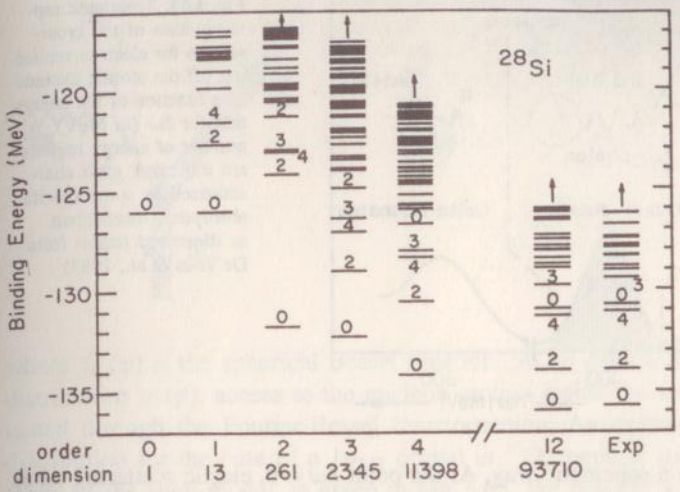


**Fig. 3.62.** Binding energy in the nucleus $^{28}$Si as a function of the number $n$ of nucleons excited out of the $1d_{5/2}$ orbital (with $0 \leq n \leq 12$)

particles have been considered is good agreement with the experimental spectrum achieved. At the same time, one notices the rather slow convergence of the energy spectrum towards its final form.

Similar types of shell-model studies have been carried out, according to the methods outlined here, in other mass regions. The *sd*-shell model space calculations, performed in great detail by Brown and Wildenthal (Brown, Wildenthal, 1988), can serve as a benchmark study in that respect.

## 3.6 Testing Single-Particle Motion in an Average Field

After a detailed discussion of the methods used to treat nucleon single-particle motion in an average field, as well as of the correlations induced by many-body effects through the residual interactions, and extensive comparison between theoretical and experimental energy spectra, one still has to prove as well as possible the very existence of independent-particle motion which is at the basis of the nuclear shell model.

One-nucleon transfer reactions (pick-up or stripping) have shown that nucleons can indeed be taken out or be put into single-particle orbitals. The ideal probe, however, to test nucleonic motion inside the nucleus is the electromagnetic interaction. When electrons scatter off the atomic nucleus, the electrons act as an almost ideal probe with which to study how nucleons move within the nucleus. By changing the electron energy ($\hbar\omega$) and its momentum ($\hbar q$), various information ranging from nuclear collective surface vibrations down to details related to the motion of individual nucleons can be obtained. In Fig. 3.63 we illustrate these

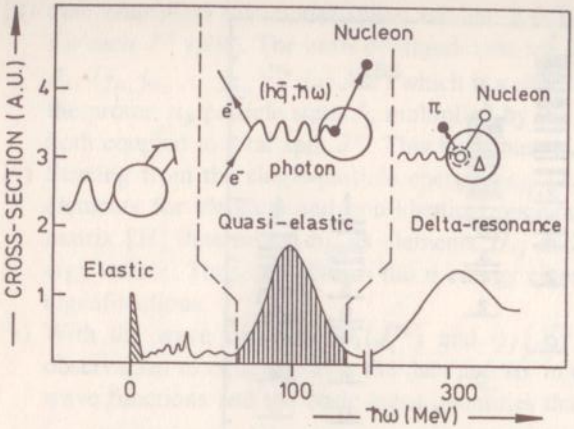


**Fig. 3.63.** Schematic representation of the cross-section for electron scattering off the atomic nucleus as a function of the energy transfer $\hbar\omega$ (in MeV). A number of energy regions are indicated, each characterized by some specific absorption mechanism, as illustrated (taken from De Vries et al., 1983)

various processes in a schematic way. At the point $\hbar\omega = 0$, elastic scattering takes place and the nucleus remains in its ground state. In the region $0 \leq \hbar\omega \leq 20\,\mathrm{MeV}$, a large number of individual resonances in the nuclear many-body system start to appear. In the region $30\,\mathrm{MeV} \leq \hbar\omega \leq 150\,\mathrm{MeV}$, one-nucleon emission occurs as the dominant process. This is one of the most interesting regions since, by measuring simultaneously the energies and momenta of the outgoing nucleon and the scattered electron, information about the velocity distribution of the nucleon inside the nucleus prior to the interaction may be obtained.

A schematic representation of the above process is given in Fig. 3.64 where we adopt the most simple reaction mechanism: the detected nucleon is ejected in a one-step knock-out reaction in which all other nucleons remain as spectator particles. This approach is called the 'quasi-free' emission approximation. Momentum conservation at the two interaction vertices in Fig. 3.64, using the laboratory system with $|\boldsymbol{p}_A| = 0$, implies

$$\boldsymbol{p}_m = \boldsymbol{p}_a - \hbar\boldsymbol{q} = -\boldsymbol{p}_B \,. \tag{3.203}$$

The momentum $\boldsymbol{p}_m$ is customarily referred to as the 'missing' momentum and represents the momentum of the detected nucleon just before it was hit by the photon, characterizing the electromagnetic interaction, and thereby absorbing a momentum $\hbar\boldsymbol{q}$.

A nucleon moving inside a nucleus will be characterized by a velocity probability distribution (related to the Fourier transform of the coordinate wave function). Within the independent particle model, one can introduce a momentum distribution $\rho_a(\boldsymbol{p})$ corresponding to a given single-particle orbital, characterized by $a$ (with $a \equiv \{n_a, l_a, j_a; \varepsilon_a\}$). This function $\rho_a(\boldsymbol{p})$ then describes the probability of finding the nucleon in the particular state $a$ with momentum $\boldsymbol{p}$. A detailed derivation of this probability, or spectral function, has been given by Ryckebusch (1988) with, as a result,

$$\rho_a(\partial) = \frac{1}{2\pi^2\hbar^3}\left[\int dr\, r^2 j_{l_a}\left(\frac{pr}{\hbar}\right)\varphi_{n_a,l_a,j_a}(r)\right]^2 v_a^2(2j_a+1)\,, \tag{3.204}$$

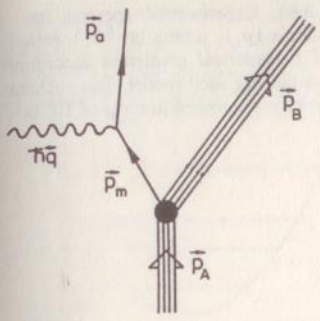


**Fig. 3.64.** One-photon exchange diagram for an electromagnetically induced one-nucleon emission process in the plane-wave impulse approximation. The various momenta ($\hbar q$, $p_a$, $p_m$, $p_A$ and $p_B$) are indicated

where $j_{l_a}(x)$ is the spherical Bessel function. So, in determining this momentum distribution $\rho_a(p)$, access to the nucleon motion inside the atomic nucleus is obtained through the Fourier-Bessel transformation. An example of a momentum distribution for the case of a $1p_{3/2}$ orbital in $^{16}$O, together with the prediction in terms of the shell-model, is given in Fig. 3.65. We observe very good agreement with the original concept of a nucleon moving inside an orbital characterized by the $1p_{3/2}$ quantum numbers.

The electron accelerator in Amsterdam (the NIKHEF-K Medium Energy Accelerator MEA) provides electrons with an energy of up to $\simeq$ 600 MeV. The electrons that are scattered off the nucleus can cause the atomic nucleus to eject certain particles or even clusters of particles. Magnetic spectrometers are now able to accurately determine the momentum of both the scattered electron and the ejected particle(s). As outlined above, the microscopic structure of the nucleon single-particle motion can be reconstructed.

A survey of the knock-out from various valence orbitals is presented in Fig. 3.66 concerning the spectroscopic strength (in % of the maximal value which amounts to $2j_a+1$ for a given orbital $j_a$). The quite important depletion of strength with respect to 100 % values, which would be the case for fully occupied orbitals in an extreme single-particle picture, is still not fully understood. Deviations could be due to (i) admixtures of low-lying collective excitations in the ground-state wave function and, (ii) the strongly repulsive short-range two-body (and eventually many-body) correlations that could scatter particles out of the occupied orbitals.

Therefore, the existence of almost fully occupied single-particle orbitals in an average, one-body field seems rather well proven, at least for those levels lying quite close to the Fermi level. If we now consider deeply-bound orbitals and try to remove a nucleon from one of these, one might expect a pattern more complex than a single one-hole state. The single-hole strength will become spread out over a number of more complex configurations, coupling to the original single-hole configuration through the residual interaction. This process is given pictorially in Fig. 3.67, where the high density of close-lying complicated configurations in the vicinity of a single-hole configuration is drawn within the dash-line region. The residual interaction can then cause the single-hole strength to be fragmented in an

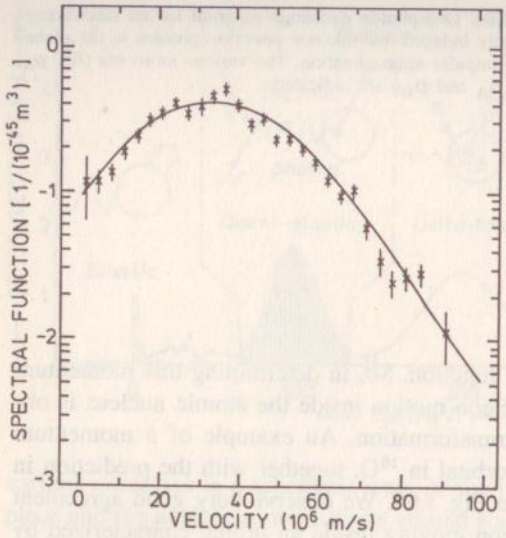


**Fig. 3.65.** Experimental spectral function for a $1p_{3/2}$ proton in $^{16}O$, together with a theoretical prediction according to the nuclear shell model. The nucleon velocity is expressed in units of $10^6$ m/s

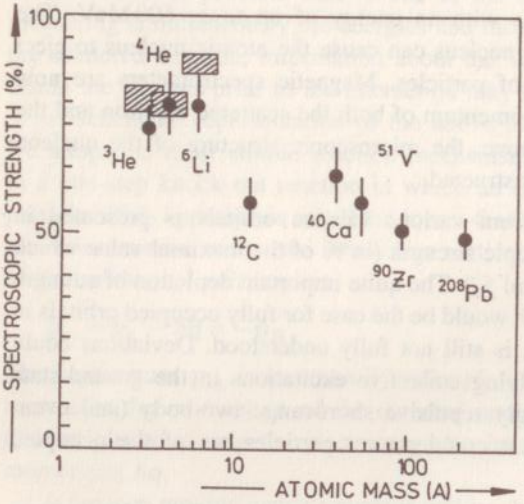


**Fig. 3.66.** Observed spectroscopic strength $S$ (relative to the full shell-model value) for knock-out from the least bound orbital and as a function of the mass number $A$. The dashed regions indicate the range of theoretical values for $A \leq 6$ systems (taken from Dieperink et al., 1990)

important way. Thereby, the very idea of undisturbed pure independent-particle motion as a zero-order picture rapidly loses credence, since the total strength becomes spread out over very many states and over a large energy region. Detailed studies, making use of Green function methods, have been carried out and are discussed by Van Neck et al. (Van Neck, 1991).

To conclude this chapter on the shell model, various tests relating to how nucleons move inside the nucleus have been discussed. Using in particular the quasi-free one-step nucleon knock-out as an experimental probe, important infor-

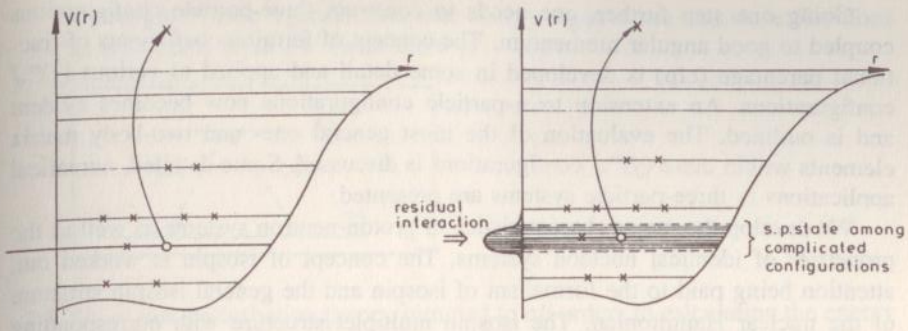


**Fig. 3.67a, b.** Pictorial representation of the way in which a nucleon is removed from a deeply-bound orbital in a potential well. On the left-hand side **(a)** a single-particle knock-out process is depicted, whereas in **(b)** interactions within a region of more complex configurations are indicated

mation on the particular nucleonic motion results. The large number of data on e.g. $(\gamma, n), (\gamma, p)(e, e'p)$, ... reactions all point towards a basic shell-model structure at least for these orbitals that are close to the Fermi level.

## 3.7 Summary

In this Chapter, having discussed the experimental evidence showing the need to consider independent-particle motion for nucleons moving in the average field built from the interactions of a given nucleon within the nucleus with all other nucleons, we described the basic structure of the nuclear shell model.

The radial equation for a harmonic oscillator average field is studied with the well-known energy spectrum. The importance of the spin-orbit interaction, which modifies the original spectrum so that it is in good agreement with the data, is discussed in detail. A number of illustrative examples of nuclei having one nucleon outside a closed shell (or one nucleon missing from a closed shell) are shown. A simple approach to Hartree-Fock theory, which underpins the microscopic structure of independent-particle motion, is given.

The next step is to consider two-particle states: the construction of appropriate two-body shell-model wave functions and a discussion of the possible forms of the residual two-body interaction is given. Starting from these basic ingredients, two-body matrix elements are evaluated in detail for central forces and, in particular, for the zero-range $\delta$ interaction. Detailed comparison with experimentally observed two-particle spectra is also given. In most nuclei, the two-particle states are not restricted to a single configuration. In most cases, all possible configurations resulting from partitioning the two particles over the available single-particle orbitals have to be constructed and the corresponding eigenvalue equation solved in this basis. Configuration mixing results and concepts such as model space, mode interaction, effective charges, ... are discussed.

Going one step further, one needs to construct three-particle configurations coupled to good angular momentum. The concept of fermion coefficients of fractional parentage (cfp) is developed in some detail and applied to various $(j)^n J$ configurations. An extension to $n$-particle configurations now becomes evident and is outlined. The evaluation of the most general one- and two-body matrix elements within these $(j)^n J$ configurations is discussed. Some detailed, numerical applications to three-particle systems are presented.

We develop the major characteristics of proton-neutron systems as well as the properties of identical nucleon systems. The concept of isospin is worked out, attention being paid to the formalism of isospin and the general isospin structure of the nuclear Hamiltonian. The isospin multiplet structure with corresponding energies is discussed. Subsequently, two- and many-particle isospin wave functions are built. The similarities and differences between the proton-neutron charge formalism and the isospin formalism are pointed out. Application to the two-nucleon($nn, pp, np$) system and isospin triplets is made. Finally, the two-body matrix elements including isospin are derived and this theoretical framework is applied to the nucleus $^{42}$Sc. A number of very special features of the proton-neutron force are pointed out: the parabolic rule and particle-particle properties are presented.

In the last two sections, a short excursion into the possibilities of present-day state-of-the-art large-scale shell-model calculations, with application to the *sd*-shell, as well as to the experimental evidence for the existence of single-particle motion in actual nuclei, is made. Here, the significance of electromagnetic interactions that probe the nucleon in its motion inside the atomic nucleus as an important proof of single-particle independent motion is clearly pointed out. Near the Fermi level, in particular, independent particle motion is shown to present a large body of evidence. For deep-lying hole states, however, important spreading over a large interval with many complex states becomes manifest.

## Problems

3.1 The three-dimensional harmonic oscillator can also be solved by separating the eigenvalue equation for the energy in cartesian coordinates $(x, y, z)$. Show that in this case $\varphi(x, y, z)$ becomes a product of three one-dimensional oscillator wave functions (product of Hermite functions). Show that a relation exists with the solutions of the eigenvalue equation in spherical $(r, \theta, \varphi)$ coordinates (see (3.16)).

3.2 Derive the Hartree-Fock equatins from the variational condition, expressed by (3.43).

3.3 Derive the antisymmetrized and normalized two-body matrix elements $\langle j_a j_b; JM|V|j_c j_d; JM\rangle_{\text{nas}}$ where $V$ is a central two-body force $V(r)$ using the Moshinsky transformation brackets.

3.4 Study the three-level model, where two levels are degenerate at the energy $\epsilon$ and only interact via the intermediate of a third level at energy $\epsilon'$ having

a strength $V$ (see figure). Study the energy eigenvalues and wave functions as a function of $\Delta\varepsilon/V$ (with $\Delta\varepsilon = |\varepsilon' - \varepsilon|$).

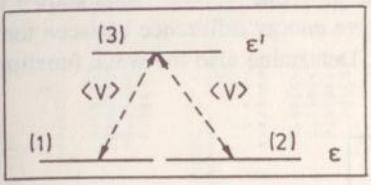


3.5 Show that perturbation theory summed to *all* orders in calculating the energy of the level (1) with unperturbed energy $H_{11}$, by including the interaction with a second level at $H_{22}(H_{22} > H_{11})$ with strength $H_{12}$ gives the result

$$\lambda_- = \frac{H_{11} + H_{22}}{2} - \frac{1}{2}\left[(H_{11} - H_{22})^2 + 4H_{12}^2\right]^{1/2} .$$

3.6 Construct the three-particle wave functions for a $(j)^3 J = j$ configuration with $j \leq 7/2$. We give the normalized $cfp$ coefficients

$$\left[j^2(J_1)jJ|\}j^3J\right] = \frac{\left[\delta_{J_1 J_0} + 2\hat{J}_0\hat{J}_1 \begin{Bmatrix} j & j & J_1 \\ J & j & J_0 \end{Bmatrix}\right]}{\left[3 + 6(2_{j_0}+1)\begin{Bmatrix} j & j & J_0 \\ J & j & J_0 \end{Bmatrix}\right]^{1/2}} .$$

and

$$\begin{Bmatrix} j & j & 0 \\ j' & j' & J \end{Bmatrix} = (-1)^{j+j'+J}\left(\hat{j}\hat{j}'\right)^{-1} .$$

3.7 Show, by explicit calculation, that the $(1_{g_{9/2}})^3 J = 9/2$ configuration has *two* independent states with $J = j$, depending on the original angular momentum of the two-particle configuration $(J_0)$ one starts from.

3.8 a) Show that the interaction energy in an $n$-particle state $|j^n \alpha JM\rangle$ with general $n(n \geq 2)$ can be expressed as a function of the two-body antisymmetrized matrix elements.

b) Show that in the calculation of a three-particle spectrum, starting from a two-body spectrum, one only needs the relative matrix elements

$$A_{J_1} = \langle j^2; J_1|V|j^2; J_1\rangle - \langle j^2; J_1 = 0|V|j^2; J_1 = 0\rangle .$$

*3.9 Given are $n$ degenerate levels $j_1, j_2 \ldots, j_n(\varepsilon_{j_1} = \varepsilon_{j_2} = \ldots = \varepsilon_{j_n})$. Determine the energy spectrum for two particles in the configuration space with $J^\pi = 0^+$ if the interaction matrix elements

$$\langle (j_i)^2; J = 0|V|(j_k)^2; J = 0\rangle = -\frac{G}{2}\hat{j}_i\hat{j}_k \quad (G > 0) .$$

Determine also the wave function corresponding with the lowest $J^\pi = 0^+$ eigenstate.